

THESIS

BIOTIC CONTROL OF LNAPL LONGEVITY - LABORATORY AND FIELD- SCALE STUDIES

Submitted by

Eric Douglas Emerson

Department of Civil and Environmental Engineering

In partial fulfillment of the requirements

For the Degree of Master of Science

Colorado State University

Fort Collins, Colorado

Spring 2017

Master's Committee:

Advisor: Susan K. De Long

Co-Advisor: Thomas Sale

Gregory Butters

Copyright by Eric Douglas Emerson 2016

All Rights Reserved

## ABSTRACT

### BIOTIC CONTROL OF LNAPL LONGEVITY - LABORATORY AND FIELD- SCALE STUDIES

Natural source zone depletion (NSZD) is an emerging strategy for managing light nonaqueous phase liquids (LNAPLs). Unfortunately, little is known about NSZD rates over extended periods of time, where heterogeneous redox conditions and changing LNAPL saturations may influence processes governing losses. Understanding long-term rates is central to anticipating LNAPL longevity under both natural and engineered conditions. Herein, laboratory and field-scale modeling studies were conducted to evaluate LNAPL longevity.

Laboratory studies evaluated loss rates as a function of total contaminant concentration under sulfate-reducing (SR) and methanogenic (MG) conditions. Biotic and abiotic loss rates were determined via tracking biodegradation products and hydrocarbons in column effluents and produced gasses over time. Furthermore, compositional weathering of LNAPL was evaluated. Loss rates with elevated sulfate averaged  $39.8 \text{ mmole carbon/day/m}^3$  ( $\pm 9.1 \text{ mmole carbon/day/m}^3$ ). Once sulfate in the soil was depleted to influent water sulfate concentrations of  $20 \text{ mg/L}$ , subsequent average loss rates were  $39.7 \text{ mmole carbon/day/m}^3$  ( $\pm 19.6 \text{ mmole carbon/day/m}^3$ ). Overall, loss rates with and without elevated sulfate were similar. Furthermore, results suggested that loss rates are independent of LNAPL concentration over the range of  $9,000$  to  $37,000 \text{ mg/kg}$  and redox conditions observed. Loss rates independent of LNAPL concentrations indicated that biologically mediated NSZD follows zero-order kinetics over the range of conditions evaluated. Column loss rates were compared to field-measured loss rates assuming an LNAPL thickness of three meters. Given this assumption, mean observed early- and late-loss rates are  $1.38$  and  $1.41 \text{ } \mu\text{mole carbon/m}^2/\text{sec}$ , respectively. Assuming decane as a representative LNAPL, observed loss rates are equivalent to  $7890$  and  $8060 \text{ L/hectare/year}$ . A

column was sacrificed at the completion of the study. Predicted mass losses of the study equate to approximately 1% total initial LNAPL mass lost. Total petroleum hydrocarbons (TPH) soil analysis of initial and final grab samples of column soil did not detect significant mass losses. Moreover, no significant shifts in the LNAPL composition were seen during the course of the study. Mass losses in this range are difficult to accurately quantify via soil-phase hydrocarbon analyses, thus highlighting the utility of the approach used herein.

An LNAPL longevity model (The Glide Path Model) was applied at a field site using a zero-order rate model for biological NSZD. LNAPL Longevity ranged from 35 to 105 years using a mean NSZD rate, plus or minus factors of 2 and  $\frac{1}{2}$ , respectively. Active recovery was shown to have little effect on the longevity of LNAPL.

## ACKNOWLEDGEMENTS

I would like to acknowledge the following groups and individuals for their part in supporting the work of this thesis. I would like to thank Dr. Susan K. De Long for accepting my research assistant application, her continued advisement throughout the course of the experiment, and continually providing positive criticism throughout my Thesis writing efforts. Dr. Thomas Sale provided his guidance, expertise with remediation, lab experience, and practical advice to a long-term column study. My gratitude goes out to Dr. Gregory Butters for being a member of my committee and opening my eyes to the world of soil physics. Thank you Shell Oil and Chevron Environmental Management Company for providing funding for this project. Technical input on application of the glide path model would not have been possible without Keith Piontek (TRC Solutions). Sanjay Garg for the direction and intuition he provided, specifically to experiment setup. My dearest appreciation to Dr. Jens Blotevogel, Dr. Mitch Olson, Dr. Kevin Saller, Gary Dick, Maria Irianni Renno, Rachael McSpadden, Emily Stockwell, Melissa Tracy, Nolan Platt, Christina Akron, Emily Mahanna, and Gabrielle Davis at the Center for Contaminant Hydrology for their introductions to analytical instruments, general advice, and overall hard work into creating this extensive column experiment. And foremost, my supportive family, for every word of advice and encouragement throughout the Master's degree experience

## TABLE OF CONTENTS

ABSTRACT.....	ii
ACKNOWLEDGEMENTS.....	iv
LIST OF TABLES.....	ix
LIST OF FIGURES.....	x
1. INTRODUCTION.....	1
1.1. Motivation.....	1
1.2. Objectives and Hypotheses.....	1
1.3. Organization.....	4
2. LITERATUE REVIEW.....	5
2.1. Introduction.....	5
2.2. LNAPL Remediation Past and Present.....	6
2.3. Fate and Transport of LNAPL.....	8
2.3.1. LNAPL as an Intermediate Wetting Phase.....	8
2.3.2. LNAPL Partitioning.....	10
2.3.3. LNAPL Subsurface Transport.....	11
2.4. Biological Degradation.....	12
2.4.1. Source Zone Microbiology.....	12

2.4.2.	Biological Degradation as a Function of Environmental Conditions.....	15
2.5.	Measuring Field Rates of Natural Losses.....	16
2.6.	Modeling of LNAPL Longevity and Natural Losses.....	19
3.	METHODS – LABORATORY STUDIES AND FIELD-SCALE MODELING.....	21
3.1.	Column Setup and Operation.....	21
3.1.1.	Column Setup.....	21
3.1.2.	Column Operation.....	25
3.2.	Analytical Methods.....	27
3.2.1.	Soil Total Petroleum Hydrocarbon Analysis .....	27
3.2.2.	Aqueous Hydrocarbons and Carbon Dioxide Analyses .....	28
3.2.3.	Gas Analysis.....	31
3.2.4.	General Water Quality Analysis .....	32
3.2.5.	Mobile LNAPL Snapshots .....	34
3.3.	Calculations .....	34
3.3.1.	Carbon Balance .....	35
3.3.2.	Molar Loss Rates.....	37
3.3.3.	Accounting for Governing Processes .....	38
3.3.4.	Statistics .....	40

3.4.	Glide Path Model .....	41
3.4.1.	Field Site.....	41
3.4.2.	Assumptions .....	43
3.5.	Glide Path Model Modification .....	43
4.	RESULTS .....	46
4.1.	Column Performance as a Function of Time .....	46
4.2.	Biodegradation Rates as a Function of Concentration .....	50
4.3.	Influence of Governing Biodegradation Processes.....	53
4.4.	Aqueous Hydrocarbon Composition as a Function of LNAPL Concentration.....	56
4.5.	Glide Path Model Results.....	58
5.	DISCUSSION AND FURTHER WORK .....	61
5.1.	Discussion .....	61
5.2.	Conclusions and Recommendations for Future Work .....	64
5.2.1.	Conclusions .....	64
5.2.2.	Future Work.....	65
6.	REFERENCES .....	67
7.	APPENDICES.....	72
7.1.	Appendix A – Draining and Saturating Procedures .....	72

7.2.	Appendix B – GRO & DRO Calibration Procedures .....	79
7.3.	Appendix C- Analytical Measurements.....	82
7.4.	Appendix D – Ultraviolet Photographic Techniques in MATLAB.....	93

## LIST OF TABLES

Table 1– Initial TPH concentrations of the 11-column laboratory study .....	25
Table 2– Sample matrix for all analytical parameters for aqueous and gaseous phases at specific operational events .....	34
Table 3– Mean NSZD molar rates for early and late periods with average and standard deviation. Control (*) and nutrient influent (***) columns are included. ....	55
Table 4 – GRO Calibration Matrix .....	79
Table 5 – Volume of GRO Standard for calibration .....	80
Table 6 – Analytical Measurements for eleven experimental columns.....	82

## LIST OF FIGURES

Figure 1– LNAPL SCM following Amos et al. (2005).....	5
Figure 2 – Column setup diagram .....	22
Figure 3 – Effluent sulfate (mg/L), cumulative methane ( $\mu\text{mole}$ ), and biodegradation rates ( $\text{mmole C/day/m}^3$ ) versus experimental months.....	47
Figure 4 – Photos of column experimental setup.....	49
Figure 5 – Log scale box-plot and linear regression models of biodegradation molar rates ( $\text{mmole C/day/m}^3$ ) versus initial LNAPL concentration (mg/kg TPH).....	52
Figure 6 – Mean NSZD molar rates ( $\text{mmole carbon/day/m}^3$ ) for contributing biological or abiotic processes vs. LNAPL concentration (mg/kg TPH) for early and late periods.....	54
Figure 7 – Log scale aqueous concentrations ( $\mu\text{g/L}$ ) of totalized n-alkanes (a), Naphthalene (b), and Benzene (c) versus experimental months.....	57
Figure 8 – Years to LNAPL depletion versus NSZD loss rate (LR) without hydraulic recovery (HR), with historical (hist.) HR, and with future hydraulic recovery.. ..	59
Figure 9 – Depiction of GPM output as total LNAPL (specific volume) for average NSZD loss rate. ....	60
Figure 10– MATLAB Output portable network graphic (png) .....	96
Figure 11– Example Slides of the UV Light Fluorescence Process and tracking of mobile LNAPL. ....	97

## 1. INTRODUCTION

The following section describes motivation, objectives, hypotheses, and organization of this thesis.

### 1.1. Motivation

Natural source zone depletion (NSZD) is becoming an important remedial strategy at weathered LNAPL sites. Specifically, NSZD often dominates mass depletion at weathered LNAPL sites, and anaerobic rates appear to be controlling LNAPL longevity. The need to remediate LNAPL where active hydraulic recovery has continually fallen short of remedial objectives remains. Site core strategies need to resolve overall efficacy of active remedies and implementing NSZD as the primary remedial strategy. Unfortunately, little is known about the effects of NSZD over extended periods of time. A primary challenge is resolving NSZD rates as either zero-order or first-order rate models. Fundamental factors that have the potential to control NSZD through time include LNAPL surface area and biological mediated degradation. Observed natural losses from multiple field sites have been shown to be within an order of magnitude from such studies as Amos et al. (2005) and McCoy et al. (2014). Each field site in the studies varied in degree of age, remaining LNAPL mass, LNAPL composition, and soil types (Amos et al., 2005, McCoy et al., 2014). An understanding of whether natural losses are dependent on mass remaining in the system and LNAPL composition is critical to applying longevity models to field sites.

### 1.2. Objectives and Hypotheses

The following section outlines objectives for this study.

Objective 1 - Determine rates of LNAPL losses as a function of LNAPL saturation, primary depletion process, and LNAPL composition.

Hypothesis: Natural losses of subsurface petroleum liquids follow a zero-order rate model independent of LNAPL saturation and predominant anaerobic biological degradation process.

Supporting activities included:

- Column studies were conducted for 411 days, and natural losses were measured via tracking degradation products and hydrocarbons in column effluent and gas produced.
- The LNAPL was collected at a former refinery and spiked with select compounds. Field soil contained residual LNAPL and was measured at a saturation of 9,000 mg total petroleum hydrocarbons (TPH) per kg soil (mg/kg). Columns had concentrations from 9,000 mg/kg to 37,000 mg/kg TPH.
- Water table fluctuations were mimicked by alternating saturated and unsaturated conditions every two weeks. Fluctuations also provided a means to measure dissolved-phase hydrocarbons and degradation products.
- De-aired influent water and gas-tight fittings kept columns anaerobic.
- Columns were plumbed to capture aqueous and vapor effluents for compositional analysis.
- To observe the impact of additional nitrogen, phosphate, and potassium, one column was provided an influent supplemented with these nutrients.
- A carbon mass balance provided molar loss rates as a function of reactor volume and time.
- To observe rates as a function of electron acceptor regime, measurements of electron acceptors, aqueous redox conditions, and off-gas composition were performed during draining events. Measurements were weighed on stoichiometric

ratios for distinguishing between sulfate-reducing and methanogenic degradation products.

- Molar loss rates were plotted versus LNAPL concentration. Statistical analysis was performed to distinguish if rates were linearly dependent upon LNAPL concentration and if regression model slopes were statistically significant from zero.
- To observe for specific compounds including risk-drivers, aqueous-phase spike compounds were resolved through time and compared to measured loss rates.

Objective 2 – Use results from the laboratory studies to forecast the longevity of LNAPL at an actual field site considering NSZD and active remediation.

Hypothesis – Late-stage hydraulic recovery will have limited effect on LNAPL longevity.

The Glide Path Model (GPM) is a developed LNAPL longevity model, which uses zero-order rates for physical processes and an assumed zero-order rate for biological processes. Via an array of loss mechanisms, the model outputs LNAPL longevity.

Supporting activities included:

- Testing of the GPM with a variety of field data and improvement of the biological component of the model with laboratory findings.
- Updated inputs of the GPM for various frequencies of hydraulic recovery. The GPM hydraulic recovery rate was updated to incorporate historical recovery events, periodic recovery, and anticipated frequency of recovery events.
- Site characteristics of a petroleum terminal site were used in a series of model runs. The GPM was calibrated against measured natural loss rates at the field site and LNAPL mass estimates collected approximately ten years apart.

### 1.3. Organization

This thesis is organized into five chapters. Chapter 1 (this section) serves as an introduction. Chapter 2 presents a review of relevant literature. The literature review introduces foundational concepts for the rest of the thesis. Chapter 3 describes methods employed in laboratory studies and field-scale modeling. Results are documented in Chapter 4. Chapter 5 provides a discussion of findings as well as conclusions and recommendations for further work.

## 2. LITERATURE REVIEW

### 2.1. Introduction

Releases of anthropogenic hazardous wastes have been detrimental to water resources, public health and the environment. When in contact with groundwater, water immiscible chemicals, or solvent/fuel mixtures, spilled to the subsurface are referred to as “non-aqueous phase liquid (NAPL)”. NAPLs that float on top of groundwater have densities lighter than water and are referred to as “light non-aqueous phase liquids (LNAPL).” Most commonly, LNAPL compounds are petroleum-based mixtures of hydrocarbons that include compounds with low maximum contaminant levels (MCL) (e.g., benzene MCL = 5 µg/L). Following Amos et al. (2005), Figure 1 presents a site conceptual model (SCM) for a shallow petroleum release undergoing biological mediated losses.

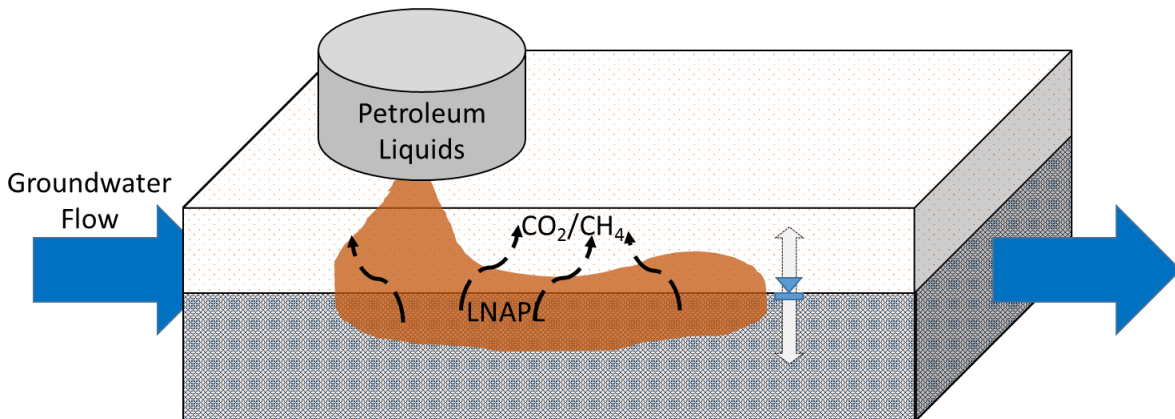


Figure 1– LNAPL SCM following Amos et al. (2005). Groundwater flow is shown with left to right gradient. Water table fluctuation is shown with a vertical two-headed arrow. Biodegradation from LNAPL to CO<sub>2</sub>/CH<sub>4</sub> is shown with an upward dashed arrow as soil vapor flux.

## 2.2. LNAPL Remediation Past and Present

Since inception in December 1970, the Environmental Protection Agency (EPA) has enforced cleanup action, or response action (RA), at hazardous substance and waste storage facilities to mitigate harm to human health and local environments. In 1980, the Comprehensive Environmental Response, Compensation, and Liability Act (CERCLA), commonly known as the Superfund Act, authorized the EPA to enforce RAs at former and active hazardous sites (EPA, 2015).

Active petroleum refining and storage facilities with aboveground storage tanks (ASTs) were early sites requiring RA. In 1995, former petroleum facilities were categorized to EPA's Brownfields and Land Revitalization program initiating subsurface remediation at neglected sites. Title 40 of the Code of Federal Regulation (CFR) Chapter 1 Subchapter D – Water Programs provides directives and guidance for AST compliance and plan of action in cases of a release (GPO, 2016). “Under Title 40 280 (CFR 280), at underground storage tank (UST) sites, where investigations indicate the presence of free product [or NAPL], responsible parties must remove free product to the maximum extent practicable as determined by the implementing agency” (GPO, 2016). In 1988, the EPA estimated approximately two million leaking USTs, or LUSTs, which were affected by CFR 280 (EPA, 2015). State and local agencies more often provided guidance and enforcement of cleanup compliance at UST sites due to regional enforcement and funding.

Most often, RA for releases at AST and UST sites saw early execution of hydraulic recovery via vertical or horizontal wells. At early stages, recovery can be effective because a large fraction of the LNAPL can be present as a continuous phase throughout the soil matrix, creating high LNAPL transmissivity (Newell et al., 1995). Over time, the effectiveness of LNAPL recovery decreased as the remaining continuous LNAPL decreased. Furthermore, groundwater

fluctuations trap LNAPL as discontinuous bodies below the water table, making recovery nearly impossible for portions of the LNAPL. Sites with similar proportions of continuous and discontinuous LNAPL fractions are referred to as “middle stage.” Sites where LNAPL remains primarily in the discontinuous fraction are referred to as “late stage” (Sale, 2016).

In an effort to remediate the discontinuous fraction of LNAPL at middle- and late-stage sites, other physical and/or chemical processes have been employed such as: dig and haul, soil vapor extraction (SVE), groundwater pump and treat (GPT), dual-phase (vapor and water) extraction (DPE), subsurface air-stripping and vapor recovery, surfactant or co-solvent flushing, oxidant injections (i.e., oxygen/ozone/Fenton’s Reagent) (McHugh, 2014). In the early 1990s, biological methods, or bioremediation, became more common and implemented at late-stage sites where dissolved hydrocarbon plumes were of highest concern. Bioremediation as a primary RA for LNAPL remediation had not been considered due to noncompliance with CFR 280. Continued operation of recovery systems was still mandated for enduring discontinuous LNAPL mass.

Recovery system operation and maintenance for small volumes of LNAPL recovery has been highly inefficient and a cost burden to stakeholders. In recent years, a critical need existed to reduce the voluntary and government funding spent on “Low Threat” sites and to shift efforts to higher-priority UST sites. Brownfields and UST sites saw the use of bioremediation technologies or monitored natural attenuation (MNA) as a means of depleting or attenuating dissolved hydrocarbon plumes via biodegradation or soil matrix adsorption (Wilson et al., 2005).

Airsparge, SVE, and bioventing technologies have been implemented at UST sites to promote aerobic degradation of dissolved hydrocarbon enhancing MNA (McHugh et al., 2014). Many of these technologies and RA strategies have been successful at lower priority sites in reducing remaining discontinuous LNAPL or dissolved hydrocarbons (McHugh et al., 2014).

“Low Threat” policies, allowing dissolved and soil hydrocarbon concentrations above regulatory limits, have been adopted by local and state agencies when considering “No Further Action” (McHugh et al., 2014). Some sites have been designated as “Low Threat” because of declining dissolved plumes with and without remedial activities where elevated dissolved concentrations or LNAPL sheens exist (McHugh et al., 2014). However, most MNA site conceptual models did not apply to higher priority LNAPL sites, as MNA typically implemented a model predicting dissolved plume degradation and not LNAPL depletion. A critical need exists to extend the accepted policies and science of MNA to NSZD.

### 2.3. Fate and Transport of LNAPL

The physical structure of porous media and chemical properties of LNAPL dictate hydrocarbon fate and transport in subsurface environments. At early-stage sites, impeding the movement of LNAPL was performed either by physical barriers and/or hydraulic capture. Decreasing mobility and eliminating fugitive hydrocarbon mass transport (i.e., vapor and dissolved) was the purpose of LNAPL recovery, and subsequently groundwater and soil vapor remedial systems. This section discusses the fate and transport of LNAPL within subsurface porous media in relation to remedial objective implementation.

#### 2.3.1. LNAPL as an Intermediate Wetting Phase

Given water-wet media and production of gases from NSZD, NAPLs act an intermediate wetting phase in soil and consolidated material. The order of fluids in porous media is controlled by the polarity of the compound. Typically, the degree of polarity is greatest in soils, then water, then LNAPL, and finally gases. In the absence of soil gases, water typically wets the soil matrix and LNAPL in a non-wetting phase.

Rising water levels often break continuous LNAPL into ganglion LNAPL blobs. Discontinuous LNAPL ganglion blobs will not move out of a pore unless pressure in the LNAPL exceeds the displacement pressure of the water in the porous media. In model aquifer sand tank experiments, Dobson et al. (2007) and Skinner (2013) both showed that water-table fluctuations led to an increased vertical extent of LNAPL source zones compared to stable model aquifers. Dobson et al. (2007) measured an increased source zone extent by a factor of 6.7. The same factor also increases LNAPL surface area proportionately, allowing more water to contact LNAPL mass (Dobson et al., 2007). LNAPL surface area is a controlling factor in physical NSZD by dissolution and volatilization (Skinner, 2013).

Hydraulic recovery reduces LNAPL thicknesses and saturations, generally making LNAPL recovery more difficult. A lingering concept behind hydraulic recovery has been that continual operation will eventually remove nearly all LNAPL mass. However, after LNAPL recovery was thought complete, immobile fractions remained at the source zone due to residual LNAPL saturation (Singh, 2004). Middle- and late-stage sites exhibit reduced LNAPL transmissivity as compared to early-stage sites. Severely reduced LNAPL transmissivity arises when the majority of LNAPL was left at residual saturation. Late-stage intermittent LNAPL mobility occurs as a consequence of coalesced discontinuous ganglion blobs exceeding displacement pressures of water. These conditions arise when water saturation falls below the critical pore pressure, retaining the ganglion blob, typically produced from either hydraulic recovery or a natural increase to groundwater gradient. Determining optimum conditions for LNAPL transmissivity often involved extensive soil core petrophysical data and extended potentiometric surface monitoring. Soil heterogeneities, in combination with variant LNAPL distribution, complicated determination of precise LNAPL transmissivity over time (Huntley et al., 2002). Because the discontinuous LNAPL at middle- and late-stage sites cannot be effectively removed by hydraulic recovery, the development of alternative remediation approaches are needed.

### 2.3.2. LNAPL Partitioning

Petroleum is composed of many different hydrocarbon compounds including non-polar long-chain alkanes or aromatics. Non-polar hydrocarbons tend to repel water molecules largely remaining in the initial phase (NAPL) or volatilizing. Polar hydrocarbons, containing carboxyl groups associated with biodegradation, partition into water more readily due to ionic attractions from water molecules. Benzene, Toluene, Ethylbenzene and Xylenes (BTEX) are primary compounds of concern for risk assessments, due to relatively high solubility and potential risks to human health. Partitioning of hydrocarbons between nonaqueous, aqueous, sorbed, and vapor phases governs subsurface mobility and biological availability of hydrocarbon for biotic depletion.

Characterizing potential areas of high hydrocarbon mass is often an objective of site RAs. Several physical laws describe how hydrocarbons partition in a subsurface environment. Raoult's law dictates the solubility of a specific hydrocarbon to dissolved phase as a function of mole fraction, often referred to as the "effective solubility." Henry's law dictates equilibrium water and vapor concentration as a function of temperature and pressure. A Freundlich isotherm predicts the amount of hydrocarbon adsorbed to a soil. Freundlich adsorption coefficients may be assumed either theoretically calculated or experimentally estimated (Schwarzenbach, 2003). Hydrocarbon adsorption often takes place at external soil particle organic surfaces, commonly referred to as the "organic content" of soil. Clay and silt soils typically have higher organic content than coarse sands and gravels, thus creating areas of high hydrocarbon adsorption. A retardation factor is often used in transport theory to express the affinity for a specific compound to the soil matrix. Retardation factors are often analytically derived or listed in environmental databases (Schwarzenbach, 2003). These laws and characteristics predict LNAPL fate and transport in the subsurface and lay foundations for LNAPL conceptual site models.

### 2.3.3. LNAPL Subsurface Transport

Phase partitioning dictates the movement of LNAPL into different physical phases; yet subsurface hydrocarbon transport is controlled by pressure gradient, transmissivity and permeability. Pressure gradients dictate the direction and velocity at which hydrocarbons are transported as well as latitudinal and longitudinal advection. SCMs often provide site hydraulic gradient measurements to assess the typical direction of LNAPL and dissolved hydrocarbon transport. Transmissivity is proportional to porous media tortuosity and hydraulic conductivity (Domenico, 1990). Gravels and sands often have high transmissivity whereas silts and clays regularly have low transmissivity. Measuring the permeability of silt and clay lenses has helped in assessing potential fate of hydrocarbon mass as dissolved or adsorbed, but it is often the case of SCMs to pinpoint highly transmissive zones and general groundwater direction.

A primary focus is contaminants of concern (COC) that have been classified as carcinogenic or possible carcinogens and readily transported in a dissolved or vapor phase. A COC like MTBE, with a common retardation factor of 1.0, less readily adsorbs to soil particles, and thus transport velocities are very similar or the same as groundwater velocity. When MTBE replaced lead in the late 1990s as a gasoline additive, petroleum UST sites had risk levels elevated due to potential hazards from rapid MTBE downgradient migration in anaerobic aquifers (EPA, 2015). On the other hand, n-hexacosane is highly hydrophobic and will be retarded near the source area by an inherent affinity to organic content. However, n-hexacosane still poses a possible carcinogenic risk to direct soil contact such as during utility construction that often occurs in redevelopment of former UST sites. Both compounds, while posing risks to different receptors, still pose an overall risk. Therefore, SCMs must accurately delineate specific routes of exposure and associated risk lifetimes as provision of stakeholder due diligence.

Projecting LNAPL weathering effects has been a primary objective of conceptual site model updates. Petrophysical characterization of field LNAPL mole fractions have provided estimates of maximum (i.e source zone) hydrocarbon concentration in water or vapor phase. During weathering processes, greater amounts of lighter, more soluble hydrocarbons flux from LNAPL to water or air than less soluble hydrocarbons as a function of effective solubility. COCs like benzene and MTBE often are used in transport models due to high risk level. A common position is that early-stage dissolved TPH composition may be significantly different from late-stage composition. As a consequence, recalcitrant LNAPL compounds are left behind prolonging environmental risk. The magnitude of COC levels above MCLs determines a site's risk category (i.e., government-mandated or voluntary program). Immediate COC risks may have been addressed in early stage, but at late-stage sites, residual LNAPL and recalcitrant compounds often extend remedial actions and monitoring under government mandated RAs. Understanding specific COC persistence under anaerobic, NSZD conditions is critical for accurately projecting site risk level.

## 2.4. Biological Degradation

This section discusses factors controlling degradation of hydrocarbons in subsurface environments under anaerobic conditions.

### 2.4.1. Source Zone Microbiology

Depletion of discontinuous LNAPL is primarily controlled by rates of biologically-mediated degradation. Anaerobic environments often dominate in LNAPL impacted media. Large oxygen demand from LNAPL often leads to depletion of available electron acceptors and methanogenic conditions that reflect reduced groundwater conditions. A secondary objective of SVE, or airsparging, has been to transition these anaerobic environments to more energetically favorable aerobic conditions. This remediation strategy is often referred to as "enhanced MNA."

However, this remedial action is energy and labor intensive. Thus, understanding anaerobic biodegradation rates of LNAPL through time is critical.

The microbial ecology of a source zone may be heavily dictated by soil types, vadose zone depths, electron acceptor abundance, and LNAPL composition (Irianni Renno et al., 2015). Microbial NSZD degradation rates are dependent upon bioavailability of substrates, ambient temperature (Zeman et al., 2014), and biofilm endurance (Zysset et al., 1994). Biofilm endurance is dependent upon shear stresses created by groundwater (Zysset et al., 1994). Fine soils may harbor greater populations of hydrocarbon-degrading microbes due to high organic content and slow groundwater velocities (Anneser et al., 2008). These zones however may be functionally separated from contaminants in groundwater flow paths due to low hydraulic conductivity and low permeability (Zysset et al. 1994).

While petroleum compounds are often hydrophobic, more soluble compounds persist beyond source areas. Persistence of hydrocarbon is a critical issue at middle- and late-stage sites. Initially, native microbial populations may not readily degrade COCs, but over an acclimation phase, the COC may become a utilized substrate (Alexander, 1994). An acclimation phase may be days, weeks, or months. Acclimation may involve a change to biofilm structure (Alexander, 1994), the production of bio-surfactants or production of specific enzymes (Zysset et al., 1994). Temperature, initial contaminant concentrations, and oxidation-reduction conditions are controlling factors of acclimation phases (Alexander, 1994). Other causes of COC persistence may be a negative consequence of toxicity, or diauxie within native microbial communities. The term “diauxie” describes microbial preferential metabolism of substrates promoting faster growth, and once depleted, microbes begin metabolism of the next preferred substrate (Alexander, 1994). Simply, the microbial communities nearest source areas may rapidly deplete paraffins (long-chain petroleum alkanes) while refusing more energy intensive compounds that

are coincidentally high risk COCs. Understanding how acclimation phases affect overall NSZD rates and LNAPL longevity is critical for modeling NSZD rates.

A concept behind site bio-augmentation strategies was to introduce known, or laboratory-cultured, hydrocarbon-degrading microbial populations to enhance degradation of specific COCs. Identifying hydrocarbon-degrading bacteria at multiple sites provided a foundation for early use of MNA as a primary site remedy (Wilson et al., 2005). When addressing NSZD in middle-and late-stage LNAPL sites, conceptual site models may assume hydrocarbon-degrading microbes are present (Skinner, 2013). Dominating a subsurface with a toluene-degrading species via bio-augmentation could be beneficial to a toluene-solvent release site as the contaminant is readily degraded. The multiple constituents encountered at petroleum sites would be bypassed by this single organism system and greatly inefficient. Additionally, survival and growth of organisms cultured ex situ and used for bioaugmentation are often limited. Furthermore, practitioners have steered away from bio-augmentation commonly due to its high implementation costs and inability to deliver precisely and maintain engineered communities. Understanding native community structure within anaerobic NSZD environments is critical for projecting biodegradation rates over time and LNAPL depletion.

Microbial DNA soil-core data show the abundance of many different hydrocarbon-degrading species that require substantially different energy for completing degradation (Irianni Renno et al., 2015). The relative abundance of species explicitly having enzymatic reactions with BTEX compounds are highly desired within a source zone (Irianni Renno et al., 2015). For example, abundant source zone organisms *Gammaproteobacteria*, *Methanomicrobia* and *Methanobacteria* have been linked with hydrocarbon degradation, achieving increased rates with increasing subsurface temperature (Zeman et al., 2014). While these organisms are often within the same anaerobic environments, substantially different Gibbs free energy is required to perform degradation (Stockwell, 2015). Evaluating specific kinetic rates for each identified

hydrocarbon-degrading species within a source zone is tedious and resource intensive. A reduction in resources is required to provide an approximate site NSZD rate for predominant microbial processes.

#### 2.4.2. Biological Degradation as a Function of Environmental Conditions

Contemporary site conceptual model consensus has been that increasingly reduced conditions lessen hydrocarbon degradation kinetic rates (Tracy, 2015). Anaerobic kinetic rates, such as sulfate-reducing and methanogenic rates, have been shown to be an order of magnitude slower than aerobic kinetic rates in homogenous microcosm studies (Alexander, 1994; Singh, 2004). Common MNA electron acceptors sampled at source zone monitoring wells and soil samples have been nitrate, sulfate, and ferric iron (Johnson et al., 2006). Ferrous iron (dissolved iron) levels compared at upgradient and downgradient locations also provide information on iron-reducing conditions from source zones. Increasingly reduced conditions arise from electron acceptor consumption, such as the depletion of dissolved sulfate leading to methanogenesis. The relative abundance, or absence, of electron acceptors may indicate a predominant electron acceptor couple. Thus, monitoring electron acceptor (e.g., anion analysis) can be critical for understanding anaerobic NSZD rates.

Nutrient and electron acceptor availability in source zones has shown to be a critical factor for identifying leading microbial degradation processes (Johnson et al., 2006). Following Stockwell (2015), steady-state subsurface nutrient cycling occurs through biomass decay. Surface nutrient leachate coupled with degradation by-product attenuation may also be assumed at steady-state for typical source zones (Zysset et al., 1994). Seasonality may influence microbial kinetics as nutrient sources and source zone temperature may transition (Coulon et al., 2005; Zeman et al., 2015). Some RAs have included in-situ nutrient mixture injections or surface application of nutrient amendments, such as a leachate. Previous experiments (Adetutu et al., 2013; Ferguson

et al., 2003; Joo et al., 2001; Sanscartier et al., 2009; Schiewer et al., 2006) were widely varied in hydrocarbon degradation to nutrient addition. Nutrient- loading duplication varied significantly in an aerobic microcosm study showing limited degradation rate dependence (Joo et al., 2001). An anaerobic column study by Chou et al. (2008) observed impairments to syntrophic degradation processes of sulfate-reducing and methanogenic communities with increased nutrient loading. Identifying if NSZD is a function of nutrient loading is critical.

Populations of subsurface microbes have been shown to be dependent upon pH and oxidation-reduction potential (ORP) (Alexander, 1994; Annesser et al., 2008). A late-stage site's source zone microbial characterization showing diversity was greatly influenced by the depth below ground surface, electron acceptor oxidation states (redox conditions), proximity to the water table and/or oxygen influx zones (Irriani Renno et al., 2015). Sulfate-reducing bacteria, such as *Desulfovibrio alcoholivorans* and *Desulfotomaculum acetoxidans* DSM 771, were shown to grow in ORP environments of -400mV, well within the range of a typical anaerobic source zones (Chang et al., 2014). Specifically, Chang et al. (2014) demonstrated sulfate-reducing bacteria diversity as a function of suspension and attached biofilms as well as ORP changes from -400 mV to -180mV. Interconnected lithological zones with ORP varying as much as 200 mV within centimeters have been observed in an tar-oil contaminated aquifer (Annesser et al., 2008). Radically different ORP environments create a range of degradation processes, which increases source zone degradation complexity. There was a critical need to understand how NSZD rates depend on predominant biological processes as a function of anaerobic environmental conditions.

## 2.5. Measuring Field Rates of Natural Losses

Singularly measuring mobile LNAPL illustrates the physical or natural depletion of only the continuous LNAPL fraction. Incomplete soil core recovery and loss of fluids during sample

retrieval can hinder accurate LNAPL saturation and mass estimates. A variety of methods and instruments have been used to measure carbon flux from LNAPL bodies. Established flux paths, as pointed out in Figure 1, define where boundary measurements may be taken. The ground surface acts as a flux boundary for carbon flux in the gas phase. Transmissive zone cross-sections act as a flux boundary for carbon flux in the aqueous phase. Multiple theories and methods for estimating natural degradation of hydrocarbons have been developed. For example, Amos et al. (2005) used the mass flux of nitrogen, argon, and methane in and out of source zones to estimate source zone degradation rates. Also, Johnson et al. (2006) proposed using source zone electron acceptor uptake as a proportional indicator of estimating natural degradation of LNAPL. Modified carbon flux measurements have provided natural loss rate estimates for total LNAPL, and importantly, these measurements account for all biodegradation processes (e.g., aerobic, sulfate-reducing, and methanogenic).

Biologically degraded hydrocarbons ultimately are converted to carbon dioxide, and thus, measurements of carbon dioxide at grade can be used to estimate hydrocarbon loss rates (Amos et al., 2005). Soil and crop scientists, primarily in environmental service and agricultural industries, have deployed carbon flux devices, both in-situ and ex-situ, for estimating soil respiration rates. Devices such as carbon dioxide traps (McCoy et al., 2014) and dynamic flux chambers (LI-COR Inc., Lincoln, Nebraska) have been implemented for measuring NSZD rates independent upon continuous or discontinuous fractions (Tracy, 2015). Alternatively, carbon gas-phase gradients, as either carbon dioxide, methane, or VOCs, have been measured with soil vapor probes and converted to carbon flux (Amos et al., 2005; Lundegard et al., 2006). Soil heterogeneities increasingly diminish the precision of not only singular measurements but repeated monitoring events (Tracy, 2015). Measurement accuracy was a function of defined geometric faces perpendicular to carbon flux (Tracy, 2015). These faces may range from simple rectangles to interpolated cross-sections established by soil core investigations. Deploying

carbon flux devices and methods requires highly detailed information of soil lithology for correctly estimating NSZD rates.

More recently, NSZD thermal monitoring was developed by Stockwell from Colorado State University (Stockwell, 2015) where NSZD was shown to be a function of the heat of reaction associated with mineralization of TPH compounds. Hydrocarbon mineralization is exothermic, and thus, complete degradation produces a measurable thermal signature. Thermodynamic models have been used to convert this thermal signature to a loss rate (Stockwell, 2015). Monitoring vertical thermal gradients from biodegradation of LNAPL produced values for the heat of reaction, while assuming subsurface thermodynamic properties such as natural decay of organic matter. In anaerobic zones, the majority of the heat is released during methane oxidation rather than hydrocarbon conversion to methane. Thus, thermal gradients must be accurately measured in methane oxidation zones. Furthermore, delineating native soil respiration from NSZD is crucial for appropriately estimating carbon flux directly related to the degradation of hydrocarbons. This background carbon flux must be subtracted from source zone carbon flux to estimate the carbon originating from contaminants.

Natural loss rates have been shown to be spatially variable due to subsurface heterogeneity. Combining various in-situ methods potentially increases accuracy of LNAPL loss rates. As shown in McCoy et al. (2014), carbon flux measurements were observed to fluctuate between 1,000 L/hectare/yr to 10,000 L/hectare/yr of naturally degraded LNAPL (rate units use benzene as LNAPL representative compound) at multiple sites. Lundegard et al. (2006) observed a range of degradation rates from 17,120 L/hectare/yr and 125,570 L/hectare/yr at a singular site. Understanding whether NSZD rates are strongly dependent upon anaerobic process is critical to delineate NSZD measurement distributions.

## 2.6. Modeling of LNAPL Longevity and Natural Losses

LNAPL longevity can be made by using differential transport equations for source zone LNAPL mass and then solving for time when remaining LNAPL equals zero. Persistence of select hydrocarbons in dissolved plumes was most often considered a function of source zone mass, as described by models from Borden et al. (1992), Dobson et al. (2007), Huntley et al. (2002) and Miles et al. (2008). Compounds that both exhibit relatively high solubility and potential risks to human health, such as MTBE and benzene, have been given greater attention in these models. Precisely predicting COC migration and risk was inherent to an accurate source term. Validating zero- or first-order NSZD is critical for accurately predicting site risk.

Source zone models, such as those presented by ASCE (1996) and Huntly et al. (2002), were primarily concerned with mass transport processes and the environmental health affects posed to aquifers and vadose zone concentrations. The LNAPL Distribution and Recovery Model (LDRM) was developed by the American Petroleum Institute (API) to simulate LNAPL recovery performance. LDRM results have been widely used in practice for evaluating RAs at early-, middle- and late-stage LNAPL sites. Model parameters incorporate site-specific petrophysical data as well as Darcy's Law for simulating LNAPL movement and recoverability of continuous fractions. While the LDRM produces recovery system effectiveness, SCMs should also account for longevity of residual LNAPL (i.e., discontinuous fractions) that still pose a risk to aquifers and potential receptors. Furthermore, the accuracy of longevity estimations is dependent upon proper inclusion of diminished LNAPL removal via hydraulic recovery.

A novel LNAPL longevity predictive model (referred to as the Glide Path Model (GPM)) was developed by Skinner from Colorado State University (Skinner, 2013) as a decision tool for predicting LNAPL source zone longevity. A series of single-component LNAPL (MTBE) sand tank experiments were used to develop LNAPL dynamic properties for a variety of site

conditions (Skinner, 2013). The sand tank experiments verified LNAPL physical NSZD processes were dependent upon LNAPL pool surface area and not mass. A quantitative study of pool dynamics validated active remedies, such as hydraulic recovery and SVE, have first-order reaction rates (Sale, 2001) dependent upon continuous LNAPL fractions remaining. Kim et al. (2002) developed similar models describing volatilization and dissolution of LNAPL on the groundwater table. Furthermore, as previously stated in Reddi et al. (1998), water table fluctuations effected distribution of LNAPL between continuous and discontinuous fractions, which ultimately controlled LNAPL mass loss rates. Discontinuous, un-recoverable LNAPL fractions appearing as ganglion blobs increased with fluctuations (Reddi et al., 1998). With respect to dissolution data, observations were in parallel with Dobson et al. (2007), showing exponential decay when remaining LNAPL had reached critical mass (i.e., total dissolved phase outweighing LNAPL fractions).

Early- stage LNAPL longevity estimates rely on physical and/or chemical remediation rates as the predominant depletion rate. At late-stage sites, where operation of recovery systems often becomes intermittent, accurate depletion rates of discontinuous fractions through NSZD are required. Models have assumed Monod or first-order kinetics for biodegradation rates (Huntely et al., 2002; Dobson et al., 2007) implying degradation was dependent upon LNAPL mass. However, the observation of equivalent NSZD rates at middle-and late-stage sites, shown in McCoy et al. (2014), suggests inconsistencies with established kinetic rates. Hydrocarbon concentrations vary between middle and late-stage field sites, but data suggests loss rates do not. This field data indicates loss rates may follow zero order kinetics (i.e., rates are independent of LNAPL concentrations). Validating zero-or first-order biodegradation kinetics for anaerobic NSZD processes is an essential element for accurate estimates of LNAPL longevity.

### 3. METHODS – LABORATORY STUDIES AND FIELD-SCALE MODELING

The following section presents methods for an 11-column laboratory study and a LNAPL longevity modeling effort.

#### 3.1. Column Setup and Operation

Section 3.1.1 describes the laboratory column experiment. A total of 11 columns were evaluated with the primary experimental variable being LNAPL saturation.

##### 3.1.1. Column Setup

Eleven tempered-glass columns were utilized. Columns were 61 cm by 41 mm ID (ACE Glass Inc., Vineland, NJ). The bottom of the columns included an ASTM 7-100 $\mu$  glass filter leading into a reduced 0.64-cm end (Figure 2). Viton® chemical-resistant tubing (3.2 mm ID & 6.5 mm ID, MasterFlex®, Vernon Hills, IL) connected columns to glass, water lines (2.5 mm ID). The experimental setup follows Borden et al. (1992). Plastic hemostats acted as valves at glass and tubing connections. Cut- and bent-glass lines (2.5 mm ID) ran from the top of the columns through rubber stoppers into an inverted 250-mL graduated cylinder. The graduated cylinder was suspended in a water reservoir to exclude air. The graduated cylinder facilitated measuring volumes of produced gases, gas sampling, and removal of excess produced gas.

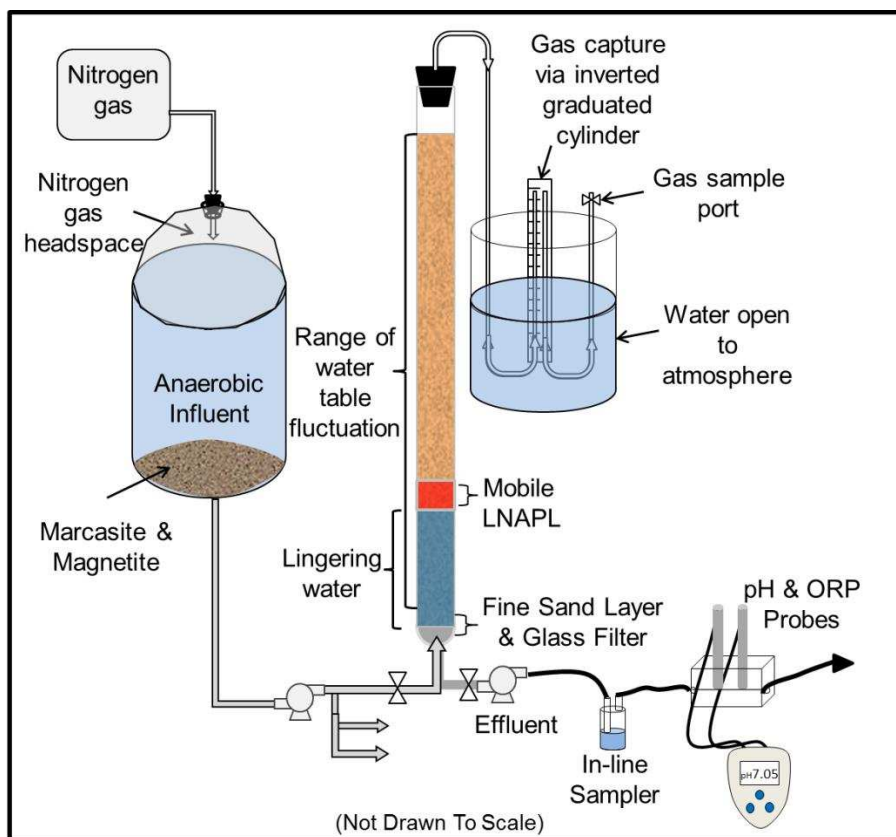


Figure 2 – Column setup diagram: a simplified representation of the experiment for a single column. Ten more columns and three more carboys were attached in this system.

Four 20-L glass carboys were setup in series to provide anaerobic influent water. Influent water was sourced from Fort Collins municipal tap water. Buffering capacity was increased by adding ACS grade sodium bicarbonate (CAS 144-55-8, EMD Chemicals Incorporated Gibbstown, NJ), resulting in an alkalinity of approximately 90 mg/L calcium carbonate and pH of 7.5. The influent was de-aired under 20 in Hg for approximately 2 hours per 20 L. Marcasite ( $\text{FeS}_2$ ) granules (0.06-0.19 in diameter) (CAS 1309-36-0, Alfa Aesar, Ward Hill, MA) and magnetite ( $\text{Fe}_3\text{O}_4$ ) powder (CAS 1309-38-2, Alfa Aesar, Ward Hill, MA) were then added as oxygen scavengers in the last carboy at 125 mg/L each, resulting in solid-phase marcasite and the presence of magnetite in the last carboy in the series throughout the experiment. The oxidation-reduction potential (silver-silver chloride) of influent water was poised between 0 mV and -20 mV throughout the experiment. Sulfate concentrations were adjusted to 15 mg/L ( $1.6 \times 10^{-4}$  M) using

sodium bisulfate monohydrate (CAS 10034-85-5 Fisher Scientific Fair Lawn, NJ), to prohibit substantial dissolution of marcasite and magnetite at the beginning of the experiment and calculated from Lindsay (1979). An interchangeable 20 L Tedlar® (Environmental Sampling Supply, Houston, TX) bag of nitrogen was attached to prevent oxygen from being present in the influent water when headspace was displaced during draining events. Carboys were elevated to maintain positive head pressure on all lines. Influent water was pumped into the columns via peristaltic pump (REGLO Digital, Model IS-1B, ISMATEC™, Glattbrugg, Switzerland) and Viton® tubing manifolds. At approximately 180 days, oxygen intruded into the water supply cascade from a small leak at the rubber stoppers, and influent sulfate concentrations increased to approximately 20 mg/L.

Field soil was excavated from a former petroleum refinery in the western United States, which has been inactive for 20 years. Soil was from an LNAPL smear zone, approximately 1.8 m to 2.4 m below ground surface (bgs). The soil was a quartz feldspar sand moderately sorted, medium to coarse with some fine gravel and trace fines. Soil color was reddish brown. After field collection, soil was immediately placed in five-gallon buckets, purged with nitrogen gas, and sealed with a 40-L Tedlar® bag (Environmental Sampling Supply, Houston, TX). Soil was kept at -20°C until needed for the experiment. A homogenized sample of moist soil had a hydrocarbon concentration of approximately 9,000 mg/kg TPH.

Field LNAPL was bailed from an on-site recovery well. LNAPL density was measured at 0.73 g/mL via a 10mL graduated cylinder and scale ( $\pm 0.01$  g). LNAPL was diluted to 1:25 in n-hexane ( $\geq 99\%$  CAS 110-54-3, Alfa Aesar, Ward Hill, MA) and analyzed using a gas chromatograph (GC) with a mass selective detector (MS) (Agilent Technologies 6890N GC & 5973 MS, Santa Clara, CA) for compositional analysis. One  $\mu\text{L}$  of solution was injected into an Rtxi-624Sii column (30 m L x 250  $\mu\text{m}$  I.D., Restek®, Bellefonte, VA). Inlet temperature was 250 °C. Initial oven temperature was 40 °C for three minutes, ramped at 15 °C per minute to 325 °C

and held for one minute for total run time of 23.0 minutes. LNAPL consisted primarily of naphthalene and long-chain alkanes between C<sub>14</sub> and C<sub>26</sub>. Field LNAPL was spiked with benzene (ACS grade, CAS 71-43-2, EMD Chemicals China), naphthalene (99.6% CAS 91-20-3 Alfa Aesar Ward Hill, MA), n-dodecane (≥99% CAS 112-40-3, Sigma-Aldrich, St. Louis, MO), n-tetradecane (≥99% CAS 629-59-4, Aldrich St. Louis, MO), and n-hexacosane (CAS 630-01-3, Sigma-Aldrich, St. Louis, MO) at 1.5 times the original LNAPL concentrations, such that these spiked compounds were identifiable over other compounds. LNAPL was kept at 5 °C until needed for the experiment.

Soil was prepared in an anaerobic chamber. Field soil was first homogenized and sieved to remove medium and large gravel. Subsamples of the homogenized field soil were spiked with predetermined volumes of modified field LNAPL to produce approximately 1,000 g samples. A column was homogenized field soil at 9,000 mg/kg without the addition of spiked LNAPL. A column contained washed and autoclaved silica-quartz sand (20-40 sieve size) mixed with spiked field LNAPL (same amount of LNAPL as nutrient addition column) at a concentration of 17,000 mg/kg. Soil TPH was analyzed before and after the spiked LNAPL addition. A fine sand layer was added above the glass filter to limit mobile LNAPL from leaving the columns (Figure 2). Columns were filled with soil to approximately 10 cm below the rims. The total weight of soil loaded into the columns ranged from 1.1 to 1.3 kg. TPH concentrations are presented in Table 1. An additional column was prepared at 27,000 mg/kg to investigate the impact of nutrient addition.

Table 1– Initial TPH concentrations of the 11-column laboratory study

---

9,000 mg/kg (no LNAPL added)
17,000 mg/kg
19,000 mg/kg
22,000 mg/kg
25,000 mg/kg
27,000 mg/kg x2
29,000 mg/kg
32,000 mg/kg
35,000 mg/kg
37,000 mg/kg

---

Nutrient addition as an NSZD enhancement strategy was investigated using the additional TPH concentration of 27,000 mg/kg. The nutrient solution consisted of ACS-grade ammonium chloride (CAS 121125-02-9, Fisher Scientific, Fair Lawn, NJ) and ACS-grade potassium phosphate monobasic (CAS 7778-77-0, Fisher Scientific, Fair Lawn, NJ). Nutrient addition followed a carbon:nitrogen:phosphate:potassium (C:N:P:K) ratio of 100:10:2:1. This ratio equated to a mass loading of approximately 37.2 g/L ammonium chloride and 47 g/L potassium phosphate per saturating event. Ammonium chloride added nitrogen nutrients in the reduced form as to prevent undesired effects to redox conditions (Schiewer et al., 2006). A precision syringe pump (Fusion 100, Chemyx, Stafford, TX) delivered nutrients with the anaerobic influent at a combined flow rate of 13.5 mL/min to achieve a TDS concentration of approximately 84,000 mg/L.

### 3.1.2. Column Operation

To mimic seasonal groundwater table fluctuations and discharged reaction by-products, water levels were raised and lowered on a two week basis. Column operation was performed over the course of 411 days. A total of 14 water cycles were conducted in this study. Columns were kept in a dark room at 20°C ± 1°C for the entirety of the experiment. Effluent water samples were

taken during draining events. Gas samples were taken before saturating and draining events. Once methanogenesis commenced, produced gas was removed prior to an event to prevent gas capture volumes from exceeding the 250 mL capacity of the inverted graduated cylinders (Figure 2). Complete operational details can be found in Appendix A.

During saturating events, a peristaltic pump (REGLO Digital, Model IS-1B, ISMATEC™, Glattbrugg, Switzerland) controlled influent flow rate. Flow rate was  $13.5 \pm 0.5$  mL/min. Influent water lines were flushed of stagnant water before saturating events. Flushing purged air that may have intruded at bends and connections between events. Pumping was terminated once water levels in the column rose to the top of the soil. Total influent water volume and gas displacement were recorded.

During draining events, a peristaltic pump (REGLO Digital, Model IS-1B, ISMATEC™, Glattbrugg, Switzerland) drew water through tubing (2.54 mm ID, MasterFlex®, Vernon Hills, IL) into a custom inline water sampler followed by a custom flow cell with water quality probes (Figure 2). Effluent flow rate began at 10 mL/min and decreased to 5 mL/min as head pressure decreased within the column. Cavitation would occur in the tubing if pump speed was increased. Two trace-clean 20-mL headspace vial (actual volume 21.4 mL, Restek®, Bellefonte, PA) in-line water samples were collected from middle sections of the columns (Figure 2). PH and oxidation reduction potential were measured during sampling every 10 mL to assume that a representative sample was collected and to resolve redox conditions. A water sample was collected after readings fluctuated less than 0.5% of prior reading. Samples had no headspace and were capped with an aluminum silver PTFE septum cap (Restek®, Bellefonte, PA). Excess water from draining (purged water) was placed in trace-clean 40-mL volatile organic analyte (VOA) vials (VWR, Radnor, PA). In most events, draining was ceased once the water level in the column had reached the fine-sand layer at the base of the column. Methane gas was removed at water cycling events from columns, producing greater than 100 mL of total gas.

Some draining events were ceased when gas capture volumes reached lower limits ( $\leq 20\text{mL}$ ). Total water volume discharged and final gas capture volume were recorded.

### 3.2. Analytical Methods

The following section describes analytical methodology used in this study for the quantification and resolution of anaerobic NSZD processes. Details of exact calibration concentrations can be found in Appendix B.

#### 3.2.1. Soil Total Petroleum Hydrocarbon Analysis

Soil samples were analyzed for TPH via a methanol extraction. For initial soil samples, approximately 20 g of homogenized soil was added to 20 mL HPLC grade methanol (CAS 67-56-1, Fisher Scientific, Fair Lawn, NJ) in a 60 mL jar. Upon homogenization and sieving, allocated sample mass amounts were less than expected and did not completely fill sample jars. Therefore, for analysis of final samples, approximately 50 g of soil and 40 mL of methanol were added to avoid excess headspace. Soil samples were vigorously shaken on a vortex for approximately one hour and then allowed to settle. Extracts were diluted in 2-mL GC vials at a 20 times dilution factor.

A 10- $\mu\text{L}$  syringe attached to an autosampler injected a one  $\mu\text{L}$  sample into a GC (Agilent Technologies 6890N, Santa Clara, CA) with a Rtx-5 column (30 m L x 320  $\mu\text{m}$  ID, Restek<sup>®</sup>, Bellefonte, VA) paired with a flame ionization detector (FID). Helium was the carrier gas at 3.5 mL/min. Injector temperature was 250  $^{\circ}\text{C}$ , and detector temperature was 300  $^{\circ}\text{C}$ . The temperature program was as follows: 40  $^{\circ}\text{C}$  for three minutes, 10  $^{\circ}\text{C}/\text{min}$  ramp to 120  $^{\circ}\text{C}$ , 20  $^{\circ}\text{C}/\text{min}$  ramp to 300  $^{\circ}\text{C}$ , and then 300  $^{\circ}\text{C}$  for three additional minutes. The carrier gas split ratio was 1:1. TPH detections were calibrated with EPAWISC gasoline range organics (GRO) and

diesel range organics (DRO) mixtures (Restek®, Bellefonte, PA) in the range of 0.005 g/L-methanol to 0.9 g/L-methanol and 0.10 g/L-methanol to 5.0 g/L-methanol, respectively.

At the completion of this study the nutrient influent column was drained and taken offline, then immediately placed in a -40°C freezer. Once frozen the soil core was extruded from the column under an anaerobic environment. The column soil was divided into five soil samples. Soil grab samples from each section were placed in pre-weighed 50 mL jars with methanol and placed in a -20°C freezer as performed at the beginning of the experiment. Upon analysis, soil samples were shaken for 30 mins and the methanol was analyzed using the soil analysis method stated earlier. Solvent dilution ratios were balanced between accuracy and spike compound peak resolution at 20:1. Sample analysis resolution was on the order of 100 mg/kg TPH. After reviewing final ultraviolet photography, the upper 10 cm and lower 10 cm grab samples of the column were shown to have an appreciable draining and accumulation of mobile LNAPL, respectively. Therefore, to represent homogenized LNAPL pores saturations only the three mid-section post-experiment grab samples were used for comparison purposes.

### 3.2.2. Aqueous Hydrocarbons and Carbon Dioxide Analyses

Equilibrium headspace concentrations were used to quantify dissolved volatile organic compounds (VOCs) and gases similar to Kampbell et al. (1998). A solvent extract was used for non-volatile DRO. A 5-mL headspace was induced on in-line water samples by removing water while attached to a Tedlar® bag of nitrogen gas (>99.5% Nitrogen gas, Airgas, Fort Collins, CO). The sample was lightly shaken for 30 minutes, and set upside down for 15 minutes to reach equilibrium before analyzing. Headspace gas was injected with a gas-tight syringe (50 µL) in two separate GCs. For DRO, the second in-line water sample was injected with two milliliters of HPLC grade n-hexane (≥99% CAS 110-54-3, Alfa Aesar, Ward Hill, MA), displacing water through an adjacently inserted needle, and shaken for approximately 45 minutes.

For VOC analysis, the same GC/FID (Agilent Technologies 6890N, Santa Clara, CA) as soil TPH analysis was utilized for VOCs and methane < 0.1 mg/L. Injector temperature was 250 °C, and detector temperature was 300°C. The temperature program was as follows: 40 °C for one minute and then 10 °C/min ramp to 78 °C for total runtime of 5.8 minutes. Two separate five-point calibrations were performed for VOCs and methane. VOC stock solution (250 mg/L total VOCs) was an aqueous mixture of equal parts n-hexane (≥99% CAS 110-54-3, Alfa Aesar, Ward Hill, MA), benzene (ACS grade, CAS 71-43-2, EMD Chemicals China), toluene (CAS 108-88-3, Fischer Scientific, Fairlawn, NJ), ethylbenzene (≥99%, CAS 100-41-4, Tokyo Chemical Industry, Tokyo, Japan), and xylenes (CAS 1330-20-7, Fischer Scientific, Fairlawn, NJ). Headspace free vials (20-mL, Restek, Bellefonte, VA) of distilled water were injected with volumes of VOC standard solution for concentrations between 0.5 and 45.0 mg/L VOCs, and shaken for 30 minutes. A 5-mL nitrogen headspace was induced, and vials were allowed to reach equilibrium before analysis. For methane < 0.1 mg/L, a gas mixture of 5% carbon dioxide and 5% methane, and 5% nitrogen, balance of helium gas (Restek, Bellefonte, VA), was diluted with nitrogen gas between 0.05% and 0.5% methane.

A Hewlett Packard 5890 Series II Gas Chromatograph paired with a Thermal Conductivity Detector (GC/TCD) measured dissolved methane (> 0.1 mg/L) and carbon dioxide. The GC/TCD had a Q-Bond 80/100 packed column (30 m L x 530 µm ID, Restek, Bellefonte, VA). Both injector and detector temperature were 110 °C. Oven temperature was constant at 40 °C for four minutes with helium carrier gas at 50 mL/min. The same gas mixture as for methane < 0.1 mg/L was diluted with nitrogen gas for a four-point calibration between 0.5% and 5% of methane and carbon dioxide.

Degradation products (methane and carbon dioxide) aqueous concentrations were determined using the following equilibrium and mass balance equations.

$$H_j = \frac{p_j}{C_{aqj}} \quad [\text{Eq. 1}]$$

$$p = \frac{nRT}{V} \quad [\text{Eq. 2}]$$

$$C_{aqj} = \frac{\frac{n_j}{V_g} * R * T}{H_j} = \frac{C_{gj} * R * T}{H_j} \quad [\text{Eq. 3}]$$

Henry's equilibrium constant ( $H$ ) is equal to partial pressure ( $p_j$ ) over aqueous equilibrium concentration ( $C_{aqj}$ ) [mole/L<sup>3</sup>] [Eq. 1]. Rearranging the ideal gas law for pressure ( $p$ ) [Eqn. 2], where  $n$  is moles,  $R$  is the ideal gas constant [V\*T/mole/P],  $T$  is temperature, and  $V$  is gas volume. From substituting Equation 2 for  $p_j$  and recognizing  $\frac{n}{V}$  is equal to gas concentration ( $C_g$ ) [mole/L<sup>3</sup>] (in this case equilibrium gas concentration), aqueous concentration simplifies to Equation 3. Henry's Law constant for methane was 657.6 L\*atm/mole (methane, SRC PhysProp). Henry's Law constant ( $H$ ) for carbon dioxide was 29.41 L\*atm/mole (carbon dioxide, SRC PhysProp).

The following mass balance equation [Eq. 4] was used for resolving the initial aqueous concentration of analytes before headspace was replaced with nitrogen.

$$n_{Tj} = C_{aq-initialj} * V_{aqinitial} = C_{aqj} * V_{aqfinal} + C_{gj} * V_g \quad [\text{Eq. 4}]$$

The initial dissolved concentration ( $C_{aq-initialj}$ ) [mole/L<sup>3</sup>] and initial 21.4 mL volume ( $V_{aqinitial}$ ) were taken from a mass balance for total moles ( $n_{Tj}$ ), using measured  $C_{gj}$  and  $C_{aqj}$  with a final sample aqueous volume of 16.4 mL ( $V_{aqfinal}$ ) and 5-mL headspace gas volume ( $V_g$ ). The rearranged equation for solving initial aqueous concentration is shown below.

$$C_{aq-initialj} = \frac{C_{aqj} * V_{aqfinal} + C_{gj} * V_g}{V_{aqinitial}} = \frac{n_{Tj}}{V_{aq}} \quad [\text{Eq. 5}]$$

Dividing Equation 4 by  $V_{aq\text{-}initial}$  separated  $C_{aq\text{-}initialj}$ . Methane calibration gas mixtures were equal to dissolved concentrations in the range of 0.0047 to 0.047 mmole/L methane [Eq. 5] for GC/FID analysis. GC/TCD calibration gas mixtures were equal to dissolved concentrations in the range of 0.047 to 0.47 mmole/L methane and 0.15 to 1.5 mmole/L carbon dioxide [Eq.1].

For DRO analysis, extracts were un-diluted and analyzed, as described for soil TPH measurements. TPH detections were calibrated to EPA/WISC gasoline range organics (GRO) and diesel range organics (DRO) mixtures (Restek®, Bellefonte, PA) in the range of 0.05 g/L-hexane to 0.75 g/L-hexane. Aqueous concentrations were calculated assuming 99.9% of DRO mass had partitioned into the hexane after equilibrium.

### 3.2.3. Gas Analysis

Gas production observations were performed on a weekly basis and gas samples were taken just before a water-table fluctuation event. Gas was analyzed for carbon dioxide, methane, VOCs, and possible semi-volatile organic compounds. Ambient temperature and barometric pressure (in Hg) were recorded during gas capture observations and water cycling events. One mL of gas was removed via a 1-mL gas-tight syringe at each event. A 50- $\mu$ L gas-tight syringe removed gas from the 1-mL syringe, and two injections were performed on the same instruments as described for dissolved hydrocarbons and carbon dioxide. The temperature program, as described for soil TPH analysis, was utilized for VOCs and methane (< 0.5% sample atmosphere), except initial hold time was one minute.

VOC standards (n-Hexane and BTEX) were employed to resolve gas concentrations, per the following equations.

$$C_{gj} = \frac{M_{Tj}}{\left(\frac{V_{aq}}{H_{dim}} + V_g\right)} \text{ [Eq. 6]}$$

$$H_{dim_j} = \frac{H_j}{RT} = \frac{C_g}{C_{aq}} \text{ [Eq. 7]}$$

For each VOC standard constituent, an equivalent headspace gas concentration ( $C_{g_j}$ ) [mole/L<sup>3</sup>] was calculated [Eq. 6], using total VOC mass added to each standard vial for each compound ( $M_{T_j}$ ) and total standard volume ( $V_{aq} + V_g$ ). Individual dimensionless Henry's Law constants ( $H_{dim_j}$ ) [Eq. 7] for VOC standard compounds (Section 4.2.2) were used for simplification. Standard concentrations were in the range of 400 to 37,000 mg/m<sup>3</sup> total VOCs. A calibration for semi-volatile organics was not performed, as these semi-volatile organics were not detected during column operation.

Methane (> 0.5% sample atmosphere) and carbon dioxide gas concentrations were analyzed as described for dissolved gases. Methane and carbon dioxide were calibrated with the same gas mixture as described for dissolved gases. A four-point gas calibration standard curve, for both gases, was in the range of 0.17 to 1.7 mmole/L, or 0.5% to 5% sample atmosphere.

#### 3.2.4. General Water Quality Analysis

General water quality analysis included: pH, oxidation-reduction potential (ORP), alkalinity, anions, and qualitative turbidity and color observations. Water quality probes were calibrated before each use. A LE407 pH probe (Mettler Toledo, Sonnenbergstrasse, Switzerland) was calibrated via a three-point calibration with buffered solutions (Tri-Check Buffer, pHYDRION, Brooklyn, NY) at pH 4, 7, and 10. Slope accuracy was an average 94.5% ± 2.4%. The gel-filled ORP probe (MN590001, Cole Parmer, Vernon Hills, IL) was calibrated against ORP Standard (Thermo Fisher Scientific, Chelmsford, MA). ORP accuracy was within ± 2.6 mV Ag/AgCl of ideal 200 mV Ag/AgCl ORP (Figure 2).

Influent and effluent water alkalinity was compared to approximate the amount of bicarbonate produced from hydrocarbon degradation. Influent water alkalinity was measured on a quarterly basis using a carbonate hardness titration kit (Mars Fishcare North America Incorporated, Chalfont, PA). The titration method was modified by using precision pipets to increase accuracy to  $\pm 3$  mg/L calcium carbonate as compared to  $\pm 10$  mg/L calcium carbonate. Effluent total carbonate hardness, or bicarbonate alkalinity, was calculated via equilibrium with measured dissolved carbon dioxide. Calculations used the  $K_{a1}$  value of  $10^{-6.35}$  (Brezonik & Arnold, *Water Chemistry*), measured pH, and dissolved carbon dioxide values. Titrations were performed on periodic draining event samples to verify methods were  $\pm 0.001$  M bicarbonate. Sample intervals of the same column were also compared, and differences were sometimes  $\geq 0.001$  M bicarbonate.

Anions (Fluoride, Chloride, Nitrate, Phosphate, and Sulfate) were measured via a Metrohm 861 Advanced Compact Ion Chromatograph with a Metrosep A Suppressed 250/4.0 column (250 mm L x 4.0mm I.D., Metrohm, Riverview, FL). For the first six water draining events, anion water samples were first diluted with deionized water at 10:1, as sulfate concentrations were in the hundreds to thousands of mg/L; thereafter, a 5:1 dilution was used as sulfate dropped below 20 mg/L. Quarterly influent water samples were not diluted.

Table 2– Sample matrix for all analytical parameters for aqueous and gaseous phases at specific operational events

<b>Hydraulic Event</b>	<b>Aqueous Analysis</b>	<b>Gas Analysis</b>
<b>Draining</b>	<ul style="list-style-type: none"> <li>• Dissolved Hydrocarbons (Gasoline/Diesel Range Organics)</li> <li>• Dissolved Gases (CO<sub>2</sub> &amp; CH<sub>4</sub>)</li> <li>• Bicarbonate</li> <li>• Anions: Sulfate, Nitrate, Phosphate, Chloride, Fluoride</li> <li>• pH / Oxidation Reduction Potential (ORP)</li> </ul>	<ul style="list-style-type: none"> <li>• Hydrocarbons</li> <li>• CO<sub>2</sub> &amp; CH<sub>4</sub></li> </ul>
<b>Saturating</b>	<ul style="list-style-type: none"> <li>• Influent Water - Sulfate , pH &amp; ORP (Quarterly Basis)</li> </ul>	<ul style="list-style-type: none"> <li>• Hydrocarbons</li> <li>• CO<sub>2</sub> &amp; CH<sub>4</sub></li> </ul>

### 3.2.5. Mobile LNAPL Snapshots

High-resolution digital photography was paired with ultraviolet light to snapshot LNAPL saturation versus column height. Before each water-cycling event, the columns were individually photographed under precise dimensions. The photographs were cropped and limited to green spectrum pixels in MATLAB (The MathWorks, Inc.). Each line of pixels with a normalized range of light intensity was integrated and displayed on a plot of intensity versus normalized column depth. Limitations with only surficial observations from the glass columns created inequivalent total intensity values across concentrations; and therefore, these snapshots were viewed to observe the movement of mobile LNAPL qualitatively. Complete LNAPL snapshot operations are included in Appendix D.

### 3.3. Calculations

This section introduces calculations used to reduce data from the laboratory experiment and application of the GPM.

### 3.3.1. Carbon Balance

Measuring NSZD rates involved a carbon mass balance accounting for the degradation, dissolution, or volatilization of LNAPL hydrocarbons. Carbon initially in the columns as LNAPL was equal to the amount of carbon released either dissolved, volatized, or accumulated. The following equation [Eq. 8] shows a simplified carbon balance.

$$\mathbf{Carbon}_{initial} = \mathbf{Carbon}_{out} + \mathbf{Carbon}_{accumulated} \quad [\text{Eq. 8}]$$

A simple molar balance was applied to the column shown in Figure 2 [Eq. 8] and then accounting for more discrete NSZD processes.

$$n_{Initial} = n_{Removed} + n_{Remaining} + n_{Precipitated} + n_{Biomass} \quad [\text{Eq. 9}]$$

Equation 9 shows the mass balance in terms of moles of carbon, where  $n_{Initial}$  is the initial moles of carbon,  $n_{Removed}$  is measured moles of carbon leaving via gas or water phases,  $n_{Remaining}$  is moles carbon remaining as hydrocarbons,  $n_{Precipitated}$  is moles carbonate precipitated, and  $n_{Biomass}$  is uptake into new biomass material. Sorption of hydrocarbons was accounted for in  $n_{Remaining}$ . To account for total change in moles carbon, Equation 9 was rearranged for the difference from initial to remaining LNAPL as moles carbon.

$$\Delta n_T = n_{Initial} - n_{Remaining} = n_{Precipitated} + n_{Removed} + n_{Biomass} \quad [\text{Eq. 10}]$$

Total change in moles carbon ( $\Delta n_T$ ) is also equal to the amount of carbon precipitated, removed, and accumulated as biomass. Carbon precipitated was not possible to measure while performing the experiment. Inorganic precipitation of carbon dioxide as carbonate minerals was assumed insignificant and at equilibrium throughout the experiment. Carbon accumulated as biomass was assumed negligible as biomass yield has been shown to be insignificant compared to carbon lost via degradation pathways (Irianni Renno et al., 2015)

Inorganic carbon, methane, or hydrocarbons were converted into moles carbon for use in the carbon mass balance. Methane, carbon dioxide, and bicarbonate only contain one mole carbon per mole species; thus, molar concentrations were converted on a 1:1 mole-to-mole ratio. A 10:1 mole-to-mole ratio was used for hydrocarbon molarity. For converting from mass of LNAPL to moles carbon, a representative compound n-decane (C<sub>10</sub>H<sub>22</sub>) was used for the LNAPL. This conversion follows the assumption made in Johnson et al. (2006) for estimating NSZD rates. A measured density of 0.73 g/cm<sup>3</sup> and a high fraction of paraffins in the range of C<sub>10</sub> to C<sub>16</sub> align with decane. The equations below describe the conversion of analyte concentrations to moles carbon.

$$n_{Removed_j}(t_i)_{aq} = C_{aq_j} * Vol_{drained}(t_i) * \frac{mole\ carbon}{mole_j} \text{ [Eq. 11]}$$

$$n_{Removed_j}(t_i)_g = \left[ \left( C_{g_j} * Vol_{gas}(t_i) \right) - \left( C_{g_{j-1}} * Vol_{gas}(t_{i-1}) \right) \right] * \frac{mole\ carbon}{mole_i} \text{ [Eq. 12]}$$

Moles carbon removed ( $n_{Removed_j}$ ) [mole] for each water cycling event ( $t_i$ ) were calculated via measured  $C_{aq_j}$  and  $C_{g_j}$ . Aqueous moles removed ( $n_{Removed_j}(t_i)_{aq}$ ) were calculated via Equation 11 and only during draining events.  $Vol_{drained}(t_i)$  was the total water drained from the column at the event. A ratio of moles carbon per mole of carbon compound  $j$  ( $\frac{mole\ carbon}{mole_j}$ ) was used as a conversion factor. For example, a ratio of 10 moles carbon per mole n-decane was used to equate measurements to moles carbon. Methane and carbon dioxide are on a 1:1 basis. Moles gas removed ( $n_{Removed_j}(t_i)_g$ ) was the difference of total gas capture moles between events [Eqn. 12]. Gas capture volumes at sampling ( $Vol_{gas}(t_i)$ ) and after the previous event ( $Vol_{gas}(t_{i-1})$ ) were multiplied to respective event gas concentrations (i.e.,  $C_{g_j}$  or  $C_{g_{j-1}}$ ) for gas capture moles carbon.

### 3.3.2. Molar Loss Rates

Rates of NSZD were approximated from discrete intervals, as shown in the below equations.

$$\frac{\Delta n_T}{t_{exp}} = \frac{n_{Initial} - n_{Remaining}}{t_{final} - t_{initial}} = \frac{n_{Precipitated}}{t_{final} - t_{initial}} + \frac{n_{Removed}}{t_{final} - t_{initial}} + \frac{n_{Biomass}}{t_{final} - t_{initial}} \quad [\text{Eq. 13}]$$

$$\frac{\Delta n_{T_i}}{\Delta t} = \frac{n_{T_i} - n_{T_{i-1}}}{t_i - t_{i-1}} \quad [\text{Eq. 14}]$$

NSZD molar loss rate was calculated by dividing  $\Delta n_T$  from Equation 10 by total experimental time ( $t_{exp}$ ) [Eq. 13] or explicit time differences between water cycling events ( $t_i - t_{i-1}$ ) [Eq. 14].

Carbon uptake ( $n_{Precipitated} + n_{Biomass}$ ) was not resolved in the experiment and is assumed to be zero. Similarly, field measurement devices disregard carbon uptake and rely on the carbon degradation out of a source zone (McCoy et al., 2014).

NSZD rates are ultimately dependent upon the reaction constants developed from numerical approximation, or, more specifically, regression analysis. Taking the limits of Equation 12, when  $\Delta n_{T_i}$  over as  $\Delta t$  approaches zero, the difference between zero- and first-order reaction constants is demonstrated below.

$$\lim_{\Delta t \rightarrow 0} \frac{\Delta n_{T_i}}{\Delta t} \Rightarrow \frac{dn_T}{dt} = \dot{n} = k \quad [\text{Eq. 15}]$$

$$\lim_{\Delta t \rightarrow 0} \frac{\Delta n_{T_i}}{\Delta t} \Rightarrow \frac{dn_T}{dt} = \dot{n} = n_0 e^{-kt} \quad [\text{Eq. 16}]$$

Both limits are equal to molar loss rates ( $\dot{n}$ ) [moles/time], yet zero-order functions [Eq. 15] are linear, whereas first-order functions [Eq. 16] are exponential. Zero-order reaction constants ( $k$ ) are in units of mass (or moles) per time. Therefore, in Equation 15, the rate of change in carbon, ( $\frac{dn_T}{dt}$ ), was equal to a single  $k$ . First-order reaction constants are in units of inverse time [ $T^{-1}$ ] and dependent upon initial moles carbon ( $n_0$ ) and time [Eq. 16]. Best-fit regressions as zero-order

(linear) or first-order (exponential) were used to validate anaerobic NSZD dependence upon LNAPL concentration. Regression analysis is discussed in following sections.

Volumetric loss rates, or molar flow rates, were used in the experiment to account for NSZD per unit volume of soil. A volumetric loss rate better applies to field-scale NSZD rates and follows the compartmental mass flux methods of Johnson et al. (2006), Miles et al. (2008), and McCoy et al. (2014).

$$\dot{n}_{vol} = \frac{\frac{dn_T}{dt}}{V} \text{ [Eq. 17]}$$

Molar flow rates ( $\dot{n}_{vol}$ ) [mole/time/L<sup>3</sup>] can be calculated from dividing  $\frac{dn_T}{dt}$  by an average soil column volume ( $V$ ), 870 mL [Eq. 17].

$$\dot{n}_{volj} = \frac{\frac{n_{Removedj}}{t_i - t_{i-1}}}{V} \text{ [Eq. 18]}$$

$$\dot{n}_{volj} = \frac{\frac{n_{T_i} - n_{T_0}}{t_i - t_0}}{V} \text{ [Eq. 19]}$$

Equation 18 calculates experimental molar flow rates between water cycling events, and Equation 19 calculates averaged molar flow rates for specific periods of the experiment [Eq. 19].

### 3.3.3. Accounting for Governing Processes

It was necessary to account for fractions of carbon leaving as a function of as both abiotic and biotic processes contributed to NSZD. Total NSZD was separated as either abiotic, sulfate-reduction, or methanogenic fractions. Hydrocarbon dissolution and volatilization contributed to abiotic NSZD.

To measure the amount of biotic NSZD, the representative compound n-decane was taken through complete mineralization via sulfate-reduction or methanogenesis pathways [Eq. 19 and Eq. 20] (Johnson et al., 2006).



Sulfide ions ( $S^{2-}$ ) are often scavenged in the presence of divalent mineral ions, such as ferrous iron ( $Fe^{2+}$ ) and manganese ( $Mn^{2+}$ ). Thus, the above  $[7.75H_2S]$  in Equation 20 can be substituted with  $[15.5H^+ + 7.75S^{2-}]$ .

Measurements of inorganic carbon and methane contributed to biotic NSZD. Inorganic carbon fractions were calculated using stoichiometric ratios from the above n-decane mineralization reactions [Eq. 20 and Eq. 21]. Dissolved sulfate measurements and moles of methane produced as either dissolved or gas were used to calculate biotic NSZD.

$$CO_{2\text{Removed}SR} = \frac{1.29 \text{ mole C}}{\text{mole } SO_4^{2-} \text{ reduced}} \cdot ([SO_{4IN}^{2-}] - [SO_{4OUT}^{2-}]) \text{ [moles] [Eq. 22]}$$

$$CO_{2\text{Removed}MG} = \frac{0.29 \text{ mole C}}{\text{mole } CH_4 \text{ produced}} \cdot CH_{4\text{Produced}} \text{ [moles] [Eq. 23]}$$

Moles carbon removed via sulfate-reduction ( $n_{\text{Removed}SR}$ ) were calculated via the ratio for inorganic carbon produced per mole sulfate reduced and multiplied by the difference in molar sulfate concentration from influent ( $[SO_{4IN}^{2-}]$ ) to effluent ( $[SO_{4OUT}^{2-}]$ ) water samples [Eq. 22].

Inorganic carbon produced via methanogenesis ( $n_{\text{Removed}MG}$ ) was calculated using the ratio of inorganic carbon to methane in Equation 21 and multiplied by moles methane produced ( $CH_{4\text{Produced}}$ ) for that event or period [Eq. 23]. Fractions were approximate contributions to total inorganic carbon loss rates. The larger inorganic carbon result, either directly measured or

calculated via the above method, was included in NSZD rates to appropriately adjust to experimental uncertainties and sampling methods.

#### 3.3.4. Statistics

Hypotheses may be verified or rejected by calculating a probability value (p-value) often from a dataset of variables and results and then comparing that probability with a sample statistic (e.g., 95% percentile). Other hypothesis testing may require regression analysis that evaluates how well results fit to a model, most often linear or logarithmic. Specifically, slope regression hypothesis tests evaluate whether slopes are, or are not, statistically significant from 0. Final statistical results are left to interpretation, and significance is often a matter of experimental context.

A linear model assessed whether NSZD was zero-order (null hypothesis) or first-order (alternative hypothesis) for both periods. Slopes statistically different from zero indicate that the dependent variable, in this case NSZD rates, was a function of the independent variable, LNAPL concentration. A probability value (p-value) greater than 0.05 accepts the null hypothesis of zero order, whereas a p-value less than 0.05 rejects the null hypothesis. The same statistical method evaluated NSZD as a function of predominant biodegradation condition under experimental settings. Excel (Microsoft Corp., Redmond, WA) was used to calculate the linear regression fit of average NSZD rates (mmole C/day/m<sup>3</sup>) versus LNAPL concentration (mg/kg). P-values of the slope were calculated for early- and late-stage data through Excel's Data Analysis Tool, also known as ANOVA, set on Regression. Excel was also used to display a 95% confidence interval offset of the regression fit. Slope regression tests evaluate whether slopes are, or are not, statistically significant from 0.

Statistical interpretation considered measurement accuracy and hydrocarbon concentration distribution for inferring statistical significance. Only the nine field-derived soil columns were

evaluated in the regression analysis with the control and nutrient columns placed on plots (Figures 4b and 4d) for comparison. Consideration was given for extraneous variables (e.g., water saturation, sulfate concentration, pH, ORP, etc.) not tested for in this null hypothesis. Statistical regression analysis was performed on two separate environmental phases of the experiment. An order of magnitude or more of variability in single-location field rates has commonly been observed; therefore, this degree of fluctuation provided a standard for statistically significant differences.

### 3.4. Glide Path Model

The GPM advanced in Skinner (2013) was applied to a fuel terminal in the central United States. GPM parameters assumed continuous reaction rates for active remedy input. For example, middle- and late-stage sites may continually fall short of previous conceptual model estimates for recovery. Periodic interruptions, such as mechanical systems maintenance, changeover of systems, and site conditions, hinder continuous use. The GPM was modified to incorporate periodically active LNAPL depletion via hydraulic recovery.

#### 3.4.1. Field Site

Data were acquired from an active petroleum tank terminal site located in the central United States. The site is adjacent to the Missouri River. Low water levels are observed during months of March and April before spring runoff. The site is underlain by fine to medium sand with silt and some gravel. Operations at the facility date back to the 1930s. An LNAPL smear zone begins at approximately 3.0 m bgs and continues up to 10.5 m bgs, and LNAPL impact zones were delineated as far as 8.9 hectares. Monitoring well LNAPL thicknesses  $\geq 0.15$  m from 2002 delineated the modern source zone. An extensive petro-physical site investigation in 2012 estimated the LNAPL source zone specific volume at approximately 0.13 m across a combined area of 61,500 m<sup>2</sup> (approximately  $6.8 \times 10^6$  kg LNAPL). Estimated specific volume was 0.16 m

across the same area in 2002. LNAPL well thickness within the source zone measured 10 % of wells  $\geq 0.06$  m in 2013; whereas in 2001 to 2002, thickness ranged between 0.30 m to 1.07 m. Petro-physical data and lab testing evaluated residual LNAPL saturation for vadose and saturated zones. Soil core samples revealed a low percentage of LNAPL saturations above literature residual saturations (Brost, 2000), where continuous LNAPL may have been present.

A dual-phase hydraulic recovery system began operation in 2008. Due to high water table conditions, no accumulation or recovery of LNAPL occurred in 2008. A hydraulic recovery system recovered approximately 47.3 m<sup>3</sup> in 2013 and 9.77 m<sup>3</sup> in 2014. Both recovery periods were during optimal water level conditions during the months of March and April. Since pumping was periodic, dissolved hydrocarbons removed were assumed negligible at an approximated 0.0001 m/year in specific volume. Volatile mass was assumed degraded before reaching the surface; therefore, volatilization was accounted for in biodegradation inputs.

Seven rounds of carbon flux measurements were performed from fall 2012 to fall 2014. Following methods described in McCoy et al. (2014), observed carbon dioxide efflux ranged between 0.15 and 17.0  $\mu\text{mole carbon/sec/m}^2$ . Field conditions and soil heterogeneity may have influenced such a large variance of carbon flux measurements. A reported source-zone average carbon flux was 4.10  $\mu\text{mole carbon/sec/m}^2$ .

After observations from Stockwell (2015), LNAPL smear zone temperature data was recorded using in-situ thermocouples over the course of one year (spring 2014 to spring 2015) and was used as the subsurface temperature profile in the GPM. As validated in Zeman et al. (2014), seasonal subsurface temperature fluctuation equal or greater than 4 °C has an effect on NSZD rates. Average temperature within the LNAPL smear zone was 14 °C with variable seasonal fluctuation of  $\pm 4$  °C; therefore, GPM simulations were performed as two sets, with and without temperature fluctuations.

### 3.4.2. Assumptions

The site was considered middle-stage with primarily discontinuous LNAPL, which was inferred from petro-physical data and intermittent LNAPL recovery. A maximum continuous fraction of 10 % was assumed during low water table periods seen in early spring. Minimum continuous fraction for the GPM was 0.01 % to work properly, as 0 % causes calculation errors in the wave function. The GPM was assumed applicable to only a minimal specific volume of 0.02 m (≤ 2,500 mg/kg TPH in soil), where residual LNAPL mass could be less than adsorbed mass.

While LNAPL was present, future hydraulic recovery would be required at the site. Recurring active remedy operation periods only coincided with low water table and where continuous fraction was near 10%. An amount of 48 m<sup>3</sup> was assumed to have been removed, every other year, from 2016 to 2026, as previous events followed a similar bi-annual pattern.

Discrete seasonality of carbon flux was not observed at the site, yet seasonal averages were within the range of input parameters of the simulation. GPM longevity simulations, without temperature fluctuations, assumed an average NSZD rate of 4.10 μmole C/m<sup>2</sup>/sec. Simulations were repeated with the average NSZD rate increased or decreased by 50%. Implementing a homogenous carbon flux for separate LNAPL bodies within heterogeneous soil site may under or over-estimate activity (Bundy et al., 2002). Likewise, for GPM simulations with temperature fluctuations, optimal and non-optimal NSZD rates were ± 50% of the average NSZD rate.

### 3.5. Glide Path Model Modification

Following Skinner (2013), total mass  $M_T^{i+1}$  [M] is calculated with a finite difference equation [Eq. 24], accounting for changes in mass as discontinuous ( $M_{disc}^i$ ) or continuous ( $M_{cont}^i$ ).

$$M_T^{i+1} = M_{disc}^i - \Delta t * (k_{dis} + f_{disc} * k_{bio}) + \frac{M_{cont}^i * \left(1 - \frac{\Delta t * k_{rec}}{2}\right) - \Delta t * (k_{vol} + f_{cont} * k_{bio})}{\left(1 + \frac{\Delta t * k_{rec}}{2}\right)} \quad [\text{Eq. 24}]$$

A cosine wave function adjusted fractions of discontinuous ( $f_{disc}$ ) and continuous ( $f_{cont}$ ) relative to water table fluctuations. Maximum and minimum continuous fraction input parameters set function amplitude. An input of day low water level observed adjusted the function to meet maximum and minimum values. Time steps,  $\Delta t$  [T], were set to 30 days, which also limited water level cycle period to 30 days. Zero-order reaction rates [M/T] for dissolution ( $k_{dis}$ ) and volatilization ( $k_{dis}$ ) were applied in the Glide Path Model. Biological processes were assumed as zero-order reaction rates (McCoy, 2014), where  $k_{bio}$  [M/T] is a field measured NSZD flux [M/T/L<sup>2</sup>] multiplied by lateral source zone area. Optimal and non-optimal NSZD rates (seasonal rates), if applicable, were dependent upon an optimal temperature for site specific NSZD (Zeman et al., 2014). A cosine wave function tracked annual temperature, which switched optimal and non-optimal rates for the  $k_{bio}$  input parameter. A first-order active remedy reaction rate,  $k_{rec}$  [T<sup>-1</sup>], acted only on continuous fractions. Loss characteristics each had input parameters for dates turned on and off.

Previously, the GPM used a reaction rate derived from averaged mass recovery rates and was assumed constant throughout site conditions. For middle- and late-stage use, the GPM must allow for varied conditions with respect to continuous fractions. Optimal conditions may only occur with exceptionally low water tables or after recovery well re-installation or rehabilitation. Active remedy rates ( $k_{rec}$ ) [Eq. 24], must fit field data and through deterministic iterations allow for a range of projected mass removal amounts.

$$k_{recovery} = \frac{Vol.Rec_{LNAPL}}{(Day_i - Day_{i-1}) * \frac{M_{cont_i}}{\rho_{LNAPL}}} \text{ [Eq. 25]}$$

Volume recovered as LNAPL ( $Vol.Rec_{LNAPL}$ ) over a discrete interval was converted to a reaction rate [Eq. 25]. Mass of continuous was accounted for in  $M_T^{i+1}$ , and density of the LNAPL ( $\rho_{LNAPL}$ ) was known or assumed [Eq. 24]. For SVE data, TPH vapor concentrations must be converted

before input into the model. Conditional statements also allowed historical and projected recovery rates from multiple inputs fields. Projected active remedy durations were user-prescribed and can be singular or cyclical (i.e., monthly, quarterly, annual, or every other year).

## 4. RESULTS

The following sections outline NSZD rates as a function of concentration, performance over time, and influence of governing biotic and abiotic processes measured from the 11 columns over 14 experimental months of operation. Column performance over time, including water quality and biodegradation rates, is discussed in Section 4.1. Biodegradation rates as a function of TPH concentration are discussed in Section 4.2. The influence of governing biotic and abiotic processes is discussed in Section 4.3.

### 4.1. Column Performance as a Function of Time

Columns reproduced field conditions where sulfate and methanogenic anaerobic NSZD occurred. Figure 3a depicts effluent sulfate data versus experimental months. Effluent sulfate changed dramatically over months 1 through 6. Average effluent sulfate concentrations initially were 1,500 mg/L in month 1 and decreased to 48 mg/L by month 6 (See Figure 3a). High initial aqueous sulfate concentrations originated from field soil derived sulfate minerals and reached a maximum concentration during month 2 at an average 1,770 mg/L. At month 9, average effluent sulfate had decreased to an average of 3.20 mg/L and reached an average of 2.51 mg/L at month 12. The decrease in effluent sulfate indicated that soluble soil sulfates had mostly dissolved and were removed from the system by column effluents.

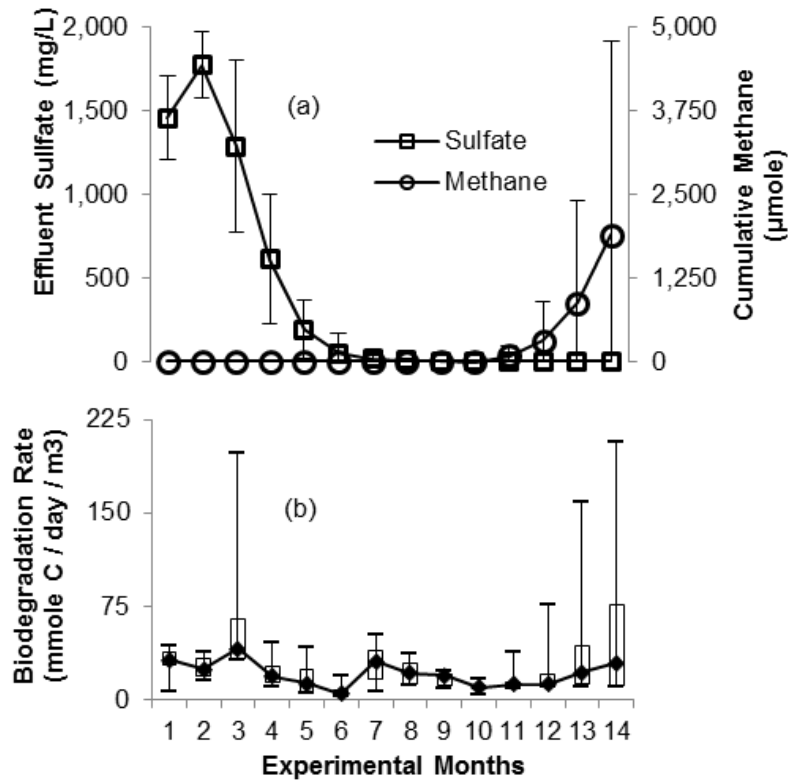


Figure 3 – Effluent sulfate (mg/L), cumulative methane ( $\mu\text{mole}$ ), and biodegradation rates ( $\text{mmole C/day/m}^3$ ) versus experimental months. Effluent sulfate and cumulative methane are shown in (a) with respective standard deviations. Biodegradation rates are shown in (b) as a whisker plot with a line connecting monthly median rates.

Methanogenesis was observed under laboratory conditions. Methane was detected at month 7 in columns with 32,000 mg/kg, 35,000 mg/kg, and 37,000 mg/kg TPH concentrations. Most effluent sulfate concentrations were less than influent sulfate concentrations of 20 mg/L at month 7 (Figure 3a). By month 12, all columns were producing methane, with the exception of the control (autoclaved sand with field LNAPL) and nutrient influent columns. A maximum methane production was observed from the 35,000 mg/kg column at a rate of 0.86 mmole/day. Columns above 27,000 mg/kg TPH were observed to produce methane gas volumes at a minimum of 10 mL per week after month 7. Methane gas accounted for greater than 90% of the total methane flux.

Biodegradation rates (mmole C/day/m<sup>3</sup>) are depicted in Figure 3b versus experimental time. The reported biodegradation rates were based on measured generation of methane and inorganic carbon. Biodegradation rates primarily ranged between 5 and 50 mmole C/day/m<sup>3</sup> with extremes reaching approximately 206 mmole C/day/m<sup>3</sup> (35,000 mg/kg, month 14). The median rate fell to 4.6 mmole C/day/m<sup>3</sup> when average sulfate concentration fell below 20 mg/L at month 6. Elevated rates, observed in month 3, may have been the result of air intrusion (See Section 4.1.2) where elevated rates were also observed in the control column (17,000 mg/kg) at 97.0 mmole C/day/m<sup>3</sup>. Interestingly, at month 11, biodegradation rates increased coinciding with an increase in methane production (Figure 3a). A significant trend was not observed with changing sulfate concentrations before dissolved concentrations were detected below 20 mg/l.

Column environments transitioned from acidic to neutral pH while ORP became increasingly reduced. Average pH across all columns, excluding the control and nutrient columns, transitioned from a slightly acidic pH of 6.62 to a neutral pH of 7.12 (See Appendix C). The control column remained near an average pH of 7.53 ± 0.14, and the nutrient column remained slightly acidic with pH ranging between 5.52 and 6.40. The control column ORP varied substantially over time and ranged between -122 and 45.4 mV. With the exception of the control column, ORP initially averaged -123 ± 19.5 mV (Ag/AgCl) up to month 7 and gradually decreased to -142 ± 18.9 mV in the remaining months (See Appendix C).

Columns dramatically shifted in appearance as NSZD progressed (Figure 4). From the first draining event, a rust-colored precipitate (presumably iron oxide) was observed on sample glassware. Effluent water was shortly exposed to air in the flow cell, likely allowing oxidation of ferrous iron (Figure 2). Black precipitates formed on soil after the saturating event in month 4. Black precipitate formation was not uniform, but began in scattered pockets and spread outward. By the end of the fifth saturating event, these precipitates completely covered visible soil and accumulated below the glass filter in thin sheets. Iron sulfide (FeS) and magnetite

( $\text{Fe}_3\text{O}_4$ ), both black in color, are typical to anaerobic environments where biological iron and sulfate reduction occurs (Ehrlich, 1996). Thus, visual observations also suggested that biological reduction of sulfate and/or iron were occurring (Sinke et al., 1998). The control column (17,000 mg/kg TPH) never formed visible precipitates throughout the experiment. The field soil contained redox sensitive manganese, iron, and sulfate minerals, whereas the control column was predominantly silica sand (see Section 3.1.1). Importantly, black precipitate formation indicated the column environments reproduced the iron- and sulfate-reducing conditions that predominate in anaerobic LNAPL smear zone environments at field sites.

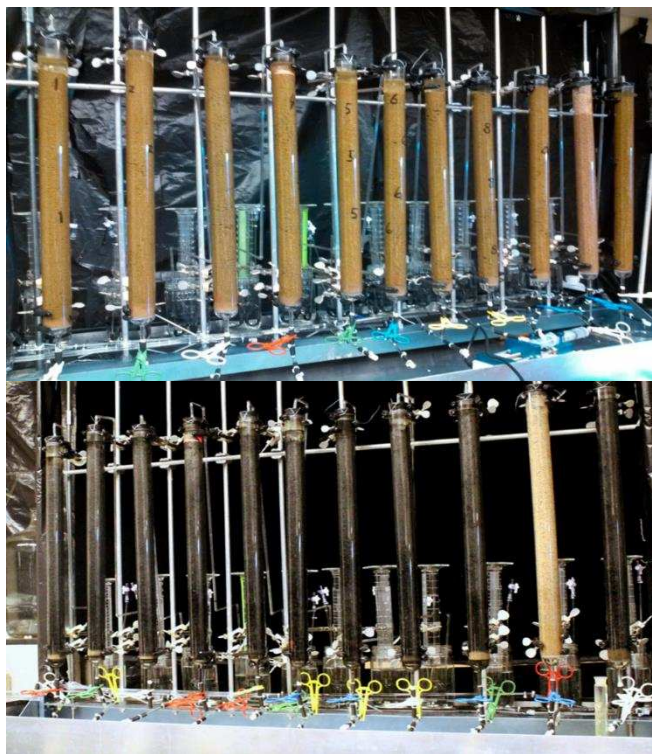


Figure 4 – Photos of column experimental setup, initially (top) when soils were brown and after six months (bottom) when black precipitates completely covered soil surfaces. The control column (second column from right) did not have black precipitates, remaining light reddish-brown throughout the experiment.

Additionally, over time, porosity may have been reduced to a significant degree due to subsidence. Initially, columns were saturated to the top of the soil with water volumes between

220 and 230 mL. Two to 4 cm of standing water was observed at two weeks into the first saturating event. Soil subsidence in the first month was due to particle settling and possibly trapped gas ebullition. By the third month, draining and saturating volumes ranged between 70 mL and 120 mL and continued in this range for the rest of the experiment. Observable soil subsidence ceased in all columns at month 4. Pore water volumes exchanged in cycling events decreased with increasing LNAPL saturation.

After draining events, some sections of the columns (approximately 4 to 12 cm) remained at water-saturated conditions. These sections were suspended above unsaturated zones. Water appeared to pass through these sections during draining; however, the pore water did not drain from these exterior, visible column sections during the draining process. Similar to a clogged filter, the discharge from these sections was possibly hindered by precipitate accumulation, not allowing complete drainage during active draining events. Beside the reduction in porosity from subsidence, pore water volume reduction may have been a result of precipitate accumulation, where pore throats were increasingly clogged with the formation of amorphous minerals.

The snapshot method was incapable to quantify a precise number for mobile LNAPL intensity (i.e., LNAPL saturation). And furthermore, the physical nature of the columns created no rationale to assume LNAPL saturation was consistent from cycle to cycle. A figure is presented in Appendix D that shows the insensitivity of snapshot measurement via MATLAB. The snapshots did however produce a qualitative observation of what had been previously observed via similar qualitative methods in Skinner (2015), Dobson et al. (2007), and Huntley et al. (2002).

#### 4.2. Biodegradation Rates as a Function of Concentration

Following Figure 5, biologically mediated NSZD rates did not significantly change with increasing TPH concentration. Thus, NSZD biodegradation rates were found to be independent

of LNAPL mass for both types of anaerobic environments observed (sulfate-reducing alone and combined sulfate-reducing/methanogenic). Sulfate-reducing (early) environment criteria were  $> 20$  mg/L effluent sulfate and  $< 5$  mmole/m<sup>3</sup> methane, whereas the sulfate-reducing and methanogenic (late) environment criteria were  $\leq 20$  mg/L effluent sulfate and  $\geq 5$  mmole/m<sup>3</sup> methane. For the control and nutrient columns, early and late periods were separated at month 7 (average transition month), because the above criteria could not be applied and to allow for comparison of chronologically equivalent rates. Early-period rates spanned two orders of magnitude (Figure 5a), but 50<sup>th</sup> percentile boxes (excluding the control column) generally were between 10 and 100 mmole C/day/m<sup>3</sup>. Late-period rates showed reduced variability (Figure 5b), specifically at TPH concentrations between 9,000 mg/kg and 25,000 mg/kg (excluding the control column). Average median biodegradation rates were approximately  $20.7 \pm 10.5$  mmole carbon/day/m<sup>3</sup> and  $19.5 \pm 10.3$  mmole carbon/day/m<sup>3</sup> for the early and late periods, respectively.

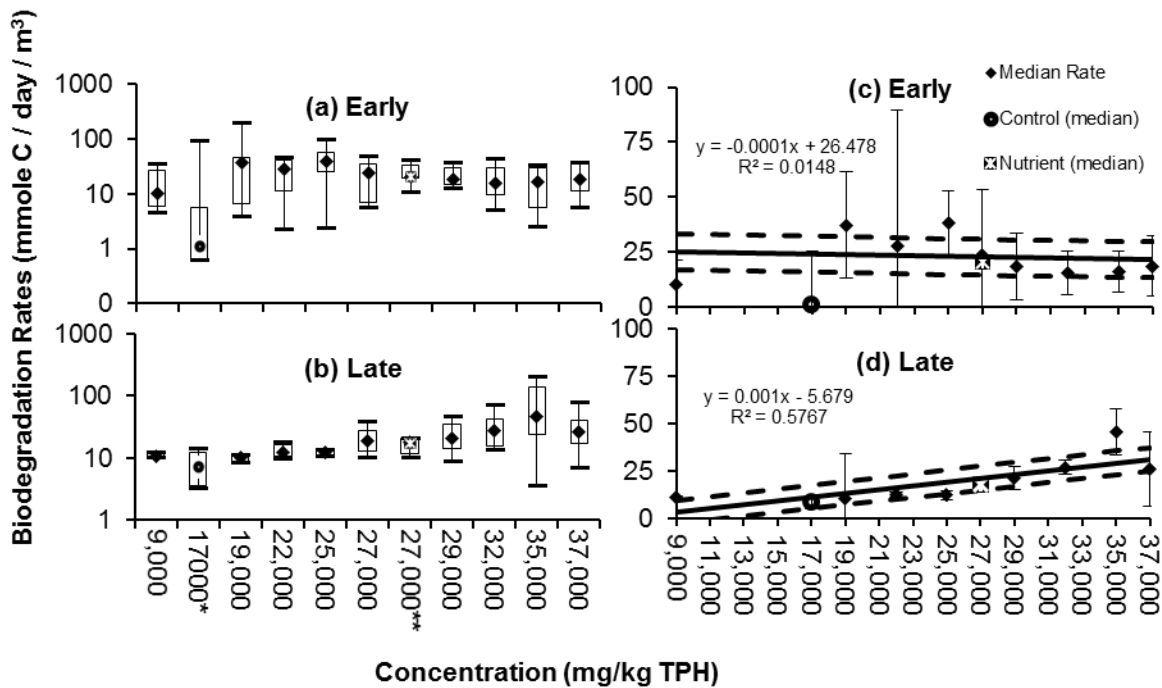


Figure 5 – Log scale box-plot ((a) and (b)) and linear regression models ((c) and (d)) of biodegradation molar rates (mmole C/day/m<sup>3</sup>) versus initial LNAPL concentration (mg/kg TPH). Figures (a) and (b) represent biodegradation rates as a standard whisker box-plot, whereas Figures (c) and (d) depict the rate data in a scatter plot and include regression equations. 95% confidence intervals (dashed lines) with standard deviation (error bars) are shown in plots (c) and (d). The early period ((a) and (c)) was predominantly sulfate-reducing. The late period ((b) and (d)) was characterized by sulfate-reduction and methanogenesis.

The early period p-value was calculated at 0.76. The early-period p-value had a substantial difference of 0.71 from the sample statistic of 0.05, suggesting the null hypothesis was accepted. Early-period rates showed an inverse relationship with increasing LNAPL concentration, and the negative regression slope for early-period data (Figure 5b) with poor model fit with an  $R^2$  of 0.0148 indicated a linear model was not appropriate. Late-period p-value was calculated at 0.02, indicating the null hypothesis was rejected ( $p$ -value < 0.05). A linear regression model for the late period (Figure 5d) was poorly fit to median rates ( $R^2$  of 0.5767). Also, a model slope of 0.001 mmole C/day/m<sup>3</sup> per unit of TPH concentration was considered insignificant for the range of LNAPL concentrations tested. NSZD rates in both periods did not show a statistically significant dependence on LNAPL mass. Therefore, NSZD rates under

predominantly sulfate-reducing and methanogenic conditions were validated to be zero-order processes.

A significant overlap was seen between the nutrient column and the un-augmented counterpart of the same initial TPH concentration (27,000 mg/kg TPH). Both early- and late-period median rates for 27,000 mg/kg columns did not differ by more than  $\pm 5$  mmole C/day/m<sup>3</sup>. These columns' rates averaged approximately 19.5 mmole C/day/m<sup>3</sup>.

A slightly wider variance of rates was observed during predominantly sulfate-reducing conditions ( $\pm 10.5$  mmole C/day/m<sup>3</sup>), as compared to combined sulfate-reducing and methanogenic conditions ( $\pm 10.3$  mmole C/day/m<sup>3</sup>). Early-period NSZD rates were often outside the confidence interval by a large degree (Figure 5c), also indicated by the R<sup>2</sup> value of 0.0148. The 90<sup>th</sup> percentile of rates across both periods was between 2.25 and 48.2 mmole C/day/m<sup>3</sup>. Rates above 50 mmole/day/m<sup>3</sup> were observed less frequently and very often not within the same column for the early period. Variations in observed biodegradation rates are due to unidentified parameters, and future work would be required to resolve rate-controlling variables given that rates were not a function of LNAPL saturation.

#### 4.3. Influence of Governing Biodegradation Processes

Both abiotic and biotic processes (abiotic dissolution and volatilization, biotic sulfate-reduction, and methanogenesis) contributed to a narrow distribution of total NSZD rates (Figure 6), relative to previously observed field rates seen in Amos et al. (2005) and McCoy et al. (2014). Sulfate-reduction NSZD fractions were generally higher than abiotic fractions for early environments across all concentrations (Figure 6a). Methanogenesis fractions were highest in columns with TPH concentrations above 29,000 mg/kg (Figure 6b). The 35,000 mg/kg column in the late period indicated a productive methanogenic environment with rates greater than sulfate-reduction NSZD seen in the early period. LNAPL concentrations between 32,000 mg/kg and

37,000 mg/kg (Figure 6b) were predominantly methanogenic NSZD environments in the late period. Interestingly, methane production in the late period was significantly higher for LNAPL concentrations between 27,000 mg/kg and 37,000 mg/kg as compared to lower LNAPL concentrations. Control and nutrient columns were observed to be not significantly different from the first half of the experiment to the second half.

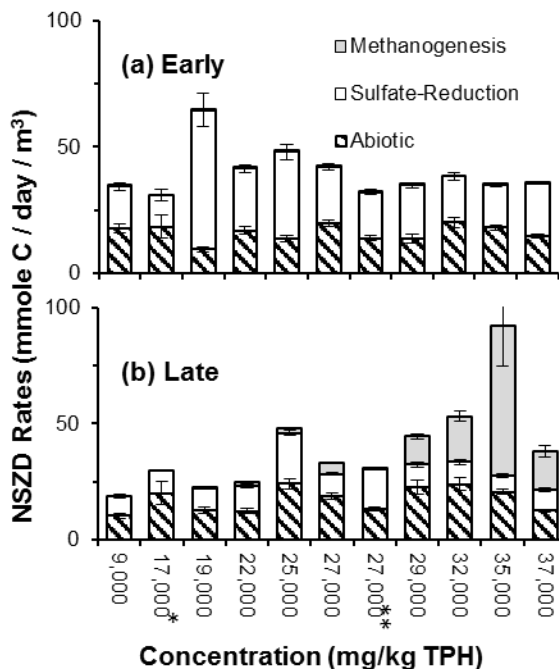


Figure 6 – Mean NSZD molar rates (mmole carbon/day/m<sup>3</sup>) for contributing biological or abiotic processes vs. LNAPL concentration (mg/kg TPH) for early (a) and late (b) periods. Stacked bar graphs separately depict abiotic and biotic NSZD rates with each processes' standard deviation. Control (\*) and nutrient (\*\*) columns rates were averaged over each seven-month period.

Total NSZD rates (Table 2) were of the same order for all TPH concentrations with a standard deviation of  $\pm 9.10$  mmole C/day/m<sup>3</sup> in the early period. When methanogenesis contributed to biotic fractions in the late period, total NSZD rates varied more; standard deviation was  $\pm 19.6$  mmole C/day/m<sup>3</sup>. Yet, total biotic fractions were relatively consistent for both phases with standard deviations of  $\pm 11.1$  mmole C/day/m<sup>3</sup> (Table 2). Abiotic dissolution and volatilization remained generally unchanged between periods, and abiotic fractions remained below 25 mmole C/day/m<sup>3</sup> (Table 2). Biotic NSZD fractions were found to be often higher than abiotic

fractions for both periods, as also depicted in Figure 6. It is important to point out that at the field scale, abiotic fractions are subsequently degraded within or along the boundaries of the source zone. Thus biodegradation rates reported here underestimate biotic fractions for combined systems of LNAPL bodies and dissolved hydrocarbon plumes.

Table 3– Mean NSZD molar rates for early and late periods with average and standard deviation. Control (\*) and nutrient influent (\*\*) columns are included.

Initial Concentration (mg/kg TPH)	Early Period NSZD Rates (mmole carbon/day/m <sup>3</sup> )				Late Period NSZD Rates (mmole carbon/day/m <sup>3</sup> )			
	Abiotic	Sulfate-Reduction	Methanogenesis	Total	Abiotic	Sulfate-Reduction	Methanogenesis	Total
9,000	17.8	16.6	0.0	34.4	10.5	8.4	0.0	18.9
17,000*	18.4	12.5	0.0	30.9	20.0	10.0	0.0	30.0
19,000	9.4	55.0	0.0	64.5	12.7	9.4	0.3	22.4
22,000	16.9	24.5	0.0	41.4	12.4	10.7	1.9	25.1
25,000	13.5	34.5	0.0	48.0	24.3	21.8	2.0	48.0
27,000	19.7	22.5	0.0	42.2	18.7	9.7	4.9	33.3
27,000**	13.7	18.4	0.0	32.2	13.2	17.5	0.0	30.7
29,000	13.8	21.1	0.0	34.8	22.6	9.8	12.1	44.5
32,000	20.0	18.4	0.0	38.4	24.0	9.6	19.6	53.2
35,000	18.1	17.1	0.0	35.2	20.7	6.9	64.8	92.4
37,000	14.6	21.1	0.0	35.7	12.7	8.8	16.9	38.4
<b>Average</b>	16.0	23.8	0.0	39.8	17.4	11.1	11.1	39.7
<b>Std. Deviation</b>	±3.1	±11.2	±0.0	±9.1	±5.0	±4.2	±18.3	±19.6

For the entire experiment, control column mean rate was  $11.6 \pm 24.1$  mmole C/day/m<sup>3</sup>, whereas field derived soils (including the nutrient column) mean rate was  $26.1 \pm 28.9$  mmole C/day/m<sup>3</sup>.

Field-derived soils contributed to biotic NSZD processes such as amorphous precipitates and methanogenesis that were not observed in the control column. However, NSZD rates were not significantly different when only considering abiotic and sulfate-reduction NSZD processes (Table 2). Field LNAPL was not sterilized and control column sand was shortly exposed to

laboratory air during setup. Possibly, organisms were unintentionally carried over from the field LNAPL or from lab exposure. Future work may require a microbial assay performed on the control column soil to compare to organisms transferred via LNAPL versus soil derived organisms.

Additionally, the supplemented nutrients appeared to inhibit methanogenesis under laboratory conditions. Interestingly, a small amount of dissolved methane (0.47 mg/l) was initially detected in the first draining event from the nutrient column indicating that methanogens were initially present in the column. However, thereafter the nutrient column did not produce methane gas (27,000\*\* mg/kg, Figure 6), while its un-supplemented counterpart and the column at 29,000 mg/kg produced significant methane gas.

#### 4.4. Aqueous Hydrocarbon Composition as a Function of LNAPL Concentration

Spiked compound dissolved concentrations did not indicate that compositional weathering occurred during the period of the experiment, as shown in Figure 7. Totalized spiked n-alkanes, naphthalene, and benzene concentrations were relatively consistent and generally ranged between one order of magnitude. High profile COCs, naphthalene and benzene, aqueous concentrations primarily ranged between 1,000 µg/L and 5,000 µg/L with no significant indication that concentrations were diminishing with time or water table fluctuations. Spiked LNAPL columns and field soil without added LNAPL had overlapping range of NSZD rates (Figures 5a and 5c), while spiked columns had mole fractions 1.5 times that of the original field LNAPL. The varying degree of aqueous hydrocarbon concentrations observed was similar across the columns and did not trend with increasing or decreasing NSZD rates.

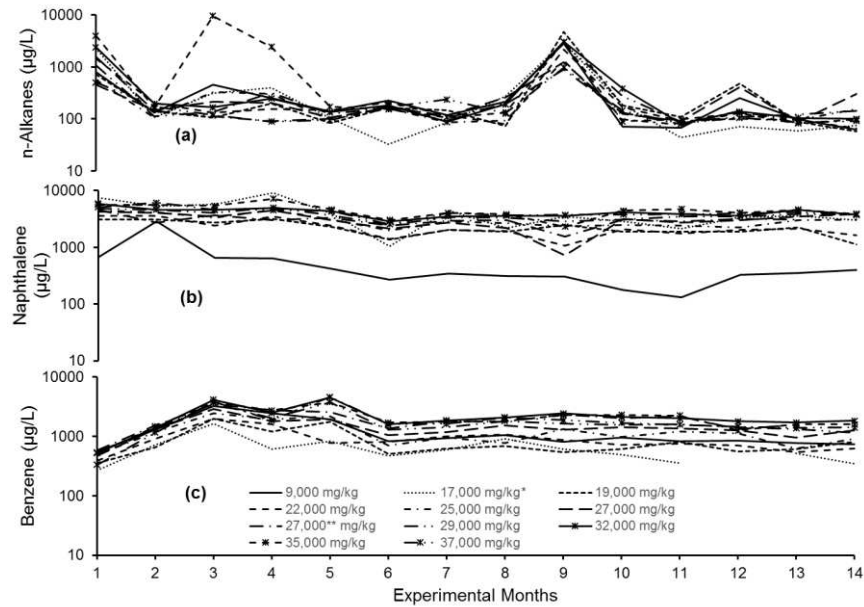


Figure 7 – Log scale aqueous concentrations ( $\mu\text{g/L}$ ) of totalized n-alkanes (a), Naphthalene (b), and Benzene (c) versus experimental months. Naphthalene was initially an LNAPL mole fraction at approximately 0.2. Benzene was initially at a LNAPL mole fraction of approximately 0.01. The 9,000 mg/kg column did not have additional LNAPL added.

Naphthalene and benzene eluted at effective solubility concentrations, yet did not vary in a significant degree as a function of early or late periods. Benzene was shown to elute independently upon initial LNAPL saturation (Figure 7a). Benzene was initially at a LNAPL mole fraction of approximately 0.01, yet median concentrations varied between 890  $\mu\text{g/L}$  (9,000 mg/kg) and 1,930  $\mu\text{g/L}$  (32,000 mg/kg) (Figure 7a). The effective solubility of naphthalene was evidently much higher after spiking, as the 9,000 mg/kg column continually eluted lower concentrations as compared to spiked columns (Figure 7b). Naphthalene dissolved at the highest concentrations as expected due to an initial spiked LNAPL mole fraction at approximately 0.2. Naphthalene concentrations ranged between 130 and 2,800  $\mu\text{g/L}$  from the 9,000 mg/kg column and between 2,500 and 6,100  $\mu\text{g/L}$  from the 37,000 mg/kg column (Figure 7b). The other spiked compounds (n-dodecane, n-tetradecane, n-hexacosane) eluted at much lower concentrations, approximately ranging between 50  $\mu\text{g/L}$  and 200  $\mu\text{g/L}$  (see Appendix C). No apparent trend in spiked compound aqueous concentrations and transition to late-period

conditions were observed. Aqueous concentrations varied to the same degree, regardless of predominantly sulfate-reduction or combination with methanogenesis conditions.

Differences in TPH concentrations and spiked compound composition was compared in nutrient column soil samples between initial homogenized soil and 3 post-experiment grab samples.

TPH concentration reduction was measured at an average 6%, however the range was 3% to 8%. The heterogeneity of the samples was too great to distinguish a quantitative reduction of mass. On the other hand, composition stability seen in Figure 7 was reaffirmed with no significantly favored reductions of benzene or naphthalene over n-alkane spiked compounds.

#### 4.5. Glide Path Model Results

The GPM predicts LNAPL longevity for the field site between 35 and 105 years, depending on the range of NSZD rates input and without considering temperature fluctuations (Figure 8).

Longevity predictions were similar with and without hydraulic recovery. With the high loss rate, LNAPL was predicted to remain (i.e., to be greater than 0.02 m LNAPL) at the field site until the year 2056 (Figure 9). When temperature fluctuations were included in the GPM, the model predicted an additional two years of LNAPL on site. Since the model is deterministic, the temperature fluctuation simulation confirmed a convergence at average-rate longevity. Thus, steady temperature simulations were best suited for providing a longevity window.

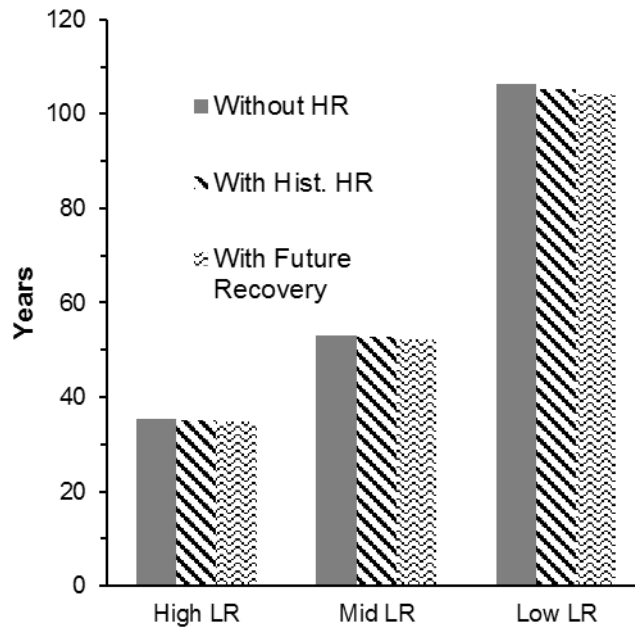


Figure 8 – Years to LNAPL depletion versus NSZD loss rate (LR) without hydraulic recovery (HR), with historical (hist.) HR, and with future hydraulic recovery. High, mid, and low LRs were 2.73, 4.10, and 6.15  $\mu\text{mole C/m}^2/\text{sec}$ , respectively.

A single output of GPM simulations is presented in Figure 8, using an average NSZD field measured flux of approximately 4.10  $\mu\text{mole C/m}^2/\text{sec}$  (Mid LR above). Hydraulic recovery into 2026 of approximately 48  $\text{m}^3$  on a bi-annual basis did not significantly reduce LNAPL longevity. To be precise, hydraulic recovery reduced longevity by 1 to 2 years, for both sets of simulations (steady and fluctuating subsurface temperature). Continuous mass was nearly non-existent when simulations reached a specific volume of 0.02 m. The majority of remaining LNAPL mass remained as immobile (yellow lines in Figure 9) and relied on NSZD for removal, while water table fluctuations changed the fraction of recoverable LNAPL (shown in green lines in Figure 9). The accuracy of the GPM was within  $\pm 8\%$  for predicted recovery versus historical field measured mass recovery in 2012 and 2014. Greater accuracy ( $\pm 5\%$ ) was achieved when recovery periods were adjusted to exactly coincide with GPM 30-day time steps.

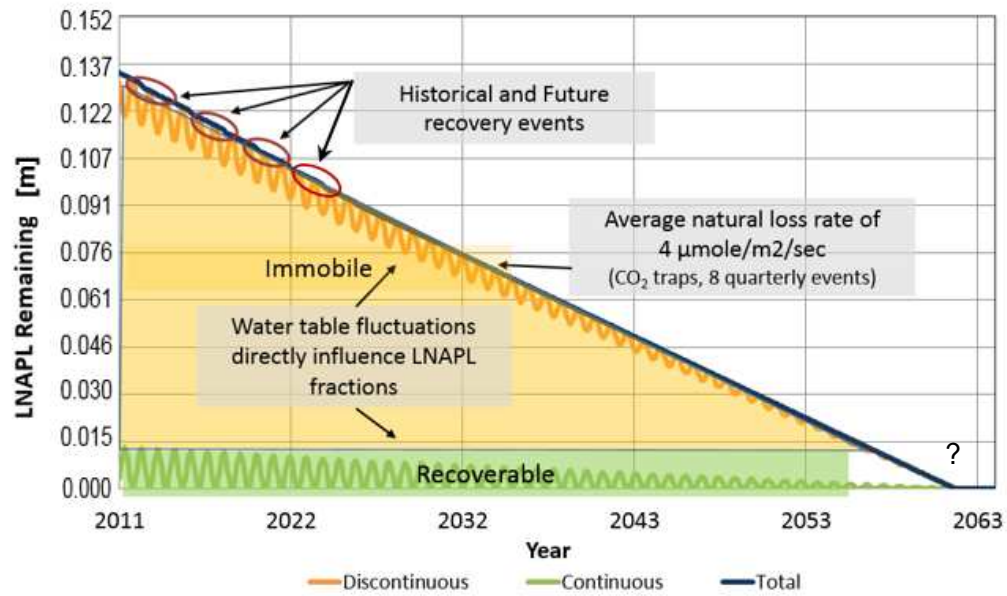


Figure 9 – Depiction of GPM output as total LNAPL (specific volume) for average NSZD loss rate. Immobile LNAPL fractions are shown in yellow shading and line. Mobile, or recoverable, LNAPL fractions are shown in green shading and line. Red circles highlight hydraulic recovery events, both historical and future. Rates are still uncertain below 9,000 mg/kg represented by the ‘?’.

## 5. DISCUSSION AND FURTHER WORK

The following sections will discuss the applicability of results, along with further work posed by evidence of both the laboratory and field-scale studies,

### 5.1. Discussion

NSZD rates were shown to be independent of LNAPL concentration following a zero-order process for LNAPL concentrations and redox conditions tested. Rates did not vary linearly (or exponentially) with LNAPL concentration, in either the early or late period (Figure 5). Under predominantly sulfate-reducing conditions in the early period, a slight negative linear trend with increasing LNAPL concentration was observed (Figure 5b); however, the poor regression fit of 0.0148 indicated rates were statistically random when comparing to LNAPL concentration. Statistical analysis also supported a zero-order hypothesis for the late-period conditions. A p-value of 0.02 rejected the null hypothesis and verified late-period biodegradation processes also were independent of LNAPL concentration. Thus, herein the hypothesis forwarded by Skinner (2015) of zero-order physical NSZD processes was supported and extended to NSZD biodegradation processes, under a specific set of field-relevant conditions. Abiotic NSZD rates represented a similar fraction of total NSZD rates across spiked LNAPL columns. Similar abiotic rates were observed in the 9,000 mg/kg column that contained original LNAPL (Table 2). LNAPL concentrations investigated were consistent with LNAPL concentration ranges observed at middle- to late-stage sites (McCoy et al., 2014; Sale et al., 2016). Therefore, NSZD rates are predicted to not change as LNAPL mass decreases over time, at least over the range of concentrations and conditions tested.

Laboratory rates were similar to previously reported laboratory rates in Joo et al. (2001) and field rates as observed in Amos et al. (2005), Lundegard et al. (2006), and McCoy et al. (2014).

The laboratory mean rate (population of all monthly biodegradation rates) was  $24.8 \pm 17.1$  mmole C/day/m<sup>3</sup> (95% confidence level). Experimental rates did not vary more than one order of magnitude; this variation was narrower than the laboratory rates of 170 to 6,800 mmole C/day/m<sup>3</sup> or measured field rates seen in Lundegard et al. (2006) and McCoy et al. (2014) that ranged one to four orders of magnitude. The laboratory studies used soil from a single site and homogenized it well, likely explaining the narrow range of observed NSZD rates. Further, Amos et al. (2005) measured advective methane gas flux at  $4.50 \times 10^{-11}$  mole CH<sub>4</sub>/s/cm<sup>2</sup>. This rate is equivalent to approximately 194 mmole C/day/m<sup>3</sup> using the 5m vertical length of the oil body in Amos et al. (2005). As Tracy (2015) proposed, field-scale measurements may vary to a significant degree due to soil water heterogeneities, lithological stratification, and in-situ preferential pathways. Since NSZD rates shown here fall within the range of the previous field measurements listed above and vary minimally, findings indicate that factors other than LNAPL mass in a source zone control NSZD rates.

Measurement of dissolved hydrocarbon concentrations (Huntley et al., 2002; McHugh et al., 2013) is not suitable for determining LNAPL deletion rates because as long as LNAPL is present in the subsurface, dissolved concentrations can be at solubility. By contrast, measurement of degradation products (CO<sub>2</sub> and CH<sub>4</sub>) can be used to calculate LNAPL loss rates. Biological NSZD eliminated LNAPL hydrocarbons evident from the amount of inorganic carbon and methane produced. LNAPL weathering was only compared between spiked columns and the 9,000 mg/kg column, but was not observed. Benzene and naphthalene losses from soil were too small to be quantified, so it was not possible to determine if their loss rates were impacted by LNAPL concentration.

Sulfate concentrations changed two to three orders of magnitude during the early-period transition to late-period methanogenic conditions. This change in dissolved sulfate was consistent with redox boundary conditions in Keijzer et al. (1998) that were established when

one electron acceptor was greater than the other by an order of magnitude or more. Methane production increased and carbon dioxide production decreased in the late period, while total NSZD rates remained similar across periods. Methanogenic NSZD processes were dormant (i.e., non-detectable methane concentrations), while effluent sulfate concentration was greater than 20 mg/L. Sulfate concentration of 20 mg/L was not verified as a definitive methanogenic threshold for this particular field soil, but such a threshold may exist in this range. In the field, methane may reach grade where oxidation may not occur, severely reducing carbon dioxide flux measurements (i.e., NSZD rates) (Tracy, 2015). Thus, for some sites, CO<sub>2</sub> trap data is underestimating NSZD rates.

LNAPL exposure did not eliminate biological activity, specifically for anaerobic NSZD processes. Previously, LNAPL was thought to be toxic to microorganisms, thus limiting hydrocarbon degradation to source-zone edges and dissolved plumes (Alexander, 1994). Hydrocarbon biodegradation observed in the control column presented the likelihood of an LNAPL toxicity adaptation behavior similar to what was observed in Irianni Renno et al. (2016). The apparent presence of hydrocarbon-degrading microbes in the control column might be explained by these microbes being present in water droplets immersed in the field LNAPL used to spike the sterilized silica. Ability of microbes to survive within LNAPL may be due to prolonged LNAPL exposure leading to microbial adaptations. Further work could test the exact mechanisms of microbial mobility in source zones and the effect on NSZD rates under natural or engineered conditions.

The experiment provided evidence that nutrients were not a rate-limiting factor for NSZD under middle- and late-stage conditions. Enhanced rates were not observed with a nutrient-supplemented influent, indicating that either field soil contained sufficient nutrients or that other factors limited NSZD rates. Ferguson et al. (2003) suggested inhibition when prescribed C:N:P ratios were followed. The anaerobic influent was sustained at 15 to 20 mg/L sulfate, and a

significant decrease in NSZD rates was not observed during transition to the late period. Experimental results showed that although the subsurface has been impacted with contaminants, natural processes remain dependent upon on general geochemical and biological conditions.

## 5.2. Conclusions and Recommendations for Future Work

### 5.2.1. Conclusions

Understanding LNAPL longevity is critical for engineering practitioners and regulators to guide decision-making regarding LNAPL source zone site management. The prevailing model of LNAPL degradation has been a first-order rate model with rates decreasing by orders of magnitude from early to late stage conditions. However, recent field site studies (McCoy et al., 2014) have reported LNAPL loss rates within an order of magnitude at middle and late-stage sites with different LNAPL saturations, suggesting that loss rates do not depend on LNAPL concentrations. The resulting hypothesis that LNAPL NSZD follows zero order kinetics was tested in this work. Results supported the zero order rate hypothesis over a range of hydrocarbon concentrations (9,000 mg/ kg to 37, 000 mg/kg) under anaerobic conditions. Laboratory mean loss rates differed by 0.1 mmole C/day/m<sup>3</sup> between the early stage of the experiment, when sulfate concentrations were >20 mg/L, and during the late stage, when sulfate was < 20 mg/L and methanogenesis was a major biodegradation pathway. Further, observed laboratory loss rates fell within the range of field-scale loss rates depleting LNAPL between 7,890 L/hectare/yr and 8,060 L/hectare/yr. Notably, laboratory rate measurements were based on detection of degradation products (CO<sub>2</sub> and CH<sub>4</sub>) and hydrocarbons in column effluents and gases produced. Determining LNAPL losses based on degradation product measurement is an emerging approach to tracking NSZD that was applied successfully in this study. Although soil from only one column was analyzed at the conclusion of the study, no

compositional weathering was observed. The Glide Path model was modified using insights from the laboratory study and applied to field data for a middle-stage LNAPL site. Modeling results predicted site longevity and demonstrated that continued active recovery would be insignificant compared to ongoing NSZD processes. Thus, this study provides a scientific basis for selecting NSZD over active remedies at later-stage sites and provides rate data to support longevity models.

### 5.2.2. Future Work

Often LNAPL thicknesses in wells or measured LNAPL saturated zones have been associated with physical mass loss rates, as shown in Miles et al. (2008) or Reddi et al. (1998). This experiment homogenized soils. While field-scale lithological heterogeneities were not investigated in this experiment, Anneser et al. (2008) and Irianni Renno et al. (2016) provided field evidence that geochemical and biological heterogeneities are on a scale of centimeters. Thus, field-scale heterogeneities may play an important role in spatially-resolved *in situ* biodegradation rates. Perhaps enhancing the precision of in-situ NSZD rate measurements with continued biological monitoring may resolve subsurface heterogeneities. Future work could also investigate NSZD rates for a broader range of LNAPL concentrations (e.g., below 9,000 mg/kg) and under completely methanogenic conditions (i.e., without any sulfate). To achieve the latter, new approaches are needed to replicate conditions in the laboratory. Longer-term, multi-year studies might also provide insight into the final stages of the LNAPL glide path.

In the GPM, longevity predictions estimated the time while LNAPL was the predominant hydrocarbon phase, often a LNAPL specific volume > 0.02 m. Below 0.02m, at late-stage sites, adsorbed hydrocarbons may outweigh discontinuous LNAPL fractions. Adsorbed mass follows nonlinear desorption, limiting available hydrocarbon mass for biodegradation (Schwarzenbach 2003). Zero-order processes may not apply beyond LNAPL concentrations tested in the

experiment where desorption of hydrocarbons may control rates. The GPM was limited to predicting total site risk; however, analytical models depicting nonlinear desorption trends, such that presented in Miles et al. 2008, may be attached to the GPM, identifying possible biodegradation kinetic rates. Continuing studies will need to address NSZD processes as LNAPL has been depleted to < 0.02 m specific volume.

## 6. REFERENCES

- Adetutu, E., Weber, J., Aleer, S., Dandie, C., Aburto-Medina, A., Ball, A., & Juhasz, A. (2013). Assessing impediments to hydrocarbon biodegradation in weathered contaminated soils. *Journal of Hazardous Materials*, 847-853. <http://dx.doi.org/10.1016/j.jhazmat.2013.01.052>
- Alexander, M. (1994). *Biodegradation and bioremediation*. San Diego, California: Academic Press.
- Amos, R., Mayer, K., Bekins, B., Delin, G., & Williams, R. (2005). Use of dissolved and vapor-phase gases to investigate methanogenic degradation of petroleum hydrocarbon contamination in the subsurface. *Water Resources Research* *Water Resources. Res.*
- Anneser, B., Einsiedl, F., Meckenstock, R., Richters, L., Wisotzky, F., & Griebler, C. (2008). High-resolution monitoring of biogeochemical gradients in a tar oil-contaminated aquifer. *Applied Geochemistry*, 23, 1715-1730. doi:10.1016/j.apgeochem.2008.02.003
- Borden, R., & Kao, C. (1992). Evaluation of groundwater extraction for remediation of petroleum-contaminated aquifers. *Water Environment Research Water Environ Res*, 64(1), 28-36.
- Brezonik, P., & Arnold, P. (2011). *Water chemistry: An introduction to the chemistry of natural and engineered aquatic systems*. New York, New York: Oxford University Press.
- Brost, E., & DeVaul, G. (2009). Non-Aqueous Phase Liquid (NAPL) Mobility Limits in Soil. *Soil and Groundwater Research Bulletin*, 9. Retrieved from [http://www.epa.gov/~media/files/ehs/clean\\_water/bulletins/09\\_bull.pdf](http://www.epa.gov/~media/files/ehs/clean_water/bulletins/09_bull.pdf)
- Bundy, J., Paton, G., & Campbell, C. (2002). Microbial communities in different soil types do not converge after diesel contamination. *J Appl Microbiol Journal of Applied Microbiology*, 22, 276-288.
- Chou, H., Huang, J., Chen, W., & Ohara, R. (2008). Competitive reaction kinetics of sulfate-reducing bacteria and methanogenic bacteria in anaerobic filters. *Bioresource Technology*, 99, 8061-8067. doi:10.1016/j.biortech.2008.03.044

- Coulon, F., Pelletier, E., Gourhant, L., & Delille, D. (2005). Effects of nutrient and temperature on degradation of petroleum hydrocarbons in contaminated sub-Antarctic soil. *Chemosphere*, 58, 1439-1448. doi:10.1016/j.chemosphere.2004.10.007
- Dobson, R., Schroth, M., & Zeyer, J. (2007). Effect of water-table fluctuation on dissolution and biodegradation of a multi-component, light nonaqueous-phase liquid. *Journal of Contaminant Hydrology*, 94, 235-248. doi:10.1016/j.jconhyd.2007.07.007
- Domenico, P., & Schwartz, F. (1990). *Physical and chemical hydrogeology*. New York, New York: Wiley.
- Ehrlich, H. (1996). *Geomicrobiology* (3rd ed.). New York, New York: M. Dekker.
- EPA. (2015, November 23). Retrieved November 25, 2015, from <http://www2.epa.gov/superfund>
- Ferguson, S.H., Franzmann P.D., Revill A.T., Snape I., Rayner J.L. (2003). The effect of nitrogen and water on mineralization of hydrocarbons in diesel-contaminated terrestrial Antarctic soils. *Cold Regions Science and Technology* 37, 197–212.
- Huntley, D., & Beckett, G. (2002). Persistence of LNAPL sources: Relationship between risk reduction and LNAPL recovery. *Journal of Contaminant Hydrology*, 59, 3-26.
- Irianni-Renno, M, Akhbari, D., Olson, M.R., Byrne, A.P., Lefevre, E., Zimbron, J., Lyverse, M., Sale, T., De Long, S.K. (2015) Comparison of bacterial and archaeal communities in depth-resolved zones in an LNAPL body. *Applied Microbiology and Biotechnology*, 100(7), 3347-3360.
- Johnson, P., Lundegard, P., & Liu, Z. (2006). Source Zone Natural Attenuation at Petroleum Hydrocarbon Spill Sites I: Site-Specific Assessment Approach. *Ground Water Monitor Remediation Ground Water Monitoring and Remediation*, 26(4), 82-92.
- Joo, Choon-sung, Young-sook Oh, & Wook-Jin Chung. (2001). Evaluation of Bioremediation Effectiveness by Resolving Rate-Limiting Parameters in Diesel-Contaminated Soil. *Microbiology and Biotechnology*, 11(4), 607-613.
- Kampbell, D., & Vandegrift, S. (1998). Analysis of Dissolved Methane, Ethane, and Ethylene in Ground Water by a Standard Gas Chromatographic Technique. *Journal of Chromatographic Science*, 36(May), 253-256.

- Keijzer, H., Zee, S., & Leijnse, A. (1998). Characteristic regimes for in-situ bioremediation of aquifers by injecting water containing an electron acceptor. *Computational Geosciences*, 2, 1-22.
- Kim, J., & Corapcioglu, M. (2002). Modeling dissolution and volatilization of LNAPL sources migrating on the groundwater table. *Journal of Contaminant Hydrology*, 65, 137-158. doi:10.1016/S0169-7722(02)00105-5
- Lindsay, W. (1977). *Chemical equilibria in soil*. New York, New York: Wiley Interscience.
- Liu, P., Wang, S., Huang, S., & Wang, M. (2012). Effects of soil organic matter and ageing on remediation of diesel-contaminated soil. *Environmental Technology*, 33(23), 2661-2672. doi:10.1080/09593330.2012.673017
- Lundegard, P., Johnson, P. (2006). Source Zone Natural Attenuation at Petroleum Hydrocarbon Spill Sites II: Application to a Former Oil Field. *Ground Water Monitor Remediation Ground Water Monitoring and Remediation*, 26(4), 93-106.
- Mccoy, K., Zimbron, J., Sale, T., & Lyverse, M. (2014). Measurement of Natural Losses of LNAPL Using CO<sub>2</sub> Traps. *Groundwater*, 53(4) 658-667. doi:10.1111/gwat.12240
- Mchugh, T., Kulkarni, P., Newell, C., Connor, J., & Garg, S. (2014). Progress in Remediation of Groundwater at Petroleum Sites in California. *Groundwater*, 52(6), 898-907. doi:10.1111/gwat.12136
- Mercer, J., Adeel, Z., & Faust, C. (ASCE 1996). A Review of NAPL Modeling Approaches for Remediation. In *Non-aqueous phase liquids (NAPLs) in subsurface environment: Assessment and remediation : Proceedings of the specialty conference held in conjunction with the ASCE National Convention, Washington, D.C., November 12-14, 1996* (pp. 46-65). New York, New York: American Society of Civil Engineers.
- Miles, B., Maji, R., Sudicky, E., Teutsch, G., & Peter, A. (2008). A pragmatic approach for estimation of source-zone emissions at LNAPL contaminated sites. *Journal of Contaminant Hydrology*, 96, 83-96. doi:10.1016/j.jconhyd.2007.10.003
- Newell, C., Acree, S., Ross, R., & Huling, S. (1995). Light Nonaqueous Phase Liquids. *Ground Water Issue, EPA/540/S-95/500*. Retrieved from <http://nepis.epa.gov>

Reddi, L., Han, W., & Banks, M. (1998). Mass Loss from LNAPL Pools under Fluctuating Water Table Conditions. *J. Environ. Eng. Journal of Environmental Engineering*, 124(12), 1171-1177.

Rittmann, B., & McCarty, P. (2001). Chapter 1. In *Environmental biotechnology: Principles and applications*.

Sale, T. 2001. Methods for Determining Inputs to Environmental Petroleum Hydrocarbon Mobility and Recovery Models. API Publication Number 4711. American Petroleum Institute.

Sale, T. 2016. Answers to Frequently Asked Questions about Managing Risk at LNAPL Sites. Bulletin #18 American Petroleum Institute Soil and Groundwater Research, 2<sup>nd</sup> Addition. Washington, DC.

Sanscartier, D., Reimer, K., Koch, I., Laing, T., & Zeeb, B. (2009). An Investigation of the Ability of a 14 C-Labeled Hydrocarbon Mineralization Test to Predict Bioremediation of Soils Contaminated with Petroleum Hydrocarbons. *Bioremediation Journal*, 13(2), 92-101.

Schiewer, S., & Niemeyer, T. (2006). Soil heating and optimized nutrient addition for accelerating bioremediation in cold climates. *Polar Record*, 42(220), 23-23.  
doi:10.1017/S0032247405004833

Schwarzenbach, R., Gschwend, P., & Imboden, D. (2003). *Environmental organic chemistry* (2nd ed.). New York, New York: Wiley.

Singh, A., & Ward, O. (2004). *Biodegradation and bioremediation*. New York, New York: Springer.

Sinke, A., Dury, O., & Zobrist, J. (1998). Effects of a fluctuating water table: Column study on redox dynamics and fate of some organic pollutants. *Journal of Contaminant Hydrology*, 33, 231-246.

Trindade, P., Sobral, L., Rizzo, A., Leite, S., & Soriano, A. (2005). Bioremediation of a weathered and a recently oil-contaminated soils from Brazil: A comparison study. *Chemosphere*, 58, 515-522. doi:10.1016/j.chemosphere.2004.09.021

U.S. Government Publishing Office (GPO) (2016). Electronic Code of Federal Regulations. ecf.gov. U.S. Government Publishing Office. First Retrieved October 14, 2015.

Wilson, J. T., Kaiser, P. M., & Adair, C. (2005). *Monitored natural attenuation of MTBE as a risk management option at leaking underground storage tank sites*. National Risk Management Research Laboratory, Office of Research and Development, US Environmental Protection Agency.

Zeman, N., Renno, M., Olson, M., Wilson, L., Sale, T., & Long, S. (2014). Temperature impacts on anaerobic biotransformation of LNAPL and concurrent shifts in microbial community structure. *Biodegradation*, 25, 569-585. doi:10.1007/s10532-014-9682-5

Zysset, A., Stauffer, F., & Dracos, T. (1994). Modeling of reactive groundwater transport governed by biodegradation. *Water Resources Research Water Resour. Res.*, 30(8), 2423-2434.

## 7. APPENDICES

### 7.1. Appendix A – Draining and Saturating Procedures

1. Prepping for draining event (week prior)
  - a. Acid Wash glassware and inline sampler unit.
    - i. Dilute Hydrochloric Acid in Tap Water (typically amounts are ~10mL in 2.5L)
    - ii. Flow diluted acid wash through pump assembly using tubing marked “CN”
    - iii. Pour acid wash into graduated cylinders (50mL) that have oxides on them
    - iv. Dry assembly via fume hood. Dry vials and graduated cylinder in oven.
  - b. pH buffer
    - i. Use pHYDRION buffer kit for 4, 7, and 10 pH buffer solutions
    - ii. Mix 100mL DI water with capsule contents in amber jars
    - iii. Put pH buffer for experiment in 40 mL VOAs
    - iv. Typically change out buffer in VOAs every third draining, i.e. three months
  - c. Print out sampling sheets if less than three spots left on either gas sampling or water sampling sheets
    - i. Template in T:\...\Shell\Eric\Notes\Templates\ColumnSamplingSheet-template.xlsx
2. Morning prep for draining event
  - a. Turn GC/FID #2 to FID-GMAN and make sure Signal 2 is less than 14.0 after 30mins (press Signal 2 button on GC to read value)
  - b. Place pH and ORP probes in Tap Water for at least 30-45min prior to calibration
  - c. Place 1L of DI water under vacuum for gas capture reservoir
  - d. Take Pictures (See Picture S.O.P. below for details)
  - e. After Signal 2 is at equilibrium shoot 50uL of nitrogen gas through (N2-1.m) to look for ‘ghost’ peaks
    - i. There typically is a negligible small peak right at 1.00min from residual methane/methanol in injector
    - ii. If quantifiable ‘ghost’ peaks are detected (use DataAnalysis intergration FID-DRO), raise oven temp to 100°C for approx. 30min
  - f. Calibrate pH and ORP probes:
    - i. pH: Using either Denver Instrument controllers or other, perform a multi-point calibration with the 4,7, and 10 buffer solutions as per instruction manuals. (If other controllers only use two-points, perform just with 7 and 10 as pH has been >7 for a while). Record pH measured after pH point is entered into controller and final slope%
    - ii. ORP: Pour approx. 15mL (just enough to cover electrode) in 40mL VOA and observe first steady reading (typically between 195 and 200) and

record (NOTE: DO NOT SWIRL VOA AS THIS CAUSES OXYGEN INTRODUCTION).

- g. Measure Gas volumes in ALL gas captures without taking sample. (Accounts for a barometric affect or gas produced just in case if draining is spanned over two days)
- h. Turn on GC/TCD to TCD-CO2-EE

### 3. Pictures S.O.P.

- a. Plug in work lamp for light during pictures
- b. Label page in Lab Notebook with date, “#th Draining Event” and columns: COL#, IMG 100-, and Obs. (observations)
- c. Setup camera on tripod
  - i. Tripod Settings:
    - 1. 11.25” (middle extension), bottom of base 33.25” from floor
    - 2. Table Angle= 10.5°
  - ii. Camera Settings: ISO=6400 (max of camera spectrum), Shutter=1/100 sec, Exposure=-3, Aperture=7.1, Auto-Focus (“AF/MF” small switch at lense)
- d. Align tripod ‘plum-bob’ with column tape on floor.
- e. Place UV light on rack at specific column with hooks at black marks to the left and right of #, hooks must go through large holes on rack and suspended on all-thread, not the rack itself
- f. Place camera at 30.5” from column. Measure from column glass to large electrode for flash on top of camera
- g. Tweak UV light at the hooks so it is parallel with the column and out of the shot
- h. Adjust tripod table and camera so column is situated between white square in frame
  - i. Rotate the table while holding camera at the column to slightly adjust frame angle
- i. Turn off work light, slightly press button down until white square turns green (you should hear the camera auto-focus to adjust for light) then take picture with full press
- j. Record IMG 100-#### for use in picture analysis
- k. Repeat for other columns

### 4. Gas Samples

- a. Record Gas Volume Measurement and circle “Y” for sampled on Gas Sampling Sheet
- b. Ambient pressure readings can be recorded from:  
<http://climate.colostate.edu/~autowx/>
- c. Attach 1mL glass syringe for gas sample to vertical port and open valve

**(NOTE: always turn valve OFF position to horizontal port to avoid air entering capture)**

- i. Purge ~0.5mL to remove air from valve
  - ii. Fluctuate syringe three times, on third fluctuation close syringe valve first then gas capture valve
  - iii. Attach septum to glass syringe end
  - iv. Inject gas sample using 50uL syringe
    1. First into GC/FID-GMAN (NOTE: make sure to put data into a folder with yr/month/dayINITIALS)
    2. Second into GC/TCD-CO2-EE (NOTE: make sure to put data into a folder with INITIALSyear/month/day)
  - v. Clean 50uL syringe by extruding 50uL nitrogen gas from Tedlar bag
  - vi. Clean 1mL syringe by removing plunger and flowing air through to remove moisture that may have accumulated
- d. Bag Removal
- i. Vacuum/clean-out column specific Tedlar bag and shut valve while bag is under negative pressure
  - ii. Attach the Tedlar bag to the vertical port and the 60mL syringe to the horizontal port
  - iii. Remove gas by turning valve to the horizontal port and the OFF position at the vertical port
  - iv. Turn valve to the vertical port and horizontal port
  - v. Open Tedlar bag (NOTE: Only one complete turn, 'mark-to-mark')
  - vi. Push gas into Tedlar bag
  - vii. **Close Tedlar bag before turning valve**
  - viii. Repeat until desired volume of gas has been removed
  - ix. No less than 130mL on draining events, no less than 20mL on saturating events
  - x. Use 50uL syringe for analysis and label data file as COL#-Bag
5. Beginning Draining
- a. Remove de-aired DI water from vacuum pump and set aside
  - b. Inline sampler assembly should be setup with the pH probe before the ORP probe
  - c. Attach column specific tubing (labeled with #) to pump and labeled 20mL sampler assembly (first samples get COL#:1)
  - d. Put 50mL graduated cylinder at the end of assembly for recording purged volume
  - e. Attach tubing to selected column and un-clasp hemostat from just the vertical 'T'
  - f. Begin the purge with the pump set at '40'
  - g. Hold vial upside down to allow entrapped air in the lines to escape
  - h. Record Start time on water sampling sheet.
6. Removing the first sample

- a. After approximately 45mL (or when water table is 6-8" below top of soil column), check probe readings and see if ORP has stabilized (pH typically is very steady by this point)
  - b. Slow pump to a setting of '10'
  - c. When ORP has stabilized and does not change 0.5% within three seconds, record readings and purge volume
  - d. Remove sample with pump no less than a setting of '10' to continue flow
  - e. Cap vial with no headspace and replace with second sample vial (COL#:2)
  - f. Set pump back on '40' setting
  - g. Place purged volume in 40mL VOA with COL# label and keep closed
7. Removing the second sample
- a. After approximately 30mL to 35mL (or when water table is 6-8" from the fine sand layer), check probe readings and see if ORP has stabilized
  - b. Slow pump to a setting of '10'
  - c. When ORP has stabilized and does not change 0.5% within three seconds, record readings and purge volume
  - d. Remove sample with pump no less than a setting of '10' to keep flow
  - e. Cap vial with no headspace and replace with blank vial
  - f. Place purged volume in 40mL VOA with COL# label
  - g. Set pump back on '30' setting (slower flow to reduce mobile LNAPL falling below the fine sand layer and into the effluent)
  - h. At this point, fill the water reservoir with 125 -150mL of de-aired DI water
8. Final Purge Volume
- a. Observe water table in the column to see how close it is to the fine sand layer
  - b. Typically purge volumes are 95-110mL, COL7 is C~75mL (except the unspiked/COL9 and LNAPL+Sand/COL10 =  $\geq 120\text{mL}$ ), if purge volume after the second sample exceeds 25mL a water quality reading can be taken, mark as 'No Sample' on sampling sheet to indicate no 20mL vial was taken
  - c. Slow the pump to '20', or '10' if needed, near the end to allow for stabilized reading
  - d. Record once readings stabilize and cease pumping
  - e. Replace hemostat at vertical 'T' and place extra purge volume in 40mL VOA, waste excess after 40mL VOA has been filled with no headspace
  - f. Record Total Purge Volume and Gas Displacement (ON BOTH SHEETS AND IN NOTEBOOK), as well as Sample Volume, # of samples, and vial sizes
  - g. Attach pump assembly to 1L beaker of Tap Water and flow ~70mL through blank vial and flow cell (Pump assembly wash should be considered 'Haz' waste)
1. REPEAT STEPS 4 THROUGH 8 FOR OTHER COLUMNS

2. Prepping for Saturating event (week prior)
  - Print out sampling sheets if less than three spots left on either gas sampling or water sampling sheets
    - i. Template in T:\...\Shell\Eric\Notes\Templates\ColumnSamplingSheet-template.xlsx
3. Morning prep for Saturating event
  - a. Turn GC/FID #2 to FID-GMAN and make sure Signal 2 is less than 14.0 after 30mins (press Signal 2 button on GC to read value)
  - b. Place 1L of DI water under vacuum for gas capture reservoir
  - c. Take Pictures (See Picture S.O.P. below for details)
  - d. After Signal 2 is at equilibrium shoot 50uL of nitrogen gas through (N2-1.m) to look for 'ghost' peaks
    - i. There typically is a negligible small peak right at 1.00min from residual methane/methanol in injector
    - ii. If quantifiable 'ghost' peaks are detected (use DataAnalysis intergration FID-DRO), raise oven temp to 100°C for approx. 30min
  - e. Measure Gas volumes in ALL gas captures without taking sample. (Accounts for a barometric affect or gas produced just in case if draining is spanned over two days)
  - f. Turn on GC/TCD to TCD-CO2-EE
4. Pictures S.O.P.
  - a. Plug in work lamp for light during pictures
  - b. Label page in Lab Notebook with date, "#th Draining Event" and columns: COL#, IMG 100-, and Obs. (observations)
  - c. Setup camera on tripod
    - i. Tripod Settings:
      1. 11.25" (middle extension), bottom of base 33.25" from floor
      2. Table Angle= 10.5°
    - ii. Camera Settings: ISO=6400 (max of camera spectrum), Shutter=1/100 sec, Exposure=-3, Aperture=7.1, Auto-Focus ("AF/MF" small switch at lense)
  - d. Align tripod 'plum-bob' with column tape on floor.
  - e. Place UV light on rack at specific column with hooks at black marks to the left and right of #, hooks must go through large holes on rack and suspended on all-thread, not the rack itself
  - f. Place camera at 30.5" from column. Measure from column glass to large electrode for flash on top of camera
  - g. Tweak UV light at the hooks so it is parallel with the column and out of the shot

- h. Adjust tripod table and camera so column is situated between white square in frame
    - i. Rotate the table while holding camera at the column to slightly adjust frame angle
  - i. Turn off work light, slightly press button down until white square turns green (you should hear the camera auto-focus to adjust for light) then take picture with full press
  - j. Record IMG 100-#### for use in picture analysis
  - k. Repeat for other columns
5. Flushing influent lines
- a. Plug in Peristaltic pump, setting ~15.00
  - b. See if Nitrogen gas headspace needs replacing before starting pump
  - c. Attach one or two influent lines in cassettes
  - d. Flush out ~200mL water, observe cascade for 'carry-over' to begin
  - e. Continue flushing until cascade is operating at steady rate
  - f. Pause pumping, leave manifold #1 connected
6. Gas Samples
- a. Record Gas Volume Measurement and circle "Y" for sampled on Gas Sampling Sheet
  - b. Ambient pressure readings can be recorded from:  
<http://climate.colostate.edu/~autowx/>
  - c. Attach 1mL glass syringe for gas sample to vertical port and open valve  
**(NOTE: always turn valve OFF position to horizontal port to avoid air entering capture)**
    - i. Purge ~0.5mL to remove air from valve
    - ii. Fluctuate syringe three times, on third fluctuation close syringe valve first then gas capture valve
    - iii. Attach septum to glass syringe end
    - iv. Inject gas sample using 50uL syringe
      - 1. First into GC/FID-GMAN (NOTE: make sure to put data into a folder with yr/month/dayINITIALS)
      - 2. Second into GC/TCD-CO2-EE (NOTE: make sure to put data into a folder with INITIALSyear/month/day)
    - v. Clean 50uL syringe by extruding 50uL nitrogen gas from Tedlar bag
    - vi. Clean 1mL syringe by removing plunger and flowing air through to remove moisture that may have accumulated
  - d. Bag Removal
    - i. Vacuum/clean-out column specific Tedlar bag and shut valve while bag is under negative pressure

- ii. Attach the Tedlar bag to the vertical port and the 60mL syringe to the horizontal port
- iii. Remove gas by turning valve to the horizontal port and the OFF position at the vertical port
- iv. Turn valve to the vertical port and horizontal port
- v. Open Tedlar bag (NOTE: Only one complete turn, 'mark-to-mark')
- vi. Push gas into Tedlar bag
- vii. **Close Tedlar bag before turning valve**
- viii. Repeat until desired volume of gas has been removed
- ix. No less than 130mL on draining events, no less than 20mL on saturating events
- x. Use 50uL syringe for analysis and label data file as COL#-Bag

#### 7. Beginning Saturating

- a. Remove de-aired DI water from vacuum pump and set aside
- b. Open first column, lower 'T', for flushing
- c. Put 50mL graduated cylinder at the end of poly-line
- d. Begin the flow at setting from previous saturating (13-15 setting)
- e. Using a stopwatch and the graduated cylinder, calibrate flow to approx. 13.5 mL/min +/- 0.5mL/min.
- f. Note: Flow-rate will slow down once column water level rises.
- g. Pause pumping after at least 50mL of discharge and flow rate has been calibrated and recorded.
- h. Remove poly-line and close 'T'.
- i. Unclasp vertical 'T', start pump, begin stopwatch

#### 8. Final Fill Volume

- a. Observe water table in the column to see how close it is to the top
- b. Typically fill volumes are 95-110mL, COL7 is C~75mL (except the unspiked/COL9 and LNAPL+Sand/COL10 =  $\geq 120\text{mL}$ )
- c. Cease pump and pause the stopwatch.
- d. Replace hemostat at vertical 'T', if needed fill water reservoir with de-aired DI water
- e. Record Total Purge Volume and Gas Displacement (ON BOTH SHEETS AND IN NOTEBOOK)
- f. Clasp influent line and move to next manifold.

#### 9. Continuing ...

- a. REPEAT STEPS 5 THROUGH 7 FOR OTHER COLUMNS
- b. If at the end of a manifold, flush ~30mL through end of next manifold before continuing to step 5

## 7.2. Appendix B – GRO & DRO Calibration Procedures

Table 4 – GRO Calibration Matrix

Initial Water GRO Concentration (mg/L)	Headspace Concentration (ppm) after equilibrium	Benzene Headspace Concentration (ppb)
0.5	1009	25
1.25	2524	63
2.5	5047	127
3.75	7571	190
5	10094	253
15	30282	760
25	50471	1267
35	70659	1774
45	90847	2281

1. Make up a stock solution just like the BTEX solution in 125mL bottle with septum cap. Add 7.13uL of each BTEX and 9.5uL n-Hexane to DI water. Let shake on tumbler overnight.
2. Fill Headspace vial with 21.4mL of DI water.
3. Cap with crimp cap.
4. With vial upside down, inject prescribed total volume (far right column) into closed vial near bottom (use long green needle) and evacuate with shorter green needle.
5. Shake on Vortex for 30min
6. With vial still upside down, remove 5mL of water and replace with nitrogen gas at same time.
7. Repeat for different concentrations.

Table 5 – Volume of GRO Standard for calibration

Water GRO Concentration (mg/L)	Vol To Add to Closed Vial
0.5	42.8uL
1.25	107uL
2.5	214uL
3.75	321uL
For Gas Samples	
5	430uL
15	1.28mL
25	2.14mL
35	3.00L
45	3.85mL

DRO STANDARDS FROM 6.23 G/L-HEXANE STOCK N-HEXANE SOLUTION

-Calibration Range from 0.05g/L-hexane to 0.75 g/L-hexane

-Need approximately 10mL pure hexane in a clean jar for dilution. Will need more for sample syringe cleaning

-Need 6 or 7 vials for standards

-Use inserts for calibration vials (total vial volume = 500uL)

-Pipet the following volumes into the 500uL inserts with rest of the volume n-Hexane:

0.05 g/L - 4uL

0.15 g/L - 12uL

0.25 g/L - 20uL

0.50 g/L - 40uL

0.75 g/L - 60uL

-Place leftover dilution hexane in a blank vial, with or without insert, depending on volume.

Label CN-1

NAPHTHALENE STANDARD FROM 250MG/L-HEXANE STOCK N-HEXANE SOLUTION

-DO NOT use 500uL inserts for naphthalene standards

-Shake standard vial on small vortex to dissolve any solid form naphthalene that may have formed (more common in methanol standard)

--Pipet the following volumes into the 2mL GC vials with rest of the volume n-Hexane:

12.5 mg/L - 100uL

25 mg/L - 200uL

50 mg/L - 400uL

100 mg/L - 800uL

### 7.3. Appendix C- Analytical Measurements

Table 6 – Analytical Measurements for eleven experimental columns

Column ( <i>Initial Soil Concentration</i> )	Date	Conditions	AQUEOUS													NOTE
			TPH (mg/L)	GRO (mg/L)	DRO (mg/L)	Benzen e (µg/L)	Naphthalene (µg/L)	n-Dodecane C <sub>12</sub> (µg/L)	n-Tetradecane C <sub>14</sub> (µg/L)	n-Hexacosane C <sub>26</sub> (µg/L)	CO2 (mg/L)	CH4 (mg/L)	Sulfate (mg/L)	Average pH	Average <sup>1</sup> ORP (mV Ag/AgCl)	
1 (19,000mg/Kg)	7/2/2014	Saturated	40.4	2.4	38.0	350	3,117	49	73	593	100	0.37	1,060	6.65	-85.4	
	7/17/2014	Drained	--	--	--	--	--	--	--	--	--	--	--	--	--	
	7/30/2014	Saturated	17.8	7.0	10.8	660	3,065	33	63	43	153	ND	1,906	6.52	-132.8	
	8/14/2014	Drained	--	--	--	--	--	--	--	--	--	--	--	--	--	
	8/27/2014	Saturated	31.3	20.6	10.7	1,950	2,707	31	69	7	176	ND	900	7.27	-149.2	
	9/10/2014	Drained	--	--	--	--	--	--	--	--	--	--	--	--	--	
	9/29/2014	Saturated	20.0	7.2	12.8	1,205	3,177	115	63	21	64	ND	130	7.26	-53.7	
	10/9/2014	Drained	--	--	--	--	--	--	--	--	--	--	--	--	--	
	10/23/2014	Saturated	22.7	17.7	5.0	1,734	2,293	24	43	17	44	ND	48	7.26	-108.1	
	11/6/2014	Drained	--	--	--	--	--	--	--	--	--	--	--	--	--	
	11/20/2014	Saturated	6.7	3.9	2.8	503	1,381	19	25	122	31	ND	21	6.73	-85.6	
	12/4/2014	Drained	--	--	--	--	--	--	--	--	--	--	--	--	--	
	12/18/2014	Saturated	11.4	1.7	9.7	622	2,016	21	81	45	31	0	8	6.66	-9.4	
	1/3/2015	Drained	--	--	--	--	--	--	--	--	--	--	--	--	--	
	1/15/2015	Saturated	13.2	6.5	6.6	682	1,878	32	26	15	27	0	8	7.10	-111.2	
	1/28/2015	Drained	--	--	--	--	--	--	--	--	--	--	--	--	--	
	2/11/2015	Saturated	55.9	2.5	53.4	544	2,496	135	114	4,436	17	0	5	7.08	-105.2	3.99(GRO), 24.07(CO2), 0.54 (Sulfate)
	2/27/2015	Drained	--	--	--	--	--	--	--	--	--	--	--	--	--	
	3/13/2015	Saturated	63.7	4.1	59.6	611	1,877	28	39	114	14	0.01	3	7.11	-110.4	
	3/28/2015	Drained	--	--	--	--	--	--	--	--	--	--	--	--	--	
	4/10/2015	Saturated	10.9	6.3	4.6	812	1,870	31	24	54	18	0.00	5	7.13	-121.3	
	4/24/2015	Drained	--	--	--	--	--	--	--	--	--	--	--	--	--	
	5/9/2015	Saturated	30.9	6.0	24.9	553	1,864	45	264	176	18	0.09	2	7.09	-125.9	
	5/22/2015	Drained	--	--	--	--	--	--	--	--	--	--	--	--	--	
	6/5/2015	Saturated	12.5	6.7	5.8	606	2,242	35	30	24	15	0.10	2	7.16	-129.5	
	6/18/2015	Drained	--	--	--	--	--	--	--	--	--	--	--	--	--	
7/7/2015	Saturated	15.9	8.2	7.7	809	1,136	24	15	18	18	0.09	0.3	7.18	-135.6		
7/21/2015	Drained	--	--	--	--	--	--	--	--	--	--	--	--	--		

Column (Initial Soil Concentration)	Date	Conditions	AQUEOUS													NOTE	
			TPH (mg/L)	GRO (mg/L)	DRO (mg/L)	Benzene (µg/L)	Naphthalene (µg/L)	n-Dodecane C <sub>12</sub> (µg/L)	n-Tetradecane C <sub>14</sub> (µg/L)	n-Hexacosane C <sub>26</sub> (µg/L)	CO2 (mg/L)	CH4 (mg/L)	Sulfate (mg/L)	Average pH	Average <sup>1</sup> ORP (mV Ag/AgCl)		
2 (22,000mg/Kg)	7/2/2014	Saturated	60.8	3.7	57.1	390	3,541	109	93	1,237	100	0.41	1,360	6.66	-155.3		
	7/17/2014	Drained	--	--	--	--	--	--	--	--	--	--	--	--	--		
	7/30/2014	Saturated	22.8	8.0	14.8	910	3,546	38	73	93	128	ND	1,700	6.51	-154.6		
	8/14/2014	Drained	--	--	--	--	--	--	--	--	--	--	--	--	--		
	8/27/2014	Saturated	36.8	26.8	10.0	1,995	2,416	47	63	23	173	ND	780	6.62	-146.8		
	9/10/2014	Drained	--	--	--	--	--	--	--	--	--	--	--	--	--		
	9/29/2014	Saturated	21.7	8.7	13.0	1,584	3,499	69	85	ND	89	ND	170	6.67	-107.8		
	10/9/2014	Drained	--	--	--	--	--	--	--	--	--	--	--	--	--		*Sample error, invalid
	10/23/2014	Saturated	12.9	5.2	7.7	762	2,422	30	84	33	12	ND	18	7.32	-123.9	DUP(aq)=16.2(GRO), 6.8(DRO), 1,839(Ben), 25(CO2)	
	11/6/2014	Drained	--	--	--	--	--	--	--	--	--	--	--	--	--		
	11/20/2014	Saturated	8.7	5.5	3.2	809	1,419	23	37	148	27	ND	1	6.70	-107.0		
	12/4/2014	Drained	--	--	--	--	--	--	--	--	--	--	--	--	--		
	12/18/2014	Saturated	10.2	6.3	3.9	1,008	2,018	22	26	72	28	0	8	7.19	-65.8		
	1/3/2015	Drained	--	--	--	--	--	--	--	--	--	--	--	--	--		
	1/15/2015	Saturated	13.4	6.4	7.0	1,067	1,951	38	34	8	26	0	5	7.13	-134.6		
	1/28/2015	Drained	--	--	--	--	--	--	--	--	--	--	--	--	--		
	2/11/2015	Saturated	44.3	8.9	35.5	871	1,075	98	144	1,919	25	0	4	7.03	-145.7		
	2/27/2015	Drained	--	--	--	--	--	--	--	--	--	--	--	--	--		
	3/13/2015	Saturated	72.4	3.9	68.5	716	2,074	36	51	83	21	0.02	4	7.03	-153.5		
	3/28/2015	Drained	--	--	--	--	--	--	--	--	--	--	--	--	--		
	4/10/2015	Saturated	9.5	4.9	4.6	753	1,732	33	27	30	17	0.02	3	7.03	-150.3		
	4/24/2015	Drained	--	--	--	--	--	--	--	--	--	--	--	--	--		
	5/9/2015	Saturated	12.6	6.9	5.7	705	2,024	37	39	24	21	0.13	2	7.02	-147.4		
	5/22/2015	Drained	--	--	--	--	--	--	--	--	--	--	--	--	--		
	6/5/2015	Saturated	10.7	5.3	5.4	544	2,112	37	36	24	17	0.22	3	7.16	-145.8		
	6/18/2015	Drained	--	--	--	--	--	--	--	--	--	--	--	--	--		
7/7/2015	Saturated	19.0	14.1	4.9	618	1,646	31	25	11	17	0.37	2	7.05	-151.6			
7/21/2015	Drained	--	--	--	--	--	--	--	--	--	--	--	--	--			

Column (Initial Soil Concentration)	Date	Conditions	AQUEOUS													NOTE	
			TPH (mg/L)	GRO (mg/L)	DRO (mg/L)	Benzene (µg/L)	Naphthalene (µg/L)	n-Dodecane C <sub>12</sub> (µg/L)	n-Tetradecane C <sub>14</sub> (µg/L)	n-Hexacosane C <sub>26</sub> (µg/L)	CO2 (mg/L)	CH4 (mg/L)	Sulfate (mg/L)	Average pH	Average <sup>1</sup> ORP (mV Ag/AgCl)		
3 (25,000mg/Kg)	7/2/2014	Saturated	39.6	4.4	35.2	490	4,518	79	86	398	88	0.32	1,030	6.71	-130.5		
	7/17/2014	Drained	--	--	--	--	--	--	--	--	--	--	--	--	--		
	7/30/2014	Saturated	23.0	9.6	13.4	1,170	4,154	35	55	16	132	ND	1,730	6.54	-150.3		
	8/14/2014	Drained	--	--	--	--	--	--	--	--	--	--	--	--	--		
	8/27/2014	Saturated	43.1	22.7	20.4	2,460	3,322	180	100	52	135	ND	250	7.07	-148.6		
	9/10/2014	Drained	--	--	--	--	--	--	--	--	--	--	--	--	--	--	
	9/29/2014	Saturated	29.6	11.8	17.7	1,911	4,636	152	121	34	58	ND	120	7.21	-118.1		
	10/9/2014	Drained	--	--	--	--	--	--	--	--	--	--	--	--	--	--	
	10/23/2014	Saturated	18.2	11.6	6.6	2,146	3,095	29	57	9	39	ND	24	7.27	-133.2		
	11/6/2014	Drained	--	--	--	--	--	--	--	--	--	--	--	--	--	--	
	11/20/2014	Saturated	8.8	4.7	4.1	695	1,985	23	37	98	31	ND	1	6.76	-113.3		
	12/4/2014	Drained	--	--	--	--	--	--	--	--	--	--	--	--	--	--	
	12/18/2014	Saturated	10.0	5.4	4.6	954	2,854	24	33	30	27	0.003	8	7.08	-73.3		
	1/3/2015	Drained	--	--	--	--	--	--	--	--	--	--	--	--	--	--	
	1/15/2015	Saturated	13.4	4.7	8.7	769	2,666	21	40	31	26	0.01	10	7.06	-131.2	DUP=8.7(GRO), 7.85 (DRO), 1,141(BEN), 19.97(CO2), 1.25 (Sulfate)	
	1/28/2015	Drained	--	--	--	--	--	--	--	--	--	--	--	--	--	--	
	2/11/2015	Saturated	46.8	6.4	40.4	1,319	2,348	51	215	1,057	19	0.01	3	7.04	-152.5		
	2/27/2015	Drained	--	--	--	--	--	--	--	--	--	--	--	--	--	--	
	3/13/2015	Saturated	67.8	7.1	60.7	965	2,493	34	33	31	17	0.02	4	7.08	-150.9		
	3/28/2015	Drained	--	--	--	--	--	--	--	--	--	--	--	--	--	--	
	4/10/2015	Saturated	14.0	8.1	5.9	1,204	2,409	35	30	13	19	0.03	3	7.04	-148.5		
	4/24/2015	Drained	--	--	--	--	--	--	--	--	--	--	--	--	--	--	
	5/9/2015	Saturated	17.6	11.7	5.9	1,121	2,219	39	36	57	19	0.10	2	7.07	-145.8		
	5/22/2015	Drained	--	--	--	--	--	--	--	--	--	--	--	--	--	--	
	6/5/2015	Saturated	15.7	8.6	7.1	625	3,007	39	35	23	15	0.17	3	7.13	-147.9		
6/18/2015	Drained	--	--	--	--	--	--	--	--	--	--	--	--	--	--		
7/7/2015	Saturated	22.8	13.3	9.5	912	3,096	42	41	71	14	0.50	1	7.14	-158.3			
7/21/2015	Drained	--	--	--	--	--	--	--	--	--	--	--	--	--	--		

Column (Initial Soil Concentration)	Date	Conditions	AQUEOUS													NOTE
			TPH (mg/L)	GRO (mg/L)	DRO (mg/L)	Benzene (µg/L)	Naphthalene (µg/L)	n-Dodecane C <sub>12</sub> (µg/L)	n-Tetradecane C <sub>14</sub> (µg/L)	n-Hexacosane C <sub>26</sub> (µg/L)	CO <sub>2</sub> (mg/L)	CH <sub>4</sub> (mg/L)	Sulfate (mg/L)	Average pH	Average <sup>1</sup> ORP (mV Ag/AgCl)	
4 (27,000mg/Kg)	7/2/2014	Saturated	41.5	5.0	36.5	470	4,248	56	86	317	78	0.21	1,500	6.73	-144.8	DUP(aq)=4.10(GRO),52.8(DRO),500(Ben),1,580(Sulfate)
	7/17/2014	Drained	--	--	--	--	--	--	--	--	--	--	--	--	--	
	7/30/2014	Saturated	23.2	10.7	12.5	1,320	4,020	43	67	38	173	ND	1,280	6.23	-112.7	
	8/14/2014	Drained	--	--	--	--	--	--	--	--	--	--	--	--	--	-Break in Gas Capture Line
	8/27/2014	Saturated	36.5	21.8	14.7	2,850	3,501	91	80	46	204	ND	1,510	6.49	-132.5	
	9/10/2014	Drained	--	--	--	--	--	--	--	--	--	--	--	--	--	
	9/29/2014	Saturated	27.6	9.3	18.3	1,816	4,484	128	76	ND	102	ND	630	6.48	-109.5	
	10/9/2014	Drained	--	--	--	--	--	--	--	--	--	--	--	--	--	
	10/23/2014	Saturated	16.4	9.1	7.3	1,935	2,985	28	64	14	22	ND	190	6.44	-129.0	
	11/6/2014	Drained	--	--	--	--	--	--	--	--	--	--	--	--	--	
	11/20/2014	Saturated	10.6	6.1	4.5	1,041	2,108	25	38	103	45	ND	1	6.55	-122.3	
	12/4/2014	Drained	--	--	--	--	--	--	--	--	--	--	--	--	--	Gas Measurement Error
	12/18/2014	Saturated	11.7	5.5	6.3	1,188	2,737	24	38	55	41	0	8	7.26	-90.7	
	1/3/2015	Drained	--	--	--	--	--	--	--	--	--	--	--	--	--	
	1/15/2015	Saturated	22.0	9.4	12.6	1,533	2,166	38	105	114	29	0.01	8	7.23	-139.3	
	1/28/2015	Drained	--	--	--	--	--	--	--	--	--	--	--	--	--	
	2/11/2015	Saturated	36.8	8.0	28.8	1,277	713	112	81	1,025	36	0.02	3	7.15	-155.3	
	2/27/2015	Drained	--	--	--	--	--	--	--	--	--	--	--	--	--	
	3/13/2015	Saturated	90.2	9.1	81.1	1,434	3,138	37	37	53	32	0.04	5	7.12	-144.4	
	3/28/2015	Drained	--	--	--	--	--	--	--	--	--	--	--	--	--	
	4/10/2015	Saturated	12.4	6.0	6.4	1,348	2,706	35	27	29	28	0.10	2	7.13	-147.6	
	4/24/2015	Drained	--	--	--	--	--	--	--	--	--	--	--	--	--	
	5/9/2015	Saturated	37.7	15.4	22.3	1,249	3,021	47	225	132	24	0.33	2	7.09	-147.0	
	5/22/2015	Drained	--	--	--	--	--	--	--	--	--	--	--	--	--	
	6/5/2015	Saturated	19.7	11.7	8.1	952	3,452	42	36	12	25	0.59	2	7.03	-146.2	
	6/18/2015	Drained	--	--	--	--	--	--	--	--	--	--	--	--	--	
	7/7/2015	Saturated	93.1	15.4	77.6	1,253	3,827	96	82	128	24	1.5	1	7.04	-155.9	
7/21/2015	Drained	--	--	--	--	--	--	--	--	--	--	--	--	--		

Column (Initial Soil Concentration)	Date	Conditions	AQUEOUS													NOTE	
			TPH (mg/L)	GRO (mg/L)	DRO (mg/L)	Benzen e (µg/L)	Naphthale ne (µg/L)	n-Dodecane C <sub>12</sub> (µg/L)	n-Tetradecane C <sub>14</sub> (µg/L)	n-Hexacosane C <sub>26</sub> (µg/L)	CO2 (mg/L)	CH4 (mg/L)	Sulfate (mg/L)	Average pH	Average <sup>1</sup> ORP (mV Ag/AgCl)		
5 (29,000mg/Kg)	7/2/2014	Saturated	58.6	4.9	53.7	490	4,809	85	78	920	99	0.02	1,700	6.59	-131.6		
	7/17/2014	Drained	--	--	--	--	--	--	--	--	--	--	--	--	--		
	7/30/2014	Saturated	17.3	10.3	7.0	1,310	4,591	30	66	19	127	ND	1,810	6.17	-102.4		
	8/14/2014	Drained	--	--	--	--	--	--	--	--	--	--	--	--	--		
	8/27/2014	Saturated	35.6	23.8	11.8	3,530	4,098	44	67	24	209	ND	1,830	6.39	-122.9	DUP(aq)=31.5(GRO),14.3(DRO), 3,955(Ben), 255.41(CO2), 1,940(Sulfate),	
	9/10/2014	Drained	--	--	--	--	--	--	--	--	--	--	--	--	--	--	
	9/29/2014	Saturated	37.6	14.1	23.5	2,003	5,011	157	74	92	110	ND	940	6.42	-108.0		
	10/9/2014	Drained	--	--	--	--	--	--	--	--	--	--	--	--	--	--	
	10/23/2014	Saturated	25.4	16.5	8.9	3,754	3,679	31	64	31	72	ND	290	6.36	-126.8		
	11/6/2014	Drained	--	--	--	--	--	--	--	--	--	--	--	--	--	--	
	11/20/2014	Saturated	12.5	7.2	5.3	1,280	2,482	27	38	101	105	ND	5	6.50	-120.7		
	12/4/2014	Drained	--	--	--	--	--	--	--	--	--	--	--	--	--	--	
	12/18/2014	Saturated	13.7	7.8	5.9	1,431	3,425	26	37	30	41	0	6	7.31	-95.2		
	1/3/2015	Drained	--	--	--	--	--	--	--	--	--	--	--	--	--	--	
	1/15/2015	Saturated	24.1	12.5	11.6	1,791	3,314	43	36	123	31	0.01	8	7.27	-147.8		
	1/28/2015	Drained	--	--	--	--	--	--	--	--	--	--	--	--	--	--	
	2/11/2015	Saturated	56.0	8.7	47.2	1,626	2,872	110	83	2,658	37	0.02	3	7.18	-152.8		
	2/27/2015	Drained	--	--	--	--	--	--	--	--	--	--	--	--	--	--	
	3/13/2015	Saturated	295.8	9.4	286.4	1,565	3,063	51	49	173	25	0.05	4	7.16	-150.3		
	3/28/2015	Drained	--	--	--	--	--	--	--	--	--	--	--	--	--	--	
	4/10/2015	Saturated	14.5	6.5	8.0	1,614	3,496	38	33	17	21	0.16	3	7.18	-146.6		
	4/24/2015	Drained	--	--	--	--	--	--	--	--	--	--	--	--	--	--	
	5/9/2015	Saturated	23.9	16.1	7.8	1,418	3,536	39	33	36	26	0.79	3	7.13	-147.9		
	5/22/2015	Drained	--	--	--	--	--	--	--	--	--	--	--	--	--	--	
	6/5/2015	Saturated	22.8	12.9	9.9	1,326	3,897	44	38	42	27	1.7	2	7.08	-140.9		
	6/18/2015	Drained	--	--	--	--	--	--	--	--	--	--	--	--	--	--	
	7/7/2015	Saturated	27.6	11.4	16.2	1,155	3,717	43	38	61	24	3.0	2	7.10	-153.8		
7/21/2015	Drained	--	--	--	--	--	--	--	--	--	--	--	--	--	--		

Column (Initial Soil Concentration)	Date	Conditions	AQUEOUS													NOTE
			TPH (mg/L)	GRO (mg/L)	DRO (mg/L)	Benzen e (µg/L)	Naphthale ne (µg/L)	n-Dodecane C <sub>12</sub> (µg/L)	n-Tetradecane C <sub>14</sub> (µg/L)	n-Hexacosane C <sub>26</sub> (µg/L)	CO2 (mg/L)	CH4 (mg/L)	Sulfate (mg/L)	Average pH	Average <sup>1</sup> ORP (mV Ag/AgCl)	
6 (32,000mg/Kg)	7/2/2014	Saturated	101.6	4.6	97.0	530	5,904	411	168	1,811	109	ND	1,720	6.50	-120.6	
	7/17/2014	Drained	--	--	--	--	--	--	--	--	--	--	--	--	--	
	7/30/2014	Saturated	16.5	1.4	15.1	1,380	4,591	44	71	80	143	ND	1,990	6.18	-98.7	
	8/14/2014	Drained	--	--	--	--	--	--	--	--	--	--	--	--	--	
	8/27/2014	Saturated	48.0	32.1	15.9	4,130	4,629	39	70	59	259	ND	1,920	6.39	-133.5	
	9/10/2014	Drained	--	--	--	--	--	--	--	--	--	--	--	--	--	
	9/29/2014	Saturated	31.2	13.8	17.4	2,490	4,973	142	68	36	122	ND	1,120	6.39	-112.9	
	10/9/2014	Drained	--	--	--	--	--	--	--	--	--	--	--	--	--	
	10/23/2014	Saturated	36.6	26.0	10.6	4,507	4,352	34	67	34	77	ND	9	6.33	-131.1	
	11/6/2014	Drained	--	--	--	--	--	--	--	--	--	--	--	--	--	
	11/20/2014	Saturated	15.0	7.7	7.3	1,592	2,898	35	39	111	56	ND	1	6.49	-127.6	
	12/4/2014	Drained	--	--	--	--	--	--	--	--	--	--	--	--	--	
	12/18/2014	Saturated	17.4	11.7	5.7	1,858	3,505	28	31	29	49	0.01	8	7.32	-102.7	DUP=10.6(GRO), 1,668(BEN), 6.77(DRO), 42.2(CO2)
	1/3/2015	Drained	--	--	--	--	--	--	--	--	--	--	--	--	--	
	1/15/2015	Saturated	22.9	11.0	11.9	2,081	3,622	44	38	111	36	0.02	4	7.34	-146.3	
	1/28/2015	Drained	--	--	--	--	--	--	--	--	--	--	--	--	--	
	2/11/2015	Saturated	126.8	11.5	115.3	2,417	3,606	118	535	2,420	42	0.03	3	7.20	-153.5	Sample Error No DRO
	2/27/2015	Drained	--	--	--	--	--	--	--	--	--	--	--	--	--	
	3/13/2015	Saturated	251.9	11.3	240.6	2,106	4,192	45	202	138	33	0.07	3	7.21	-148.0	
	3/28/2015	Drained	--	--	--	--	--	--	--	--	--	--	--	--	--	
	4/10/2015	Saturated	17.4	8.6	8.8	2,001	3,843	39	33	8	25	0.25	3	7.19	-148.9	
	4/24/2015	Drained	--	--	--	--	--	--	--	--	--	--	--	--	--	
	5/9/2015	Saturated	26.9	18.4	8.5	1,784	3,547	57	48	33	29	0.88	3	7.15	-144.7	
5/22/2015	Drained	--	--	--	--	--	--	--	--	--	--	--	--	--		
6/5/2015	Saturated	23.3	13.2	10.2	1,712	4,531	55	45	5	31	2.1	2	7.14	-145.8		
6/18/2015	Drained	--	--	--	--	--	--	--	--	--	--	--	--	--		
7/7/2015	Saturated	24.1	13.9	10.2	1,831	3,717	39	36	24	30	3.7	1	7.15	-151.7		
7/21/2015	Drained	--	--	--	--	--	--	--	--	--	--	--	--	--		

Column (Initial Soil Concentration)	Date	Conditions	AQUEOUS													NOTE
			TPH (mg/L)	GRO (mg/L)	DRO (mg/L)	Benzene (µg/L)	Naphthalene (µg/L)	n-Dodecane C <sub>12</sub> (µg/L)	n-Tetradecane C <sub>14</sub> (µg/L)	n-Hexacosane C <sub>26</sub> (µg/L)	CO2 (mg/L)	CH4 (mg/L)	Sulfate (mg/L)	Average pH	Average <sup>1</sup> ORP (mV Ag/AgCl)	
7 (35,000mg/Kg)	7/2/2014	Saturated	88.8	4.0	84.8	520	5,640	99	102	3,817	127	0.18	1,550	6.46	-115.3	
	7/17/2014	Drained	--	--	--	--	--	--	--	--	--	--	--	--	--	
	7/30/2014	Saturated	29.2	12.2	17.0	1,460	5,577	76	58	28	136	ND	1,940	6.33	-122.9	
	8/14/2014	Drained	--	--	--	--	--	--	--	--	--	--	--	--	--	
	8/27/2014	Saturated	73.3	24.9	48.4	3,690	5,401	3,349	5,806	416	207	ND	1,440	6.37	-125.6	
	9/10/2014	Drained	--	--	--	--	--	--	--	--	--	--	--	--	--	
	9/29/2014	Saturated	41.4	16.9	24.5	2,736	7,147	734	1,544	140	100	ND	620	6.42	-101.7	DUP=16.6(GRO), 2,424(Ben), NP (DRO), 108.15(CO2), 650 (Sulfate)
	10/9/2014	Drained	--	--	--	--	--	--	--	--	--	--	--	--	--	
	10/23/2014	Saturated	34.8	24.3	10.5	3,739	4,640	60	56	56	63	ND	425	6.29	-115.6	
	11/6/2014	Drained	--	--	--	--	--	--	--	--	--	--	--	--	--	
	11/20/2014	Saturated	15.3	9.6	5.7	1,707	3,049	31	27	94	62	ND	4	6.49	-132.5	
	12/4/2014	Drained	--	--	--	--	--	--	--	--	--	--	--	--	--	
	12/18/2014	Saturated	16.4	9.5	6.9	1,759	4,018	30	31	47	53	0.02	4	7.35	-116.5	
	1/3/2015	Drained	--	--	--	--	--	--	--	--	--	--	--	--	--	
	1/15/2015	Saturated	20.1	8.4	11.7	1,816	3,813	44	21	68	34	0.07	6	7.36	-137.9	
	1/28/2015	Drained	--	--	--	--	--	--	--	--	--	--	--	--	--	
	2/11/2015	Saturated	59.8	9.9	49.9	2,260	2,324	56	35	2,940	46	0.09	3	7.21	-149.3	
	2/27/2015	Drained	--	--	--	--	--	--	--	--	--	--	--	--	--	
	3/13/2015	Saturated	118.1	12.2	105.9	2,272	4,433	50	21	20	31	0.25	4	7.22	-148.0	
	3/28/2015	Drained	--	--	--	--	--	--	--	--	--	--	--	--	--	
	4/10/2015	Saturated	22.0	11.3	10.7	2,219	4,750	44	36	17	31	0.68	4	7.22	-142.5	
	4/24/2015	Drained	--	--	--	--	--	--	--	--	--	--	--	--	--	
	5/9/2015	Saturated	17.9	8.2	9.7	1,252	4,091	41	36	53	36	1.25	3	7.19	-140.5	
	5/22/2015	Drained	--	--	--	--	--	--	--	--	--	--	--	--	--	
	6/5/2015	Saturated	25.1	15.5	9.5	1,586	4,633	44	39	0	38	3.7	2	7.18	-137.5	
	6/18/2015	Drained	--	--	--	--	--	--	--	--	--	--	--	--	--	
	7/7/2015	Saturated	21.6	13.3	8.3	1,591	3,832	35	29	35	47	5.4	1	7.22	-142.7	
	7/21/2015	Drained	--	--	--	--	--	--	--	--	--	--	--	--	--	

Column (Initial Soil Concentration)	Date	Conditions	AQUEOUS													NOTE
			TPH (mg/L)	GRO (mg/L)	DRO (mg/L)	Benzen e (µg/L)	Naphthale ne (µg/L)	n-Dodecane C <sub>12</sub> (µg/L)	n-Tetradecane C <sub>14</sub> (µg/L)	n-Hexacosane C <sub>26</sub> (µg/L)	CO2 (mg/L)	CH4 (mg/L)	Sulfate (mg/L)	Avera ge pH	Average <sup>1</sup> ORP (mV Ag/AgCl)	
8 (37,000mg/Kg)	7/2/2014	Saturated	40.1	2.9	37.2	330	5,089	56	77	372	118	0.24	1,450	6.68	-122.8	
	7/17/2014	Drained	--	--	--	--	--	--	--	--	--	--	--	--	--	
	7/30/2014	Saturated	27.4	9.8	17.6	1,160	6,109	69	65	38	157	ND	1,860	6.32	-114.5	
	8/14/2014	Drained	--	--	--	--	--	--	--	--	--	--	--	--	--	
	8/27/2014	Saturated	38.5	22.7	15.8	3,770	4,579	87	31	ND	198	ND	1,280	6.45	-118.8	
	9/10/2014	Drained	--	--	--	--	--	--	--	--	--	--	--	--	--	
	9/29/2014	Saturated	28.3	14.4	14.0	1,875	4,564	36	53	ND	106	ND	620	6.49	-109.5	
	10/9/2014	Drained	--	--	--	--	--	--	--	--	--	--	--	--	--	
	10/23/2014	Saturated	33.7	25.4	8.3	4,558	4,382	32	51	12	77	ND	230	6.42	-121.9	
	11/6/2014	Drained	--	--	--	--	--	--	--	--	--	--	--	--	--	
	11/20/2014	Saturated	15.8	9.3	6.6	1,590	2,562	24	38	107	51	ND	2	6.57	-120.0	DUP=5.2(GRO),1214.7(Ben), 4.65 (DRO), 41.7(CO2), 0(CH4)
	12/4/2014	Drained	--	--	--	--	--	--	--	--	--	--	--	--	--	
	12/18/2014	Saturated	23.8	8.8	15.0	1,629	4,038	32	145	59	42	0	4	7.31	-95.2	
	1/3/2015	Drained	--	--	--	--	--	--	--	--	--	--	--	--	--	
	1/15/2015	Saturated	24.3	13.5	10.9	2,059	3,652	41	31	56	36	0.02	3	7.31	-140.8	
	1/28/2015	Drained	--	--	--	--	--	--	--	--	--	--	--	--	--	
	2/11/2015	Saturated	43.8	9.7	34.1	1,867	3,754	66	32	875	37	0.03	2	7.20	-139.0	
	2/27/2015	Drained	--	--	--	--	--	--	--	--	--	--	--	--	--	
	3/13/2015	Saturated	93.3	8.1	85.2	1,675	3,807	47	29	69	30	0.06	3	7.15	-139.8	
	3/28/2015	Drained	--	--	--	--	--	--	--	--	--	--	--	--	--	
	4/10/2015	Saturated	16.2	7.5	8.7	1,564	3,875	39	34	9	27	0.12	2	7.14	-142.0	
	4/24/2015	Drained	--	--	--	--	--	--	--	--	--	--	--	--	--	
	5/9/2015	Saturated	25.9	17.0	8.8	1,464	3,954	41	34	30	28	0.66	2	7.11	-136.8	
	5/22/2015	Drained	--	--	--	--	--	--	--	--	--	--	--	--	--	
6/5/2015	Saturated	21.3	12.4	8.9	1,377	4,200	48	31	6	26	2.0	2	7.11	-138.8		
6/18/2015	Drained	--	--	--	--	--	--	--	--	--	--	--	--	--		
7/7/2015	Saturated	26.0	16.4	9.6	1,408	3,857	37	28	25	26	3.9	2	7.13	-136.4		
7/21/2015	Drained	--	--	--	--	--	--	--	--	--	--	--	--	--		

Column (Initial Soil Concentration)	Date	Conditions	AQUEOUS													NOTE
			TPH (mg/L)	GRO (mg/L)	DRO (mg/L)	Benzen e (µg/L)	Naphthale ne (µg/L)	n-Dodecane C <sub>12</sub> (µg/L)	n-Tetradecane C <sub>14</sub> (µg/L)	n-Hexacosane C <sub>26</sub> (µg/L)	CO2 (mg/L)	CH4 (mg/L)	Sulfate (mg/L)	Average pH	Average <sup>1</sup> ORP (mV Ag/AgCl)	
9 (9,000mg/Kg)	7/2/2014	Saturated	42.3	6.1	36.2	550	677	63	113	626	12	0.03	1,730	6.64	-105.9	
	7/17/2014	Drained	--	--	--	--	--	--	--	--	--	--	--	--	--	
	7/30/2014	Saturated	29.1	17.9	11.2	1,290	2,845	41	82	9	139	ND	1,740	6.18	-97.3	
	8/14/2014	Drained	--	--	--	--	--	--	--	--	--	--	--	--	--	
	8/27/2014	Saturated	65.8	43.5	22.3	3,260	651	257	160	34	169	ND	1,660	6.30	-104.8	
	9/10/2014	Drained	--	--	--	--	--	--	--	--	--	--	--	--	--	
	9/29/2014	Saturated	49.7	33.8	15.9	2,459	632	171	79	ND	86	ND	1,160	6.31	-92.0	
	10/9/2014	Drained	--	--	--	--	--	--	--	--	--	--	--	--	--	
	10/23/2014	Saturated	24.3	18.9	5.4	1,948	418	26	102	11	38	ND	500	6.28	-112.9	
	11/6/2014	Drained	--	--	--	--	--	--	--	--	--	--	--	--	--	
	11/20/2014	Saturated	12.2	9.2	3.0	834	270	20	77	128	45	ND	395	6.38	-118.7	
	12/4/2014	Drained	--	--	--	--	--	--	--	--	--	--	--	--	--	
	12/18/2014	Saturated	12.7	9.9	2.8	938	348	21	48	49	43	0	80	7.10	-86.9	
	1/3/2015	Drained	--	--	--	--	--	--	--	--	--	--	--	--	--	
	1/15/2015	Saturated	17.3	9.5	7.7	1,053	309	36	107	69	39	0	31	7.29	-119.1	
	1/28/2015	Drained	--	--	--	--	--	--	--	--	--	--	--	--	--	
	2/11/2015	Saturated	58.4	22.3	36.1	811	302	88	73	2,699	31	0	3	7.15	-117.9	
	2/27/2015	Drained	--	--	--	--	--	--	--	--	--	--	--	--	--	
	3/13/2015	Saturated	38.5	11.2	27.3	951	177	31	23	18	22	0	4	7.03	-112.3	
	3/28/2015	Drained	--	--	--	--	--	--	--	--	--	--	--	--	--	
	4/10/2015	Saturated	8.9	6.7	2.2	832	132	33	30	5	19	0	6	7.03	-106.0	DUP=18.8(CO2)
	4/24/2015	Drained	--	--	--	--	--	--	--	--	--	--	--	--	--	
	5/9/2015	Saturated	15.0	10.8	4.2	843	328	33	37	183	21	0	3	7.05	-99.8	
	5/22/2015	Drained	--	--	--	--	--	--	--	--	--	--	--	--	--	
	6/5/2015	Saturated	17.1	14.5	2.6	774	349	35	36	27	16	0	5	7.09	-94.3	
	6/18/2015	Drained	--	--	--	--	--	--	--	--	--	--	--	--	--	
7/7/2015	Saturated	24.9	17.3	7.6	730	396	29	27	6	14	0	3	7.14	-93.6		
7/21/2015	Drained	--	--	--	--	--	--	--	--	--	--	--	--	--		

Column (Initial Soil Concentration)	Date	Conditions	AQUEOUS													NOTE
			TPH (mg/L)	GRO (mg/L)	DRO (mg/L)	Benzene (µg/L)	Naphthalene (µg/L)	n-Dodecane C <sub>12</sub> (µg/L)	n-Tetradecane C <sub>14</sub> (µg/L)	n-Hexacosane C <sub>26</sub> (µg/L)	CO <sub>2</sub> (mg/L)	CH <sub>4</sub> (mg/L)	Sulfate (mg/L)	Average pH	Average <sup>1</sup> ORP (mV Ag/AgCl)	
10 (17,000mg/Kg)	7/2/2014	Saturated	103.6	2.4	101.2	270	7,549	641	79	1,559	2	ND	170	7.28	-64.1	
	7/17/2014	Drained	--	--	--	--	--	--	--	--	--	--	--	--	--	
	7/30/2014	Saturated	23.6	8.1	15.5	720	5,362	41	53	13	7	ND	30	7.49	-103.4	
	8/14/2014	Drained	--	--	--	--	--	--	--	--	--	--	--	--	--	
	8/27/2014	Saturated	45.4	21.2	24.2	1,625	5,716	252	42	23	53	ND	23	7.47	-121.9	
	9/10/2014	Drained	--	--	--	--	--	--	--	--	--	--	--	--	--	
	9/29/2014	Saturated	36.2	3.4	32.8	607	9,172	235	52	109	4	ND	18	7.48	45.4	
	10/9/2014	Drained	--	--	--	--	--	--	--	--	--	--	--	--	--	
	10/23/2014	Saturated	17.3	8.8	8.5	825	3,997	28	32	44	4	ND	16	7.34	-92.1	
	11/6/2014	Drained	--	--	--	--	--	--	--	--	--	--	--	--	--	
	11/20/2014	Saturated	5.9	3.1	2.8	473	1,053	8	25	0	5	ND	19	7.30	-28.3	
	12/4/2014	Drained	--	--	--	--	--	--	--	--	--	--	--	--	--	
	12/18/2014	Saturated	13.1	5.1	8.1	597	4,521	31	7	49	5	0	12	7.53	-67.4	
	1/3/2015	Drained	--	--	--	--	--	--	--	--	--	--	--	--	--	
	1/15/2015	Saturated	25.2	6.5	18.7	913	2,203	37	147	88	7	0	16	7.52	18.8	
	1/28/2015	Drained	--	--	--	--	--	--	--	--	--	--	--	--	--	
	2/11/2015	Saturated	73.2	15.9	57.3	604	3,532	62	29	2,890	8	0	11	7.64	21.0	
	2/27/2015	Drained	--	--	--	--	--	--	--	--	--	--	--	--	--	
	3/13/2015	Saturated	153.2	5.8	147.4	491	2,861	33	118	39	4	0	16	7.68	22.6	DUP=5.1(GRO), 208.4 (DRO), 2035(Ben), 2.10(CO <sub>2</sub> ), 16.44(Sulfate)
	3/28/2015	Drained	--	--	--	--	--	--	--	--	--	--	--	--	--	
	4/10/2015	Saturated	9.6	4.6	5.0	354	2,159	29	7	8	10	0	19	7.63	11.5	
	4/24/2015	Drained	--	--	--	--	--	--	--	--	--	--	--	--	--	
	5/9/2015	Saturated	10.5	3.9	6.6	0	3,444	32	18	21	7	0	17	7.68	21.5	
	5/22/2015	Drained	--	--	--	--	--	--	--	--	--	--	--	--	--	
	6/5/2015	Saturated	17.8	10.8	6.9	511	3,552	34	20	5	6	0	16	7.72	16.0	
	6/18/2015	Drained	--	--	--	--	--	--	--	--	--	--	--	--	--	
7/7/2015	Saturated	14.4	5.5	8.9	348	3,021	29	16	30	4	0	15	7.71	19.2		
7/21/2015	Drained	--	--	--	--	--	--	--	--	--	--	--	--	--		

Column (Initial Soil Concentration)	Date	Conditions	AQUEOUS													NOTE
			TPH (mg/L)	GRO (mg/L)	DRO (mg/L)	Benzen e (µg/L)	Naphthale ne (µg/L)	n-Dodecane C <sub>12</sub> (µg/L)	n-Tetradecane C <sub>14</sub> (µg/L)	n-Hexacosane C <sub>26</sub> (µg/L)	CO2 (mg/L)	CH4 (mg/L)	Sulfate (mg/L)	Average pH	Average <sup>1</sup> ORP (mV Ag/AgCl)	
11 (27,000mg/Kg)	7/2/2014	Saturated	71.9	4.8	67.1	580	4,631	125	102	1,336	181	0.47	1,720	6.40	-174.1	
	7/17/2014	Drained	--	--	--	--	--	--	--	--	--	--	--	--	--	
	7/30/2014	Saturated	23.2	13.2	10.0	1,510	2,702	32	62	50	183	ND	1,980	5.52	-147.9	DUP(aq)=15.3(GRO), 194.9(Ben), 20.2(DRO), 1,906(Sulfate), 177.79(CO2)
	8/14/2014	Drained	--	--	--	--	--	--	--	--	--	--	--	--	--	
	8/27/2014	Saturated	41.8	26.8	15.0	3,500	3,635	39	75	ND	239	ND	2,070	5.73	-160.3	
	9/10/2014	Drained	--	--	--	--	--	--	--	--	--	--	--	--	--	
	9/29/2014	Saturated	24.6	13.7	10.9	2,712	3,027	34	58	ND	201	ND	1,250	5.70	-124.9	
	10/9/2014	Drained	--	--	--	--	--	--	--	--	--	--	--	--	--	
	10/23/2014	Saturated	22.3	14.9	7.4	2,566	3,331	31	57	15	125	ND	470	5.76	-133.8	
	11/6/2014	Drained	--	--	--	--	--	--	--	--	--	--	--	--	--	
	11/20/2014	Saturated	15.2	9.6	5.6	1,367	2,427	28	50	101	142	ND	182	5.86	-139.7	
	12/4/2014	Drained	--	--	--	--	--	--	--	--	--	--	--	--	--	
	12/18/2014	Saturated	16.4	10.4	6.0	1,789	2,917	23	35	48	165	0	150	5.95	-116.4	
	1/3/2015	Drained	--	--	--	--	--	--	--	--	--	--	--	--	--	
	1/15/2015	Saturated	21.0	9.8	11.2	1,766	3,009	43	47	105	185	0	97	5.96	-142.4	
	1/28/2015	Drained	--	--	--	--	--	--	--	--	--	--	--	--	--	
	2/11/2015	Saturated	39.9	12.2	27.7	2,337	1,546	49	25	810	183	0	29	6.01	-155.60	
	2/27/2015	Drained	--	--	--	--	--	--	--	--	--	--	--	--	--	
	3/13/2015	Saturated	94.0	12.0	82.0	2,035	3,068	46	39	47	176	0	37	5.95	-166.90	
	3/28/2015	Drained	--	--	--	--	--	--	--	--	--	--	--	--	--	
	4/10/2015	Saturated	17.7	10.6	7.1	2,143	2,834.6	36.5	37.2	5.9	167	0	20	6.07	-163.50	
	4/24/2015	Drained	--	--	--	--	--	--	--	--	--	--	--	--	--	
	5/9/2015	Saturated	26.7	17.5	9.3	1,330	3,190	40	40	63	87	0	18	6.08	-147.9	
	5/22/2015	Drained	--	--	--	--	--	--	--	--	--	--	--	--	--	
6/5/2015	Saturated	26.0	18.5	7.5	1,562	3,069	40	40	5	151	0	10	6.15	-146.2		

**NOTE:**

<sup>1</sup> - Average or lowest stabilized reading.

Yellow Signifies Late Stage Criteria

#### 7.4. Appendix D – Ultraviolet Photographic Techniques in MATLAB

Throughout the experiment high resolution photographs were taken just before a saturating event or a draining event. The camera was positioned at approximately 20.75 inches from the front of each column on a tripod, and centered at a permanent sticker placed on the floor. An ultraviolet light was hung from rack above the columns and placed to the side so that light illuminated the LNAPL within the columns.

The raw image was adjusted using a photograph editing software so that the column was exactly vertical. At times the tripod was used for other experiments or the tripod legs would slide vertically at one leg, but not others just slightly enough to displace the camera from exactly level.

Using MATLAB code, shown below, the raw image was automatically cropped to just the illuminated column. Each image was placed in the same folder as the MATLAB code so that the program was “grabbing” the correct image. The code could process all 11 images of each column at once. The code pixelated the image and sorted out just the green hue from the illuminated LNAPL. Each row of pixels was evaluated on an arbitrary intensity scale provided by MATLAB. Then each row was cumulated into a single value for the position along the image, or in other words the length of the column. Using a plotting function the intensity values were plotted along a normalized vertical axis of the image to provide LNAPL intensity versus the length of the column.

The following pages describe the exact MATLAB code, show an example MATLAB plot, and how mobile LNAPL was visualized to move throughout the experiment.

#### MATLAB RAW CODE

```
function point_source_plotting
% global green_channel y
clc

%%%%%%%%%%%%%%%%%%%%%%%%%%%%%%%%%%%%%%%%%%%%%%%%%%%%%%%%%%%%%%%%%%%%%%%%Column1%%%%%%%%%%%%%%%%%%%%%%%%%%%%%%%%%%%%%%%%%%%%%%%%%%%%%%%%%%%%%%%%%%%%%%%%
%%%%%%%%%%%%%%%%%%%%%%%%%%%%%%%%%%%%%%%%%%%%%%%%%%%%%%%%%%%%%%%%%%%%%%%%

img{1}=imread('Column 1','jpg'); %name and extention, have to be in same folder as this file

aa = size(img{1});
```

```

ymax = aa(1)
xmax = aa(2)
img{1} = imcrop(img{1}, [24*xmax/50 0 xmax/25 ymax]); % crop the image if
% you want
aa = size(img{1});
ymax = aa(1)
xmax = aa(2)
% figure,imshow(img{1}{:,:,:}) % shows original picture
im_green = img{1};
im_green(:,1) = 0; %equates all blue to zero values
im_green(:,3) = 0; %equates all red to zero values
% shows the green channel for the pic
% return %stops the program here
x = linspace(0,1,xmax); % array from zero to one divided xmax times
    y = linspace(0,1,ymax);
    parameters = zeros(2,length(x));
colors = jet(length(x));

    for i=1:length(y)
        green_channel(i,:) = double(img{1}(i,:,2)); % creates array of only green values
        green_channel(i,:) = abs(green_channel(i,:) - min(green_channel(i,:))*1.5);
%subtracts smallest
        %green_channel(i,:) = green_channel(i,:)/ max(green_channel(i,:)); %normalizes
intensity values to 1
        napl_1(i,:) = sum(green_channel(i,:));
    end

```

```

%MASS_1 = cumsum(napl_1,1)%Sums up all Points in continuous matrix

%Points_1 = cumsum(napl_1,2) %creates 3456x1 matrix of of napl points per

%pixel line

%%%%%%%%%%%%%% plotting
%%%%%%%%%%%%%%

window_x = 900;

window_y = 900;

offset_x = 25;

offset_y = 25;

fig1 = figure(1);

set(fig1,'Position',[ offset_x offset_y window_x window_y],'PaperPositionMode','auto')

    %surf(x,y,green_channel,'EdgeColor','none');

    subplot(1,2,2)

    imshow(im_green);

    xlabel('Visual','FontSize',22)

subplot(1,2,1)

plot(napl_1,y,'g')

axis ij

axis([0 18000 0 1])

    hold off

    figure(gcf)

set(gca,'FontSize',18)

title('Column 1 ','FontSize',22)

xlabel('Intensity (Summation)','FontSize',16)

ylabel('Green Intensity','FontSize',28)

ylabel('Length Along Column (normalized)','FontSize',16)

% legend('Column 11')

```

view(2) %makes it a 2-D view instead of 3d iso

This code is repeated another 10 times to complete the process of plotting intensity versus normalized column length. The following image shows an example of the output file.

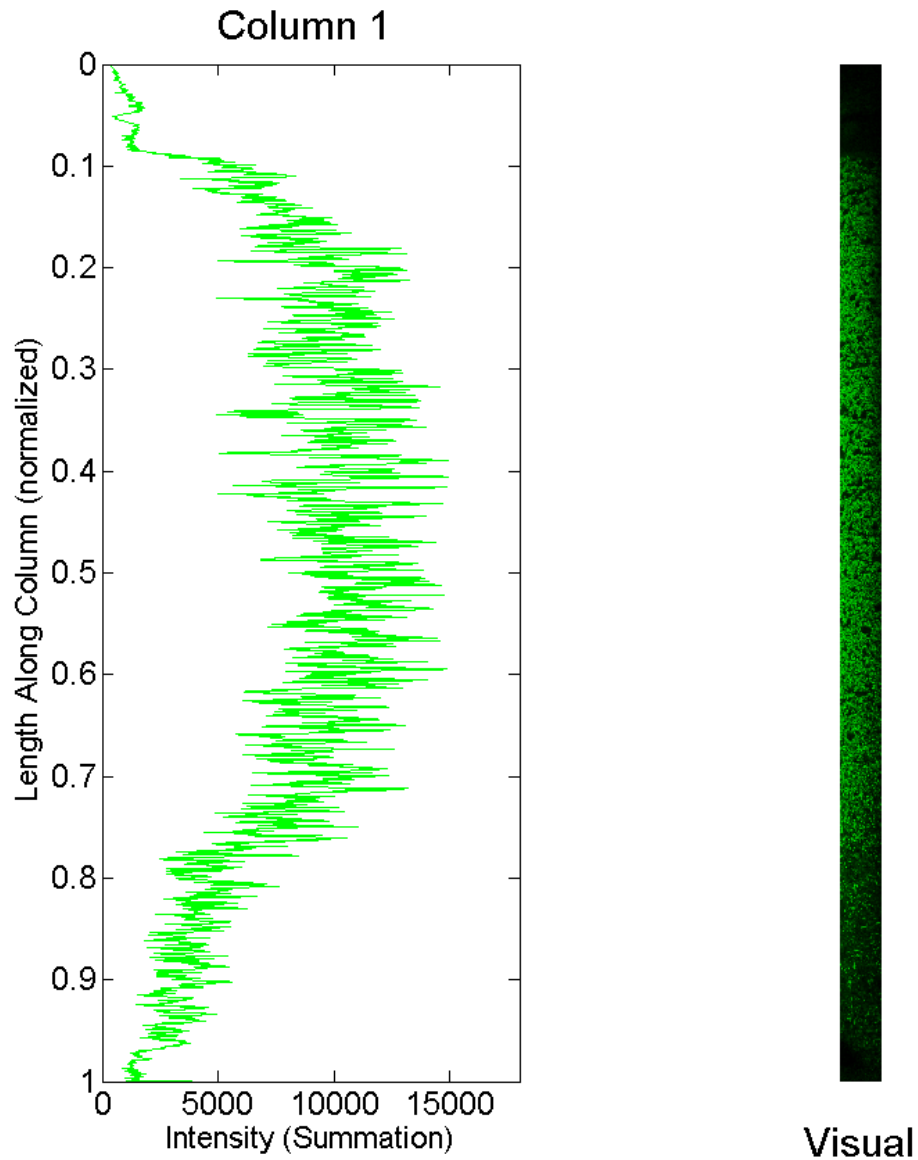
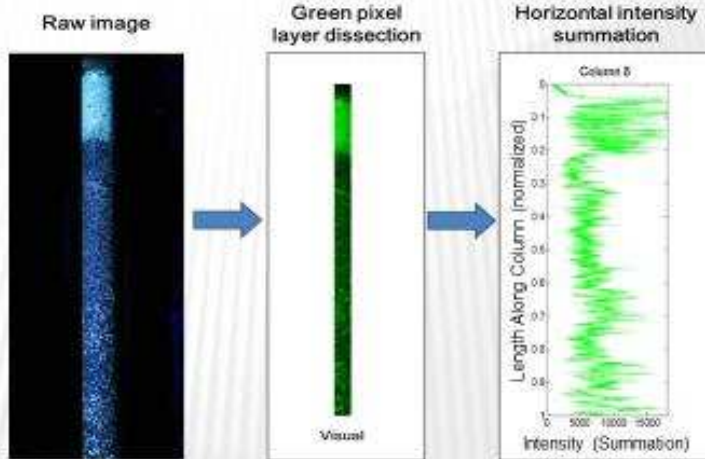


Figure 10– MATLAB Output portable network graphic (png)

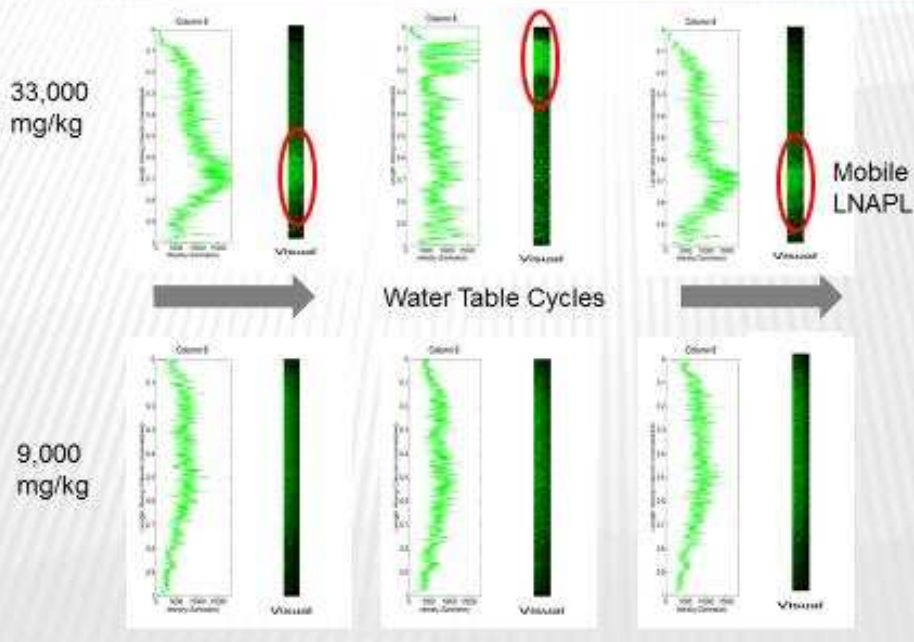
# UV LIGHT LNAPL FLUORESCENCE

- Individual pictures of columns under UV light
- High fraction of naphthalene causing fluorescence



13

# LNAPL CONCENTRATION VS. DEPTH



14

Figure 11– Example Slides of the UV Light Fluorescence Process and tracking of mobile LNAPL.